ELECTRON TRANSPORT THROUGH SINGLE GOLD ATOMS AND HYDROGEN MOLECULES

switching on the atomic scale

M.L. Trouwborst

University of Groningen
Zernike Institute
for Advanced Materials

NWO
Netherlands Organisation for Scientific Research

Zernike Institute PhD thesis series 2009-01
ISSN: 1570-1530
ISBN: 978-90-367-3658-9
ISBN: 978-90-367-3660-2 (electronic version)

The work described in this thesis was performed in the research groups Physics of Nanodevices of the Zernike Institute for Advanced Materials at the University of Groningen, the Netherlands. This research was financed by the 'Nederlandse Organisatie voor Wetenschappelijk Onderzoek (NWO)', via a Pionier grant.

Cover image: Micrograph made by a scanning electron microscope, of a mechanically controllable break junction. The metal bridge is made of gold and has a cross section of 100 $\times$ 100 nm (at the constriction).

Cover design by: Peter Musschenga, www.pjot.nl
Printed by: PrintPartners Ipskamp, Enschede

RIJKSUNIVERSITEIT GRONINGEN

ELECTRON TRANSPORT THROUGH SINGLE GOLD ATOMS AND HYDROGEN MOLECULES

switching on the atomic scale

Proefschrift

ter verkrijging van het doctoraat in de
Wiskunde en Natuurwetenschappen
aan de Rijksuniversiteit Groningen
op gezag van de
Rector Magnificus, dr. F. Zwarts,
in het openbaar te verdedigen op
vrijdag 30 januari 2009
om 16:15 uur

door

Marius Leendert Trouwborst

geboren op 29 maart 1977
te Woerden

Promotores:	Prof. dr. ir. B. J. van Wees
	Prof. dr. B.L. Feringa
Copromotor:	Dr. ir. S.J. van der Molen
Beoordelingscommissie:	Prof. dr. E. Scheer
	Prof. dr. ir. H.S.J. van der Zant
	Prof. dr. D.M. de Leeuw

Contents

Preface

At the time of writing this thesis, Intel Corporation announced the production of 32 nm "node" processors in 2009. Hence, in the very near future, computers will be build from transistors with line widths of less than 300 atoms. Even more fascinating is the number of dopants in such processors: less than 30 atoms are used for the doping of a single transistor.

Meanwhile the race for miniaturization continues, clearly requiring an understanding of the physical processes on the atomic scale. These processes can be investigated by atomic or molecular junctions, where only a few atoms or molecules provide the connection between two electrodes. Since the electrical conductance of the whole system is dominated by this small number of atoms or molecules, one can learn about the physical phenomena on the (sub-)nanometer scale. Quantum tunneling, (local) phonon heating, electron-phonon coupling and electromigration (related to the force of electrons on the metal ions), form just a few intriguing examples.

For this thesis, electronic conductance measurements are performed on atomically sharp electrodes, fabricated by so called mechanically controllable break junctions. Such electrodes are created by pulling a metallic wire. For ductile materials, like gold, stretching such wires creates a neck of atoms at the weakest point of the wire. With further stretching, the wire breaks, resulting in two atomically sharp electrodes.

Such electrodes can be used to measure the mechanical and electrical properties of single atoms and/or molecules. For example, with our experimental setup we can control the electrode separation with an accuracy of 5 pm. This gives us the opportunity to investigate the mechanical properties of metallic wires, at electrode separations smaller than the size a single atom. As will be shown in this thesis, a detailed description can now be given of the adhesive forces between the apex atoms of the two electrodes.

Furthermore, measurements are presented on hydrogen molecules. The hydrogen molecule, as on of the most simple molecules in nature, can very well be used for understanding the role of molecular vibrations on the electrical properties of molecular junctions. As will be shown, by vibrationally exciting hydrogen molecules, a strong heating effect can be observed. Interestingly, this heating mechanism has some remarkable consequences. For example, a new type of memory is presented, based on molecular hydrogen. The operating voltage of the switch is simply given by the vibration frequency of the molecule. Hence, this thesis gives new physical insights in the mechanical properties and conductance properties of single atomic and molecular junctions.

Marius Trouwborst
Zürich, Switzerland, June 2008

Thesis Outline

Chapter 1. Basic concepts. (p. 1)

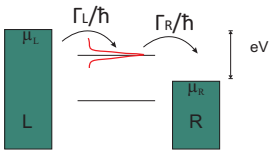

In the first chapter, we discuss the basic theoretical concepts in the research field of molecular electronics. Furthermore, typical conductance measurements are discussed on both atomic wires and molecular junctions.

Chapter 2. Experimental setup and techniques. (p. 27)

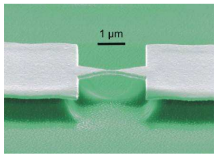

Most of the experimental work presented in this thesis, is done on a mechanically controllable break junction. In this chapter, the experimental setup is described in detail and characterized by typical conductance measurements.

Chapter 3. Calibration of lithographically defined break junctions. (p. 43)

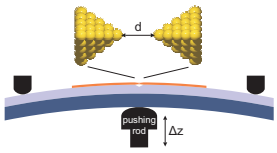

For understanding the experimental results, it is crucial to know the electrode separation. In this chapter, the calibration factor, or the ratio between the electrode separation and the bending of the substrate, is determined.

Chapter 4. Single atom adhesion in optimized gold nanojunctions. (p. 61)

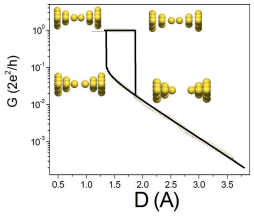

We present a "training" method to obtain atomically sharp electrodes, such that one can close and open the electrodes with perfect reproducibility. This way, we can model and calculate the elasticity of the electrodes, giving insight in the attractive forces on the atomic scale.

Chapter 5. Molecular heating in hydrogen-gold junctions. (p. 71)

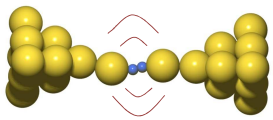

We measure the vibration spectra of molecular hydrogen, contacted in between two gold electrodes. Large hysteresis effects are observed, with response times up to 200 ms, which are explained by phonon heating of the contacted molecule(s).

Chapter 6. Switching with hydrogen molecules. (p. 93)

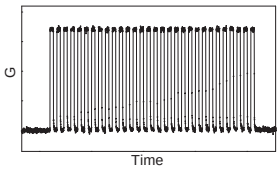

We demonstrate a new type of memory, based on molecular hydrogen in between two electrodes. The operating voltage of the switch is simply given by the vibration frequency of the molecule.

Chapter 7. Two level fluctuations in hydrogen covered nanogaps. (p. 101)

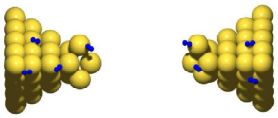

Here, gold nanogaps are investigated in the presence of molecular hydrogen. Two level fluctuations are observed, which can be understood by vibrationally induced hopping of the molecules in between two different positions.

Chapter 8. Joule heating in electromigration induced nanogaps. (p. 113)

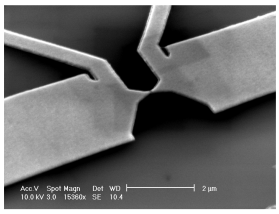

In the final chapter, we present our measurements on electromigration induced nanogaps. In particular, we show that Joule heating plays an crucial role in the electromigration process, which increases the mobility of the gold atoms.

Chapter 1

Basic concepts of the research field

Abstract

In this chapter, the basic concepts of electrical conductance in atomic and molecular junctions are discussed. Depending on the size of the contact, different regimes are expected. Electron tunneling and conductance quantization is explained together with characteristic measurements. Finally, we discuss how atomic or molecular levels and also vibrations can be observed in the measurements.

1.1 Conductance at the atomic scale

1.1.1 Semiclassical description

When considering a metallic wire of macroscopic dimensions, the electrical resistance of such a wire is simply given by Ohm's law. This relation states that the current through a wire (I), is proportional to the voltage over the wire (V), with 1/R as the proportionality constant (R is the resistance):

$$I = \frac{V}{R} \tag{1.1}$$

This relation was first found by Henry Cavendish in 1871, but named after Georg Ohm, who was the first to publish his experiments [1]. The existence of resistance is an important issue in daily life. For example, the resistance of a wire in a light bulb leads to lighting, or is used in heating systems, as described by Joule heating (given by I^2R). Interestingly, although these systems are of macroscopic size, the origin of resistance lies at the nanometer scale. Finally, it is all described by how easy electrons can move through a metallic conductor.

This can be explained by the following: Let us assume a metallic wire, at zero temperature, where the atoms are perfectly ordered in a lattice. When a voltage is applied over the wire, the electrons will be accelerated from one side of the wire to the other. In this hypothetical case, the electrons will not be hindered, leading to an infinite current through the wire. However, it is not possible to create such a wire. A metal will always have impurities or imperfections of the lattice. Hence, electrons can only travel a limited length, before they are scattered to these irregularities in the metal. This scattering always gives a nonzero resistance, leading to the relation described above.

We note here that scattering can actually occur in two ways: When energy is exchanged during the scattering process, one talks about inelastic scattering. This happens when electrons scatter with other electrons, or when electrons excite lattice vibrations (phonons). This process is responsible for macroscopic processes like heating. Besides inelastic scattering, elastic scatter events take place. In general, this refers to scattering with ions in the lattice. Since these ions have a much larger mass then the electron, no energy is transferred and the phase of the electron is conserved. We briefly state here that this process can result in conductance fluctuations; according to quantum mechanics, a moving electron can also be described as a wave. Due to elastic scattering, an electron can follow the same path for multiple times, without losing its phase information. Hence, this can result in destructive interference, which can have a large influence on the conductance properties of mesoscopic systems. Finally, we note that both quantities are described by length scales; the mean length the electron travels before scattered elastically (inelastically), is called the elastic (inelastic) scattering length.

This raises the interesting question about the conductance of a small constriction. When the dimensions of the constriction are smaller than the mean free path of the electron, Ohm's law can no longer be used. This problem was first investigated by Sharvin [2]. He considered two electron reservoirs, separated by a circular orifice (see Fig. 1.1). Since there is no scattering near the contact, all electrons moving in the right direction (with positive wavevector, $k_z > 0$) come from the left side of the contact, and vice versa. Hence, when a bias voltage is applied, the electrons at the left electrode will have a different energy than the electrons at the right electrode. Or, stated differently, in this case the right moving electron states will be occupied to an energy eV higher than the left moving states (as drawn in Fig. 1.1). Due to this imbalance, the number of electrons

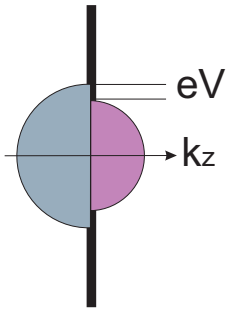

Figure 1.1: *Model for calculating the Sharvin resistance. For the model, an electron reservoir is assumed, separated by a small circular orifice (in between the two black lines). The electron energies in the two reservoirs are shifted by a bias voltage eV, leading to a current density j.*

moving in the right direction will be higher than the number of electrons moving in the left direction. When a constant voltage is applied, this imbalance leads to a net current density j:

$$j = e\langle v_z \rangle \rho(E_F) \cdot eV/2 \tag{1.2}$$

where e is the electron charge, $\langle v_z \rangle$ is the average velocity in the positive z direction (at E_F) and $\rho(E_F)/2$ is the density of states of these electrons (the factor 1/2 is since only 1 direction is considered). For free electrons, $\langle v_z \rangle = \hbar k_F/2m$ and $\rho(E_F) = mk_F/\pi^2\hbar^2$, leading to the following expression for the conductance through a circular orifice:

$$G_S = \frac{2e^2}{h}(\frac{k_F a}{2})^2 \tag{1.3}$$

where a is the contact radius, h is the Planck constant and k_F is the Fermi wave number. This is the famous formula for the so-called Sharvin conductance, which can be applied in the semiclassical regime. This is the regime where the constriction size is smaller than the mean scattering length, but much larger than the Fermi wavelength. At smaller constrictions, like the atomic wires used in this thesis, the wave character of the electrons start to be of importance.

1.2 Conductance quantization

1.2.1 Conductance in a ballistic channel

When the dimensions of the conductance channel are in the same order as the Fermi wavelength, one reaches the so-called quantum ballistic regime. Now, not all electron wavelengths are allowed, which thereby limits the conductance. This is schematically drawn in Fig. 1.2. Since the width of the channel W (and height H) has approximately the same size as the Fermi wavelength, only an half-integer number of wavelengths are allowed. Other wavelength cannot exist in this direction, due to interference (so called "destructive" interference). As shown below, this has dramatic consequences for the conductance of the wire. Let us assume a channel where the width W and height H are comparable to the Fermi wavelength λ_F, and the length L of the channel follows $L >> \lambda_F$.

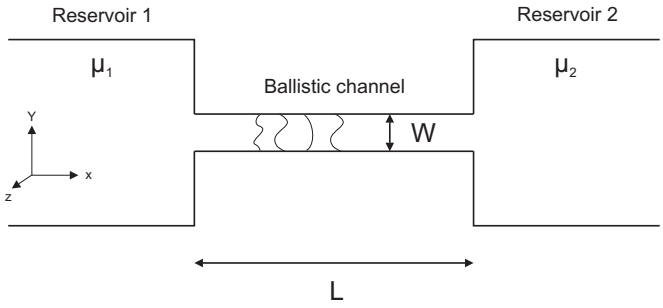

Figure 1.2: *Schematic drawing of a ballistic channel of length L, width W and height H. The electrons traversing this channel are confined in the y-direction and z-direction. Hence, only transversal wavelengths are allowed with $\lambda_y = 2W/j$ and $\lambda_z = 2H/j$, where j is an integer. The ballistic channel is connected on both sides to a reservoir with electrochemical potentials μ_1 and μ_2.*

To show the confinement of the transversal modes, we calculate the the local density of states of the electrons, within the channel. The time-independent Schrödinger equation is given by:

$$\frac{\hbar}{2m}\left(\frac{\partial^2}{\partial x^2}+\frac{\partial^2}{\partial y^2}+\frac{\partial^2}{\partial z^2}\right)\psi(x,y,z) = E\psi(x,y,z) \tag{1.4}$$

Using the general solution, $\psi(x,y,z) = e^{(ik_x x + ik_y y + ik_z z)}$, and for the total wave vector $k^2 = k_x^2 + k_y^2 + k_z^2$, we find for the wave vector:

$$k^2 = \left(\frac{n_x \pi}{L}\right)^2 + \left(\frac{n_y \pi}{W}\right)^2 + \left(\frac{n_z \pi}{H}\right)^2 \tag{1.5}$$

When assuming an infinitely long constriction ($L = \infty$), one obtains the following expression for the total electron energy inside the channel:

$$E_n(k) = \frac{\hbar^2 k^2}{2m} = \frac{\hbar^2}{2m}\left(k_x^2 + \left(\frac{n_y \pi}{W}\right)^2 + \left(\frac{n_z \pi}{H}\right)^2\right) \tag{1.6}$$

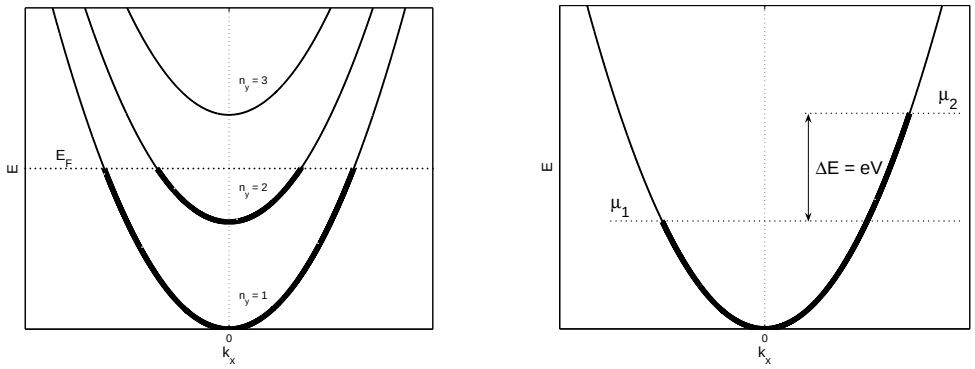

(a) Occupation of electron states for multiple energy modes n_y

(b) Occupation of electron states for single conducting mode with applied bias voltage

Figure 1.3: *Dispersion relations. (a) The parabolic shape of the curve is from the (free) longitudinal wave vectors, while the (quantized) shift in the y-direction is from the confined transversal modes (increasing in energy by a factor 1, 4, 9, ..). Here, two modes are filled up to the Fermi energy (dotted line). (b) Biased electron system with $\Delta E = \mu_2 - \mu_1$. Electrons with an energy between μ_1 and μ_2 contribute to the transport, and have positive wave numbers k_x. Note that, in practice, $eV << E_F$.*

Expression 1.6 shows that the energy and wave vector of an electron are quantized in the y-direction, while being continuous in the x-direction. The relation between energy and wave vector is called the dispersion relation and is drawn schematically in Fig. 1.3(a). All available k-states are filled up to the Fermi energy, indicated by the thick line. For the case shown in Fig. 1.3(a), only the modes $n_y = 1$ and $n_y = 2$ are relevant for electron transport through the system, since these have free electron states right above the Fermi energy.

Having calculated the electron energy, the conductance of a ballistic channel can now be evaluated. For a single dimension, the current through the channel is given by the product of the density of states and the velocity for all occupied states. This gives for a single dimension:

$$J_{n_y} = \frac{1}{2}\int_{\mu_1}^{\mu_2} v_{n_y}(E) D_{1D}(E) dE \tag{1.7}$$

where $v_{n_y}(E)$ is the electron velocity at a certain energy and mode n_y. Furthermore, μ_1 and μ_2 are the electrochemical potentials of the reservoirs 1 and 2, respectively. The factor 1/2 is introduced because only electrons with a positive k-vector are taken into account, as depicted in Fig. 1.3(b). The total particle current can then be calculated by summing over all occupied modes n_y:

$$J(\mu) = \sum_{n_y=1}^{N_{ymax}} \frac{1}{2}\int_{\mu_1}^{\mu_2} v_{n_y}(E) D_{1D}(E) dE = \sum_{n_y=1}^{N_{ymax}} \frac{1}{2}\int_{\mu_1}^{\mu_2} \sqrt{\frac{m}{2\hbar^2 E}}\sqrt{\frac{2E}{m^*}}\frac{g_s}{\pi} dE \tag{1.8}$$

where $N_{y_{max}}$ is the highest occupied mode. The current through the contact can now be evaluated (using $g_s = 2$ due to 2 spin states):

$$I = \sum_{n_y=1}^{N_{ymax}} -eJ_{n_y} = -N_{y_{max}}\frac{2e}{h}(\Delta\mu) = N_{y_{max}}\frac{2e^2}{h}V_{bias} \tag{1.9}$$

Or, in terms of conductance:

$$G = N_{y_{max}}\frac{2e^2}{h} \tag{1.10}$$

Expression 1.10 is the well-known result for ballistic transport, and crucial in the field of mesoscopic physics. It tells us that conductance is quantized, in integers of $2e^2/h$ (or 1/12.9 $k\Omega$). Note that in real contacts, some scattering can still occur. Therefore, the formula can be written in a more generalized way, leading to the famous formula as obtained by Landauer (and later more generalized by Büttiker) [6]:

$$G = N_{y_{max}}\frac{2e^2}{h}\sum_{n_y=1}^{N_{ymax}} T_n \tag{1.11}$$

where T_n is called the transmission probability, meaning the probability for a wave to reach the other side of the system ($0 \leq T_n \leq 1$). The existence of quantized conductance was demonstrated for the first time by van Wees *et al.* in 1988, and shortly after by Wharam *et al* [3, 4]. Here, a two dimensional electron gas (2DEG) was used to confine the electrons in two dimensions. By changing the electronic landscape using an electrostatic gate, the width of the channel was tuned from

0 to 360 nm. This resulted in a stepwise change in conductance, where in total 16 steps could be observed, each separated by $2e^2/h$. Actually, also in nanowires one has observed quantized conductance. However, an important difference is that a nanowire is a three dimensional structure (in contrast to a 2DEG). So for nanowires, the same confinement as in the y-direction, is also expected in the z direction. Finally, we note that the channels, as discussed for equation 1.11, have independent eigenstates. Hence, the transmissions in equation 1.11 actually depend on the energy, so that we can rewrite the relation as:

$$I = \frac{2e}{h} \int_0^\infty T(E)(f_l - f_r)dE \tag{1.12}$$

where f_l and f_r are the Fermi-Dirac distributions of the left and right electrode respectively.

1.3 Electron tunneling

In the previous section we discussed the conductance of strongly coupled systems which are confined in two directions, thereby creating an effective one-dimensional conductance channel. However, if we now break the contact, the transmission will be strongly suppressed. The electrodes are now separated by a vacuum gap, having a barrier height equal to the work function of the electrodes (5 eV for gold). Since the height of this barrier is much larger than the energy of the electrons, classically speaking, the electrons cannot cross the gap. However, since the width of the gap is relatively small, the electrons can still quantum mechanically tunnel through the barrier. To estimate the tunnel current, one can use a simplified energy diagram, by assuming a square potential barrier (see Fig. 1.4(a)):

$$V(x) = \begin{cases} 0 & \text{for } x < 0 \\ V_0 & \text{for } 0 < x < d \\ 0 & \text{for } x > d \end{cases}$$

Using this strongly simplified barrier, the Schrödinger equation can be solved in a straightforward manner:

$$-\frac{\hbar^2}{2m}\frac{d^2\psi(x)}{dx^2} + V_0\psi(x) = E\psi(x) \tag{1.13}$$

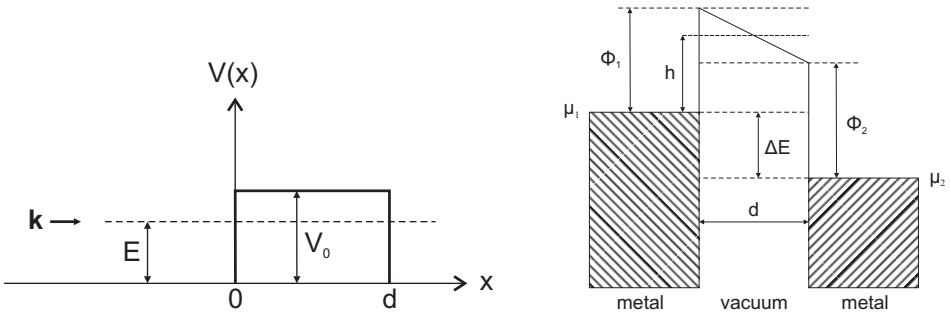

(a) Square potential barrier.

(b) Energy diagram with applied voltage.

Figure 1.4: *(a) Square barrier of width d and height V_0 (no bias voltage applied). An electron, with wave vector k and energy E, approaches the barrier. (b) Energy diagram for two metal surfaces, separated by a vacuum gap. When applying a bias voltage, the effective Fermi energy of the electrons get shifted for the left and right electrode. This energy is now given by the electrochemical potentials μ_1 and μ_2 for the left and right electrode respectively.*

Considering only $0 < E < V_0$ and using:

$$k = \frac{\sqrt{2mE}}{\hbar}, \qquad k' = \frac{\sqrt{2m(V_0 - E)}}{\hbar}$$

one finds three solutions to the Schrödinger equation, at the left of the barrier, in the barrier and at the right of the barrier:

$$\psi(x) = \begin{cases} e^{ikx} + (t_1 - 1)e^{-ikx} & \text{for } x < 0 \\ t_1 e^{-k'd}[e^{-k'(x-d)} + (t_2 - 1)e^{k'(x-d)}] & \text{for } 0 < x < d \\ t_1 t_2 e^{-k'd} e^{ik(x-d)} & \text{for } x > d \end{cases}$$

where t_1 and t_2 are the amplitude transmission coefficients for the transmission at 0 and at d, respectively. By satisfying the boundary conditions for continuity of $d\psi/dx$ and ψ at $x = 0$ and $x = d$ one finds:

$$t_1 = \frac{2k}{k + ik'}, \qquad t_2 = \frac{2ik'}{k + ik'}$$

Which results in the following approximation for the transmission probability T:

$$T = \left| t_1 t_2 e^{-k'd} \right|^2 \approx \frac{16E(V_0 - E)}{V_0^2} exp\left(\frac{-2d}{\hbar} \sqrt{2m(V_0 - E)} \right) \tag{1.14}$$

When a small bias voltage is applied (much smaller than the workfunction), the shape of the barrier does not rigorously change and the height of the barrier can be approximated by ϕ (see Fig. 1.4(b)). This results in the following relation for the tunnel conductance:

$$G = \frac{2e^2}{h}T = \frac{2e^2}{h}e^{-2\kappa d} \tag{1.15}$$

where $\kappa = \sqrt{2m\phi}/\hbar$.

We emphasize that this relation is only valid for small voltages. At higher voltages, one has to take into account the exact shape of the barrier, and the potential landscape in the region outside the barrier, as calculated by Simmons [5]. Nevertheless, for small voltages, Eq. 1.15 describes the experimental data remarkably well (as we will show in section 3.3.1). The main outcome of the formula, the exponential dependence of conductance on the gap distance, is an important result in the field of molecular electronics. Actually, this is the basic concept of the scanning tunneling microscope (STM), where one can visualize atoms and molecules on a surface. Note that the resolution of such a microscope is, in theory, not limited by the distance. In contrast to an ordinary optical microscope, with an STM one can in principle scan surfaces at a large distance away, with the same (atomic) resolution when scanning closer by. The only limit is set by the signal to noise ratio for measuring the conductance. In practice, tunneling currents can be measured down to 1 pA, and the maximum voltage which can be applied is around 1 V. Taking a typical value for κ, $1/\mathring{A}$, Eq. 1.15 gives 1 nm for the maximum working distance from the surface.

1.4 Conductance through single atoms

1.4.1 Theoretical background

In a 2DEG, the width of the channel can be carefully tuned [3]. In contrast, in metallic nanowires, the width of the constriction is proportional to the number of atoms in the contact. For a single gold atom contact, the diameter is 2.5 $\mathring{A}$, whereas the Fermi wavelength is about 2 $\mathring{A}$. Together with the fact that the level spacing in metal atoms is large (in the order of 1 eV), this indicates that only a small number of modes is present.

This is indeed the case, as can be shown by a self-consistent tight binding model (see Fig. 1.5). In fact, for gold, the net current flows through a single

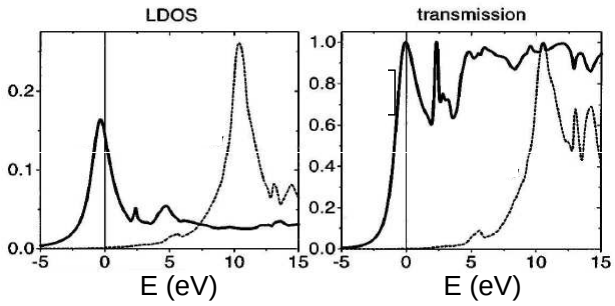

Figure 1.5: *Local density of states (left) and transmission (right) of a single gold atom contact, as a function of energy (in the ideal configuration). The solid line results from the 6s orbital, and the dotted line from the p orbital. The graphs are a direct result from a tight binding model. The vertical line denotes the position of the Fermi energy. Picture from Ref. 10.*

channel only. In many cases, the number of channels is determined by the chemical valence of the atoms [7]. This is exactly as expected, since these electrons interact with the electrons of the neighboring atoms, thereby creating conductance channels. The transmission of the channels strongly depends on the coupling of the atoms. It is found that, for noble metals like gold, silver and copper, the current is transferred through the s-orbital (at the Fermi energy). For these metals, the transmission of this orbital is nearly 1, as shown in Fig. 1.5.

1.4.2 Conductance histograms

The conductance of a single atom can be measured by recording so called conductance traces. An example of such a trace is given in the insert of Fig. 1.6. Here, the conductance is measured while breaking the wire. During pulling, the diameter of the contact decreases, leading to a decrease in conductance (for $G > 10\ G_0$, this behavior can be described by Sharvin's rule). Remarkably, the conductance does not decrease in a smooth way. Instead, sudden steps can be observed in the conductance. This is due to the fact that the minimum cross section of the wire is given by the number of gold atoms in the cross section, which decreases stepwise. Interestingly, around 1 G_0, a conductance plateau can be observed, just before the wire breaks. Since this is the minimum conductance value before breaking, this configuration can be attributed to the smallest possible crosse section: a single gold atom.

As investigated by Scheer *et al* [7], this conductance value indeed originates from a single conductance channel. This was shown by investigating the IV char-

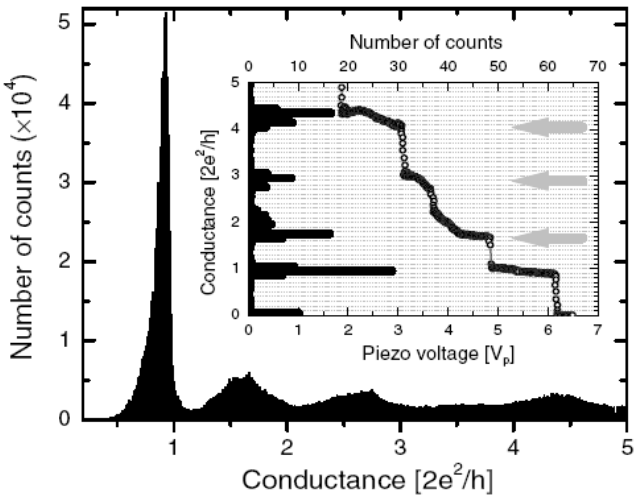

Figure 1.6: *Conductance histogram of Au, constructed from 2000 independent conductance traces while opening the contact. The number of counts correspond to how often a certain value for the conductance is measured. The inset shows an example of a single measurement trace, together with a histogram of this single trace.* $V_{bias} = 40\ mV$, *T=9K. Picture from Ref. 11.*

acteristics of a aluminum-gold contact at low temperatures (below 100 mK). Due to the so called proximity effect, at these low temperatures, the gold layer behaves as a superconductor. By measuring the Andreev reflection, the number of eigenchannels can be directly deduced by the IV characteristics of the contact. They observed a single mode, with transmission 1, for gold contacts with conductance 1 G_0. Later on, this result was confirmed using two different experimental methods. First, by investigating the noise spectrum of a quantum point contact (the so called "shot noise"), van den Brom *et al* found that the conductance of a single gold atom contact is carried by a single channel (with T=1) [8]. Second, Ludoph *et al* found that the conductance fluctuations have a minimum around an integer number of $2e^2/h$ [9]. This is as expected, since a fully transmitting channel has no conductance fluctuations. Furthermore, by investigating the amplitude of the fluctuations, they could derive a number for the elastic mean free path of the electrons. This was found to be in the order of 5 nm for a gold quantum point contact.

However, the conductance is not always exactly equal to 1 G_0, as can be directly observed from the conductance trace. In fact, the conductance slightly varies when stretching the contact. This is due to the fact that the conductance depends on the exact configuration of the electrodes. Backscattering of the

electrons, universal conductance fluctuations, or parallel tunneling paths lead to deviations from the perfect transmission. Therefore, each trace shows different fine structure. To average out these fluctuations, often many traces (typically >1000) are measured and collected in conductance histograms (see Fig. 1.6). These histograms are made by counting how many times a certain value of the conductance appears. Hence, the most frequently occurring conductance values will show up as a peak in the histogram. For gold, peaks close to 1,2 and 3 G_0 are always observed. Clearly, the peak at 1 G_0 has the highest weight. This behavior was studied by Yanson *et al*, where they discovered that the strong peak at 1 G_0 is related to the formation of so called atomic chains (as will be further discussed in the next section) [11]. Furthermore, they found that the peak at 1 G_0 is strongly asymmetric. This is exactly as expected when considering a single conductance channel. As discussed in the previous paragraph, scattering near the contact could give a transmission <1. However, a transmission >1 is not possible in a single mode. Therefore, when averaging over many traces, the conductance peak is only broadened towards lower conductances values, leading to an asymmetric peak.

Finally, we return to the discussion that the peak at 1 G_0 corresponds to a cross section of a single gold atom. This was shown by density functional calculations [17] and numerous experimental data [7, 16, 18, 19, 20, 21, 22]. In contrast, the peaks at higher conductance values (like the ones near 2 G_0 and 3 G_0), can not be simply attributed to two or three gold atoms, since also more modes with a lower transmission can add up and explain these conductance peaks in the histograms.

1.4.3 Atomic chains

As shortly mentioned in the previous section, the plateau around 1 G_0 is much longer than the plateaus at other conductance values. This effect is particularly visible in conductance histograms, like the one in Fig. 1.6. The peak around 1 G_0 is more than 10 times larger than the peaks at other conductance values. Remarkably, even though the contact has a cross section of only a single atom, this configuration can be stretched over a much longer distance than for any other configuration. This interesting effect was first observed in Leiden by J.M. Krans, and later extensively studied by Yanson *et al* [11]. They found plateaus around 1 G_0 of more than 20 $\AA$ long. Which is more than 8 times larger than the diameter of a single atom (2.5 $\AA$ for gold). These observations could only

be explained, when assuming the formation of *atomic chains*. When pulling an one atom contact between two gold electrodes, an atomic chain was created, with a cross section of a single atom. Since the conductance of such a chain is independent of the length of the chain (as explained in section 1.2), this gives a stable conductance around 1 G_0.

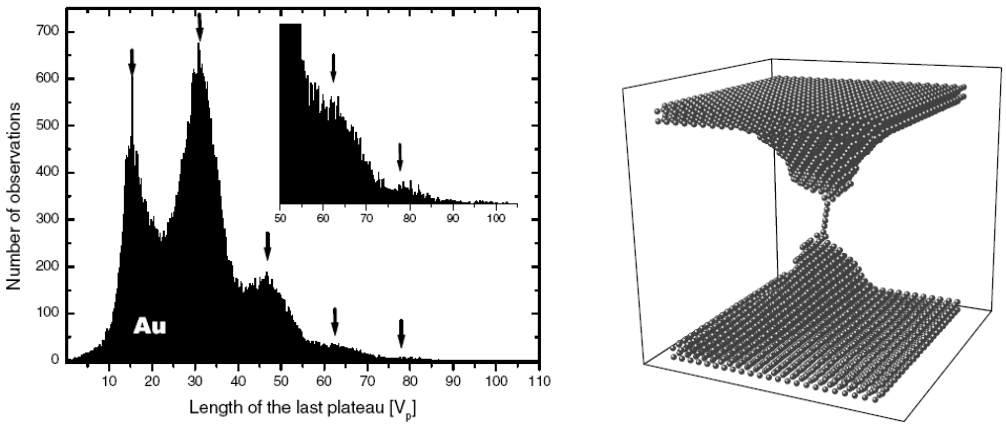

(a) Plateau length histogram (b) MD simulation

Figure 1.7: *(a) Histogram from the length of the plateau around 1 G_0, for 100.000 individual opening traces. T=4 K and the applied voltage is 10 mV. The spacing between the peaks is equal to 2.5 Å. Picture from Ref. 11. (b) Snapshot of a Molecular Dynamics simulation of stretching a Au nanowire along the [100] direction. Just before the wire breaks, an atomic chain is formed of 6 atoms long. T = 12 K. Picture from Ref. 14.*

That this picture is correct, was shown by Yanson *et al* [12]. They recorded many opening traces (≈100.000), and calculated for each trace the length of the plateau in between 0.5 and 1.1 G_0. When plotting the lengths of all these traces in a histogram, peaks were observed, at equidistant positions (see Fig. 1.7a). Interestingly, the distance between the peaks is equal to 2.5 $\mathring{A}$, or the diameter of a gold atom captured in an atomic chain [13]. This observation is consistent with the formation of chains before breaking: Just before the contact breaks, an atomic chain is created, consisting of an integer number of gold atoms.

The experimental results can also be simulated using a Molecular Dynamics simulation. An example is shown in Fig. 1.7b, as obtained by Sørensen *et al* [14]. Also here, atomic chains are observed, just before breaking. Using these simulations, one has found the origin of this remarkable phenomenon. This is related to the fact that the binding energy of the atoms is larger in an atomic

chain than in the bulk [15]. Hence, during the pulling of a contact, it can be energetically favorable for an atom to "participate" in an atomic chain, instead of breaking the atomic bond. This will be discussed in more detail in chapter 4. To conclude this section, we note that this phenomenon is not restricted to gold. Chain formation also occurs for metals like Pt and Ir and, less pronounced, Cu, Ag, Ni and Pd [15].

1.5 Conductance of molecular junctions

In the previous sections we discussed two different conductance regimes. When two electrodes are strongly coupled, one can observe conductance quantization. In contrast, when the electrodes are weakly coupled, resulting in a large barrier between the contacts, the electrons can only tunnel through the barrier.

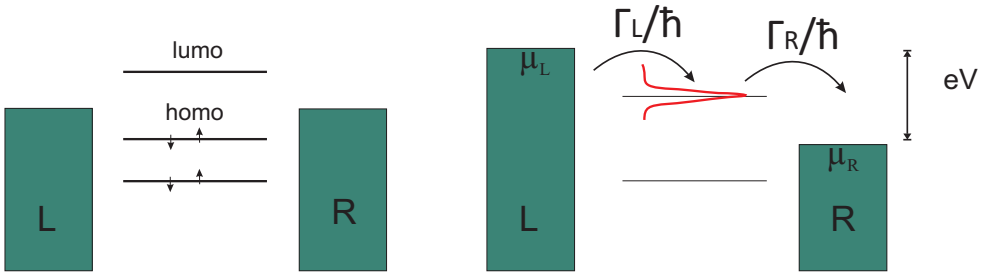

(a) molecular levels (b) molecular contact

Figure 1.8: *(a) Schematic drawing of a molecule, in between two electrodes, without coupling and bias voltage. (b) Drawing of a molecular contact at bias V. Due to the finite coupling* Γ*, the molecular level is broadened..*

When a molecule is contacted between two electrodes, the conductance is also strongly affected by the strength of the coupling. As will be discussed in this section, the coupling will lead to broadening of the molecular levels. We will first discuss the hypothetical case that there is no broadening. In this case, the energy diagram would look similar to the one drawn in Fig. 1.8(a). The molecular levels of the molecule lie at a well defined energy, where only the levels below the Fermi energy are occupied. The two levels above and below the Fermi energy are defined as follows: The highest occupied molecular level is called the HOMO, and the lowest unoccupied molecular level is called the LUMO. In this case, no current will flow, since the number of right flowing electrons is equal to the number of left flowing electrodes. This can change when a bias voltage is applied. As a result,

the maximum energy of the electrons in the right and left electrode get shifted (see Fig. 1.8(b)). This energy is called the electrochemical potential μ (at zero temperature). At a bias eV, the electrochemical potentials are $\mu_L = E_F + eV/2$ and $\mu_R = E_F - eV/2$ for the left and right electrode respectively. When the bias voltage is large enough, so that a molecular level lies in between the chemical potential of the two electrodes, a current will flow in between the two electrodes. This is due to an imbalance between the number of electrons on the left and right electrode. If we define the energy of the molecular level by ϵ, then the number of electrons with this energy depends on the temperature T and μ, and is given by the Fermi-Dirac distribution, $f(\epsilon, \mu) = \frac{1}{1+e^{\frac{\epsilon-\mu}{kT}}}$. Now, the number of electrons flowing from the left to the right is given by $2f(\epsilon, \mu_L)$, where the factor of two is from the spin degeneracy. And the number of electrons from right to left equals $2f(\epsilon, \mu_R)$. Due to the bias voltage, this number is different for both electrodes $(f\epsilon, \mu_R) < f(\epsilon, \mu_L)$. Which results in a net current flow. Note that only the levels which lie in between μ_L and μ_R, contribute to the current. For example, the lower level drawn in Fig. 1.8(b) does not contribute. Here, at this relatively low energy, all levels of the electrodes are filled ($f(\epsilon, \mu_L) = f(\epsilon, \mu_R) = 1$). Hence, there is no imbalance for this molecular level.

Till thus far, we assumed zero broadening of the molecular level. However, when a molecule is coupled to an electrode, a chemical bond will be created, between the molecule and the electrodes. In other words, a redistribution occurs of the charges or orbitals, a process which is called hybridization. This leads to broadening of the molecular levels. Actually, the stronger the coupling of the molecule to the electrode, the stronger the broadening. This is schematically drawn in Fig. 1.8, and is an important issue in molecular electronics. The coupling is defined by the parameters Γ_L and Γ_R for the coupling to the left and right lead respectively. Using these values, the broadening of the molecular level can be described by a Lorentzian-shaped density of states [29]

$$D(E) = \frac{\Gamma/2\pi}{(E-\epsilon)^2 + (\Gamma/2)^2} \tag{1.16}$$

where $\Gamma = \Gamma_L + \Gamma_R$ and ϵ is the energy of the molecular level (without broadening). Using this relation for the broadening, one can now calculate the total current through the molecule. This is done using the same arguments as used in the upper paragraph, only one should now integrate over the full energy range:

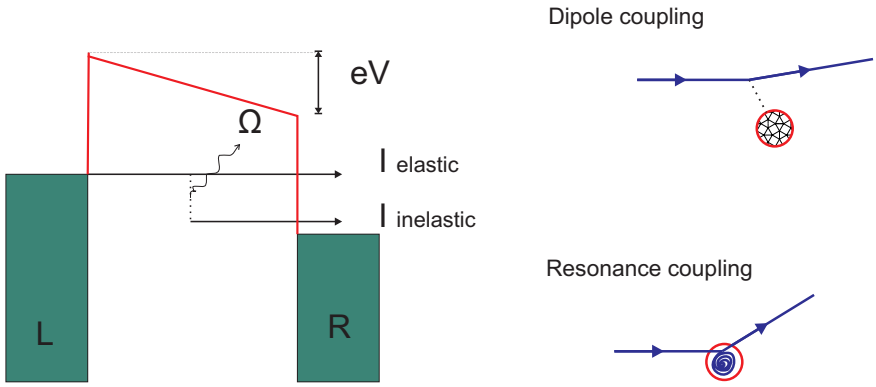

(a) Inelastic tunneling.

(b) Two limiting IETS processes

Figure 1.9: *(a) When the bias voltage exceeds the vibration energy Ω, an extra inelastic path is created. The electron loses energy, thereby exciting the molecule, before being injected into the right electrode. The total current is simply the sum of the elastic and inelastic current. (b) Two different cases of inelastic scattering. Top figure: Dipole scattering. Here, the momentum exchange is due to an approaching electron. Due to the induced electric field, the electron can exchange energy to the molecule. Which is then left behind in an higher vibrational mode. Lower figure: Resonance scattering. The electron is temporarily trapped in a molecular orbital. Only when the electron tunnels out the molecule, a molecular vibration is excited.*

$$I = \frac{2e}{\hbar}\frac{\Gamma_l\Gamma_r}{\Gamma_l+\Gamma_r}\int_0^\infty D(E)[f_l(E,\mu_l) - f_r(E,\mu_r)]dE \tag{1.17}$$

Which is the final result for the current through a molecular junction.

1.6 Vibrational levels in nano junctions

1.6.1 Inelastic electron tunneling spectroscopy

As introduced in section 1.1.1, even for ballistic contacts, electrons have a small probability of being scattered near the contact, thereby transferring energy to the molecule or atom in the contact (see Fig. 1.9(b)). Interestingly, this energy is often used to excite a vibration. When this occurs, an extra conductance path is created, where the electrons lose energy before being injected into the other electrode (as shown in Fig. 1.9(a)). Since this particular conductance path is

not present at lower voltages, ($| V | < \hbar\Omega$), a stepwise increase in the differential conductance can be observed, at $V = \pm\hbar\Omega$ (see Fig. 1.10(b)). In general, this step is in the order of 1 %. We note here that, in the case where the transmission is close to 1, a *decrease* instead of an increase is observed in the conductance, as will be discussed in the next section. Furthermore, we emphasize that the phonon excitation takes place at a certain energy. Hence, the position of the step in the dI/dV curves should be perfectly symmetric. This is independent of the coupling strength to the left and right lead. In contrast, a step in dI/dV due to an elastic current, can be asymmetric. This is an important signature of vibration excitations, and makes it possible to distinguish between vibrations and for example an increase in elastic current (see Fig. 1.10(a)). Hence, inelastic tunneling spectroscopy, often denoted as IETS, is a popular method in molecular electronics. The fact that one can indirectly observe the phonon spectrum of the specific molecule, is a strong tool for analyzing differential conductance spectra. Finally, we note that the drawings in Fig. 1.10 are simplified. More complicated structures can show up in the IV curves, as we will show in chapter 5.

1.6.2 Point contact spectroscopy

In the previous chapter we have shown that the opening of an inelastic conductance path, gives a stepwise increase in the differential conductance at $V = \pm\hbar\Omega$. However, this actually depends on the transmission of the channel. When the transmission is high, say close to 1, the differential conductance will show a stepwise *decrease* at $V = \pm\hbar\Omega$. This is related to the fact that, for high transmission, only electron states are available on the left electrode. This is shown schematically in Fig. 1.11. When the electron excites a molecular vibration, it will lose energy. However, all electron states with positive wave vector k_F, are occupied. Hence, the electron can only fall down to electron states with negative k_F vector. That is, the electron is scattered back to the electrode where it came from. Thus, the differential conductance will show a *decrease* in the conductance at $V = \pm\hbar\Omega$. This type of spectroscopy is called point contact spectroscopy (PCS). Note that the transition between PCS and IETS lies at a conductance of 0.5 G_0 [30].

The atomic chains, as discussed in section 1.4.3, are a model system for PCS measurements. As first shown by Agraït *et al*, steps in dI/dV can be observed at energies equal to the vibration mode [26]. In this case, they measured gold chains, and observed steps in dI/dV at 10 and 18 meV. They related these peaks to the transversal and longitudinal vibration modes of gold. Interestingly, one

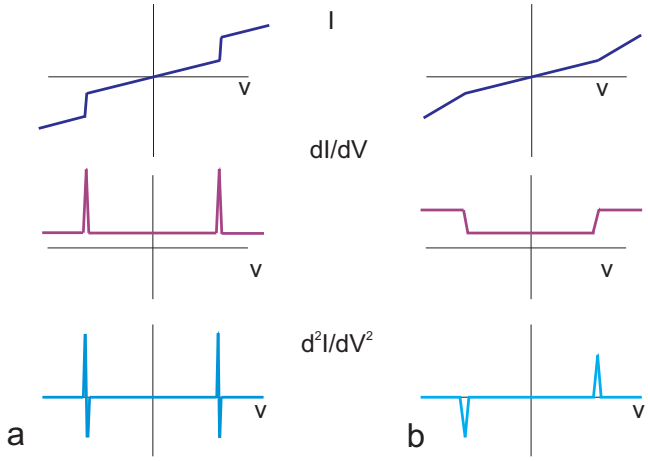

Figure 1.10: *Illustration of IV, dI/dV and d^2/dV^2, as a function of the voltage, when (a) a molecular level, or (b) an inelastic tunnel path is present. When an extra molecular level starts to participate, a step or spike in the current can be observed. In contrast, when a molecular vibration is induced, as shown in (b), a step can be observed in the differential conductance (here, $G < 0.5\ G_0$).*

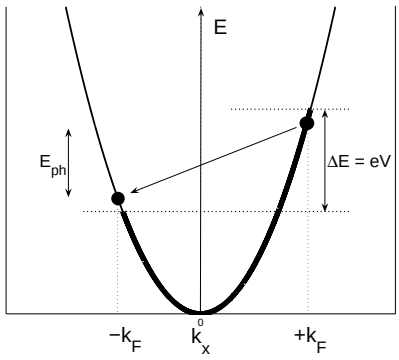

Figure 1.11: *Local density of states, under a bias voltage, assuming a single conductance channel. The thick line represents the occupied states. When an electron is scattered and thereby exciting a phonon, the electron releases energy equal to the phonon energy. Since only states at $-k_F$ are available, the electron is forced to scatter back away from the contact. This gives a decrease in conductance, at $V = V_{ph}$. Note that in practice, the voltage eV is much smaller than the Fermi energy.*

can directly compare these results with other methods, like electron energy loss spectroscopy (EELS). In Fig. 1.12, an example is shown of a neutron scattering and PCS measurement on gold. Clearly, both measurements lead to similar results, showing the gold phonons at 10 and 18 meV. Remarkably, at $V > 20$ meV, a flat background is still present, even though no more phonon modes are available. This is attributed to spontaneous emission of phonons, so that the phonon spectrum is not in thermal equilibrium [24].

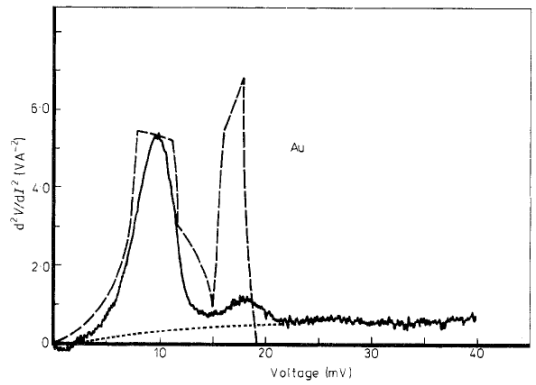

Figure 1.12: *Gold phonon spectra, as measured by PCS and neutron diffraction. Continuous line: d^2/dV^2 spectrum from gold contact with $R_0 = 3.3\Omega$ and $T = 1.2K$. Dashed line: phonon density of states, as measured by neutron diffraction. For the PCS data, the second peak is lower than the one obtained from neutron diffraction. This is due to the weaker coupling with the longitudinal phonons with PCS. Picture from Ref. 25.*

1.7 Conductance measurements on molecules

1.7.1 Vibrational levels of a single hydrogen molecule

In the previous section, we discussed how atomic vibrations can be observed in conductance measurements. However, when a molecule is contacted in between two electrodes, vibrations of the molecule can also be observed. In this section, we discuss the measurements on molecular hydrogen. Thanks to the simplicity of the molecule, hydrogen has become a model system, both for theoretical and experimental work. We start the discussion with the remarkable results of Smit *et al* [27]. Here, they contacted a (single) hydrogen molecule in between two Pt electrodes. and used PCS to identify the molecule. As expected, they observed a

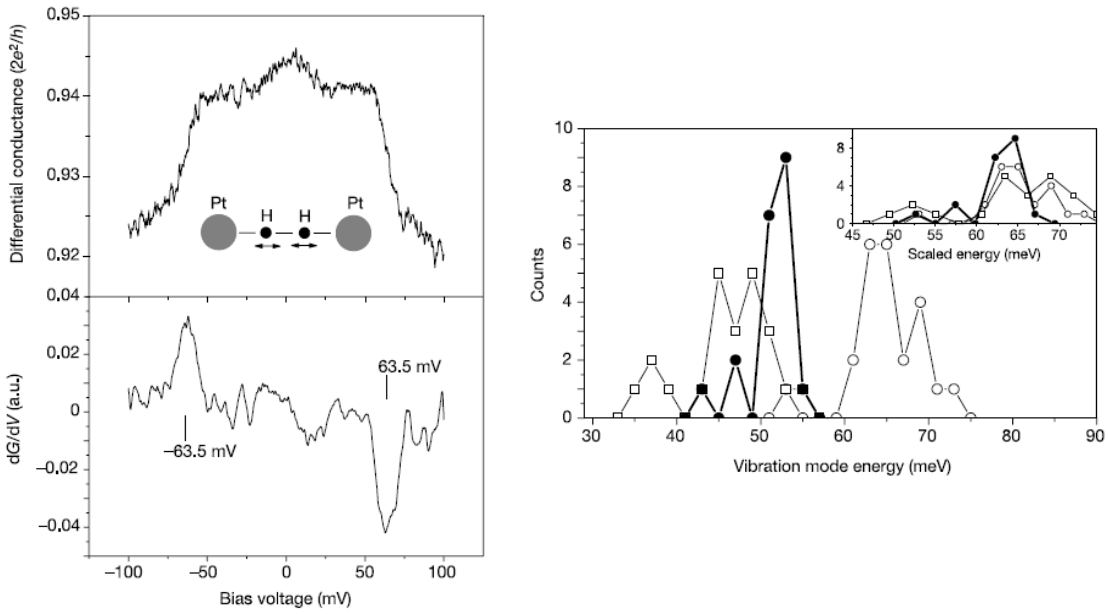

Figure 1.13: *(Left) Differential conductance of a Pt/H_2 contact, and, below, its numerical derivative. At 63.5 meV, the vibration of the hydrogen molecule is excited, leading to a decrease in the conductance at $V = \pm\hbar\Omega$. (Right) Distribution of vibration energies for various point contacts on Pt/H_2 (open circles), Pt/D_2 (open squares) and Pt/HD (filled circles). Inset: the same data with the energy axis scaled by the factors expected for the isotope shifts of the hydrogen molecule, $\omega_{H_2}/\omega_{D_2} \propto \sqrt{m_{D_2}/m_{H_2}} = \sqrt{2} \approx 1.414$ (open squares) and $\omega_{H_2}/\omega_{HD} \propto \sqrt{m_{HD}/m_{H_2}} = \sqrt{3/2} \approx 1.225$ (filled circles). Picture from Ref. 27.*

decrease in conductance, around the vibration frequency of the H_2 molecule (see Fig. 1.13). Interestingly, by repeating the measurements on H_2 isotopes, they observed a shift in this vibration energy. Since the vibration frequency scales with the mass of the molecule, $\Omega \propto \sqrt{k/m}$, one expects a $\sqrt{2}$ difference in energy, when the mass m is doubled. Indeed, measurements on H_2, D_2 and HD perfectly scaled with the mass. Secondly, they found a zero-bias conductance of a single hydrogen molecule to be nearly $2e^2/h$. At that time, this was an unexpected high conductance for the molecule. Later on, DFT calculations showed that H_2 could strongly hybridize with the Pt electrodes, leading to an transmission close to 1 [28]. This was one of the first results showing the importance of the coupling and broadening of the molecule, when connected to two electrodes.

After the first publication of these PCS measurements, numerous measurements followed on H_2, D_2 and HD, revealing more exciting results on these simple

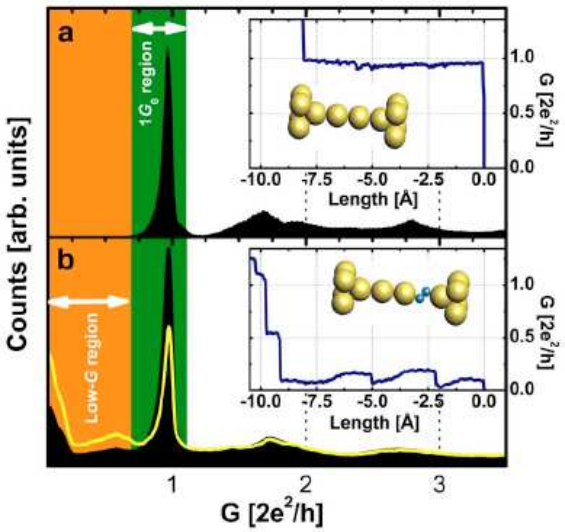

Figure 1.14: *Upper picture: typical pulling trace of a gold nanowire. A plateau can be observed around 1 G_0, after which the contact breaks. Lower picture; Pulling trace of a gold nanowire in a H_2 environment. Here, long conductance plateaus can be observed, in between 0.05 and 0.7 G_0. Remarkably, for a large part of the trace, the conductance increases, as a function of distance. This is attributed to the formation of atomic chains, with hydrogen incorporated within the chain. Picture from Ref. 32.*

molecules. For example, again using PCS, three different vibration modes can be distinguished, as measured by Djukic *et al* [31]. By studying the stretching dependency of the vibration energies,they could ascribe all vibration modes, to the exact nature of the vibration. Furthermore, Csonka *et al* observed that the binding of $Au - H_2$ can be as strong as the Au-Au bond. Hence, the hydrogen clamp is strong enough to pull a chain of gold atoms (as drawn schematically in the lower inset of Fig. 1.14). Which then results in long conductance plateaus in between 0.05 and 0.7 G_0. Note the remarkable shape of these plateaus: The conductance first increases, even though the contact is stretched. Only after $\pm$ 2.5 $\AA$, the conductance suddenly drops. This behavior can be explained by considering atomic chains, with one or more H_2 molecules incorporated. When pulling such a contact, the hydrogen molecule is first stretched. As calculated by Barnett *et al*, this gives a higher conductance [33]. When fully stretched, the forces overcome the binding forces of the gold atoms, and an extra gold atom hops into the atomic chain.

Finally, we note that we have performed spectroscopy measurements on this

system. Remarkable hysteresis effects appear, as will be presented in chapter 5.

1.8 Functional molecules

Although many details in the field of molecular electronics are not yet understood, there have been some great achievements in the past years. Organic chemists have created a variety of interesting molecules, some of which can switch between two conductive states. The switching is done using a voltage pulse (redox switches), or using light (photochromic switches), which is clearly getting close to future applications. An example of an interesting molecular system, are the diarylethene switches. In solution, these molecules can be switched reversibly between a high and a low conductive state, using light of different frequencies. However, also when grafted on a gold surface, these molecules retain their switching properties [34, 35]. This was shown in Groningen, and is presented in Fig. 1.15 [34]. The molecule which was used is shown in Fig. 1.15(a). It consists of a switching unit, which is coupled to the gold by a thiol unit. Thiols are known to form a chemical bond with gold, and are often used in molecular electronics as the "alligator clip", for the binding between molecule and electrode. The molecular system was investigated by STM and UV-VIS spectroscopy. As expected, the molecules can be switched from the ON state to the OFF state, by applying light of different wavelengths. For the STM, the molecule in the ON state, has a higher conductance than its environment, and will therefore show a white spot in the STM graph (Fig. 1.15(b)). Regarding the UV-VIS spectroscopy, the transmission of the molecules depends on their conductance state. Hence, a clear difference was observed in the transmission spectra, between the two different states of the molecule.

It is interesting to note that this result was actually a follow up of an earlier study on very similar molecules. Here, the only difference between the molecules was that the end group was a thiophene ring instead of a benzene ring. So two carbon atoms were replaced by a sulphur atom. Interestingly, although these molecules could also switch reversibly in solution, the switching was prohibited when grafted on gold [36]. Dulic *et al* showed that this molecule could only switch one way, from the ON to the OFF state. The other direction was quenched, due to the presence of the gold, as was shown by both UV-vis spectroscopy and electrical measurements. Consequently, the results of Dulic *et al* could be explained by the stronger coupling of the thiophene unit to the gold, in comparison with the benzene ring. Hence, replacing a single atom in a relatively large molecule, can

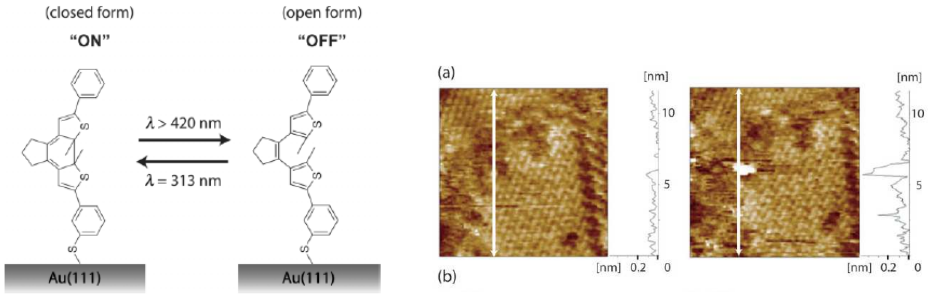

(a) Diarylethene switch (b) SEM graph of the switch in both states

Figure 1.15: *(a) Diarylethene switch, grafted on Au using a thiol bond. By applying light of 313 nm, the molecule switches to the high conductive state. The molecule can be switched back to the ON state, using light of 420 nm. (b) Reversible switching, as shown using an scanning tunneling microscope. The white spot, corresponding to a high current state, shows the molecule in the ON state (right picture). After the exposure to light of >420 nm., the molecule is in the OFF state (left picture). Pictures from Ref. 34 .*

have a dramatic influence on its electrical properties. This was one of the first examples showing the importance of the anchor group, for the properties of the molecule.

References

[1] Electricity, Encyclopedia Britannica (1911).

[2] Y.V. Sharvin, Zh. Eksp. Teor. Fiz. **48**, 10369 (1965).

[3] B.J. van Wees, H. van Houten, C.W.J. Beenakker, J.G. Williamson, L.P. Kouwenhoven, D. van der Marel and C.T. Foxon, Phys. Rev. Lett. **60**, 848 (1988).

[4] D.A. Wharam, T.J. Thornton, R. Newbury, M. Pepper, H. Ahmed, J.E.F. Frost, D.G. Hasko, D.C. Peacock, D.A. Ritchie and G.A.C. Jones, J. Phys. C **21**, L209 (1988).

[5] J.G. Simmons, J. Appl. Phys. **34**, 6 (1963).

[6] R. Landauer, IBM J. Res. Dev. **1**, 223 (1957); M. Büttiker, Phys. Rev. Lett. **57**, 1761 (1986).

[7] E. Scheer, N. Agraït, J.C. Cuevas, A.L. Yeyati, B. Ludoph, A. Martín-Rodero,

G. Rubio Bollinger, J.M. van Ruitenbeek and C. Urbina, Nature **394**, 154-157 (1998).

[8] H.E. van den Brom and J. M. van Ruitenbeek. Phys. Rev. Lett. **82**, 1526 (1999).

[9] B. Ludoph, M. H. Devoret, D. Esteve, C. Urbina, and J. M. van Ruitenbeek. Phys. Rev. Lett. **82**, 1530 (1999).

[10] J. C. Cuevas, A. Levy Yeyati, A. Martin-Rodero, G. Rubio Bollinger, C. Untiedt, and N. Agraït, Phys. Rev. Lett. **81**, 2990 (1998).

[11] A.I. Yanson, PhD thesis, Leiden University 2001.

[12] A.I. Yanson, G. Rubio Bollinger, H.E. van den Brom, N. Agraït and J.M. van Ruitenbeek, Nature **395**, 783 (1998).

[13] C. Untiedt, A.I. Yanson, R. Grande, G. Rubio-Bollinger, N. Agraït, S. Vieira and J.M. van Ruitenbeek, Phys. Rev. B **66**, 085418 (2002).

[14] M. R. Sørensen, M. Brandbyge and K. W. Jacobsen, Phys. Rev. B **57**, 3283 (1998).

[15] S.R. Bahn and K.W. Jacobsen, Phys. Rev. Lett. **87**, 266101 (2001).

[16] H. Ohnishi, Y. Kondo, and K. Takayanagi, Nature **395**, 780 (1998).

[17] M. Brandbyge, M. R. Sørensen, and K. W. Jacobsen, Phys. Rev. B **56**, 14956 (1997).

[18] J. M. Krans, C. J. Muller, I. K. Yanson, T. C. M. Govaert, R. Hesper, and J. M. van Ruitenbeek, Phys. Rev. B **48**, 14721 (1993).

[19] N. Agraït, J. G. Rodrigo, and S. Vieira Phys. Rev. B **47**, 12345 (1993).

[20] L. Olesen, E. Lægsgaard, I. Stensgaard, F. Besenbacher, J. Schitz, P. Stoltze, K. W. Jacobsen, and J. K. Nørskov, Phys. Rev. Lett. **72**, 2251 (1994).

[21] J. M. Krans, J. M. van Ruitenbeek, V. V. Fisun, I. K. Yanson, and L. J. de Jongh, Nature **375**, 767 (1995).

[22] M. Brandbyge, J. Schiøtz, M. R. Sørensen, P. Stoltze, K. W. Jacobsen, J. K. Nørskov, L. Olesen, E. Lægsgaard, I. Stensgaard, and F. Besenbacher, Phys. Rev. B **52** 8499 (1995).

[23] W.H.A. Thijssen, PhD thesis, Leiden University 2007.

[24] B.N.J. Persson, Physica Scripta **38**, 282 (1988).

[25] A.G.M. Jansen, A.P. van Gelder and P. Wyder, J. Phys. C: Solid St. Phys. **13**, 6073 (1980).

[26] N. Agraït, C. Untiedt, G. Rubio-Bollinger and S. Vieir, Phys. Rev. Lett. **21**, 216803 (2002)

[27] R.H.M. Smit, Y. Noat, C. Untiedt, N.D. Lang, M.C. van Hemert, J.M. van Ruitenbeek, Nature **419**, 906 (2002).

[28] K.S. Thygesen and K.W. Jabobsen, Phys. Rev. Lett. **94**, 36807 (2005).

[29] S. Datta, Quantum Transport: Atom to Transistor, Cambridge university press (2005).

[30] O. Tal, M. Krieger, B. Leerink and J.M. van Ruitenbeek, Phys. Rev. Lett. **100** 196804 (2008).

[31] D. Djukic, K.S. Thygesen, C. Untiedt, R.H.M. Smit, K.W. Jacobsen and J.M. van Ruitenbeek, Phys. Rev. B. **71**, 161402 (2005).

[32] Sz. Csonka, A. Halbritter and G. Mihály, Phys. Rev. B **73**, 75405 (2006).

[33] R.N. Barnett, H. Hakkinen, A.G. Scherbakov and U. Landman, Nano Lett. **4**, 1485 (2004).

[34] N. Katsonis, T. Kudernac, M. Walko, S.J. van der Molen, B.J. van Wees and B.L. Feringa, Adv. Mater. **18**, 1397 (2006).

[35] J. He, F. Chen, P. A. Liddell, J. Andrasson, S. D. Straight, D. Gust, T. A. Moore, A. L. Moore, J. Li, O. F. Sankey and S. M. Lindsay, Nanotechnology **16**, 695 (2005).

[36] D. Dulic, S. J. van der Molen, T. Kudernac, H. T. Jonkman, J. J. D. de Jong, T. N. Bowden, J. van Esch, B. L. Feringa and B. J. van Wees, Phys. Rev. Lett. **91**, 207402 (2003).

Chapter 2

Experimental setup and techniques

Abstract

In this chapter, a description is given of the experimental setup which is used for the measurements on the gold nanowires. Furthermore, a brief overview is given concerning the fabrication of lithographically defined break junctions. Finally, typical measurements are shown and discussed, like the conductance in and out of contact, and the drift of the setup.

2.1 Mechanically controllable break junction technique

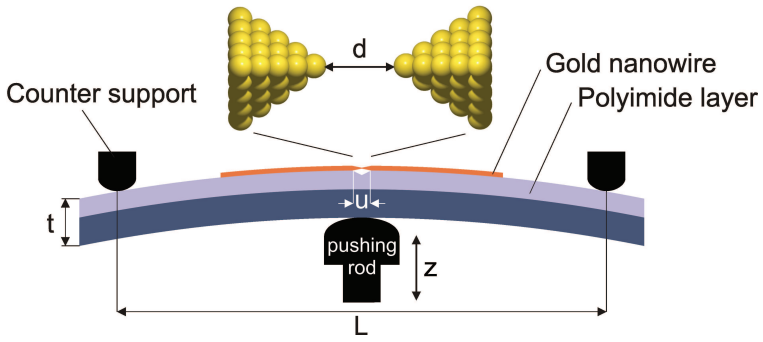

Figure 2.1: *Schematic drawing of the break junction, in 3 point bending mechanism.*

In the 1980's, Moreland and coworkers studied the tunnel characteristics of superconductors. However, to measure these currents in small wires, a method was needed to create atomic sized tunnel contacts, with a stability higher than

the Scanning Tunneling Microscopes available at that time. For this purpose, Moreland *et al* developed the break junction technique [1]. Here, they put a thin wire of a superconductor material, in between two glass plates, to study the tunneling characteristics . Later on, modifications were made in Leiden (and partly in Saclay) by Van Ruitenbeek, Muller and Krans *et al*, leading to the Mechanically Controllable Break Junctions (MCBJ) as we know them today [31, 3]. Basically, they consist of a flexible substrate, on top of which a metal wire is attached (as drawn schematically in Fig. 2.1). In the center of the substrate, the wire has a constriction and is made free hanging. Below this constriction, a pushing rod can give a vertical displacement ΔZ, which leads to bending of the substrate. As a result of this bending, the wire will be stretched in the horizontal direction, finally leading to breaking of the wire near the constriction. After breakage, the distance between the electrodes, Δd, varies proportional to the displacement of the pushing rod. However, as we will show, the displacement of the electrodes is strongly reduced by the use of the relatively large substrate. The reduction factor, or attenuation factor, r, is given by [3, 11]:

$$r = \frac{\Delta d}{\Delta z} = \frac{6tu}{L^2} \cdot \zeta \tag{2.1}$$

where t is the thickness of the substrate, u the length of the constricted area and L the distance between the two counter supports. Finally, the relation has to be multiplied with a correction factor, ζ, which depends on the exact sample design (for our samples, ζ equals 2.6). This factor is due to the softness of the polyimide layer, and will be discussed in the next chapter. For our MCBJ samples, the dimensions are as follows: $t = 0.42$ mm, $u = 2.4$ μm and $L = 18.8$ mm. This leads to a -corrected- attenuation factor of $r \approx 4.4 \cdot 10^{-5}$. One can now immediately see the impressive resolution of the break junction. By displacing the pushing rod with 0.1 μm, the electrode separation changes by only 4.4 pm. This value can be compared with the diameter of a gold atom (2.5 $\mathring{A}$). Hence, a single gold atom is more than 50 times larger than the spatial resolution of our break junctions.

Different types of break junctions

Before discussing the sample fabrication, we note here that there are actually two types of break junctions. Mostly used are the so called "notched wire" break junctions. Here, polycrystalline wires are used with a typical diameter of 20 to 100 μm. These wires (often after annealing) are then placed and glued on the

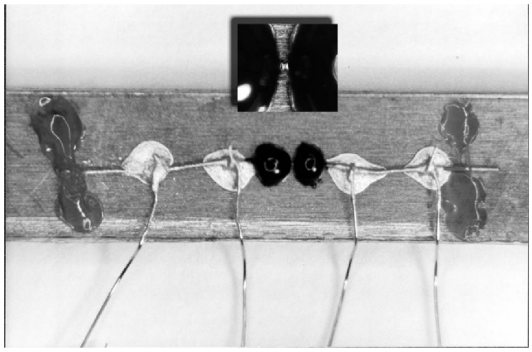

Figure 2.2: *Photograph, made by an optical microscope, of a "notched wire" break junction, as used in the pioneering work of Van Ruitenbeek et al and Muller et al (top view). The horizontal wire is the gold wire, attached to the substrate by 4 dots of epoxy glue (black). For the connections to the electronics, four wires are attached using silver paint. The width of the substrate is 4.5 mm. Picture from Ref. 5*

substrate with an epoxy glue. Finally, to create the constriction in the middle of the wire, a notch is created. This is done by carefully cutting the wire with the help of a sharp blade. After the notch is made, the sample is ready for the measurements (see Fig. 2.2). The other type of break junctions are the so called lithographically defined fabricated break junctions, and are the ones we have used for our experiments. Here, the wire is defined using electron beam lithography, and is thermally evaporated onto the substrate (to be explained in the next paragraph). Another difference between the two types, is the larger attenuation factor for the "notched wire" break junctions. In general, this factor is 100 times larger than the value for the lithographically defined junctions. Furthermore, lithographically fabricated junctions are often driven by a motor, while the "notched wire" junctions are driven by a piezo stack. Although both type of junctions can be used for the same measurements, each type has its own advantages. In general, the lithographically defined break junctions are less sensitive to vibrations and have a negligible drift (as discussed in section 2.6.3). On the other hand, the notched wire break junctions can be closed and opened in a shorter time scale, and are therefore more suitable for statistical measurements, when a large number of traces is needed for averaging.

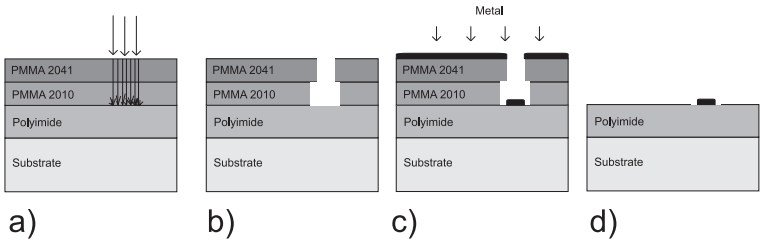

Figure 2.3: *Schematic layout of the electron beam lithography process. a) After spin coating 2 PMMA layers on the substrate, the layers are exposed by the electron beam, according to a pre defined pattern. b) After development, the exposed part is dissolved, leaving a mask on top of the substrate. c) Gold evaporation. Since the two PMMA layers have a different molecular weight, the bottom layer is more affected, resulting in a thin evaporation mask. This gives a sharp gold strip in the middle. d) Finally, the lift off process. The sample is put in heated aceton, thereby removing all the PMMA, leaving only the gold nanowire.*

2.2 Sample fabrication

The fabrication of a lithographically defined break junction is a many-step process, and is briefly described below (a more detailed description is given in the appendix):

1. One starts by cutting a phosphor bronze plate into small substrates (22.5 x 10.2 x 0.5 mm). Subsequently, these substrates are flattened using a polishing machine. This process is repeated on 4 different polishing papers, where the final one has a grain size of 1 μm.

2. After carefully cleaning, the sample is spin-coated with pyrralin polyimide (HD MicroSystems) such that a smooth insulating top layer is formed with a thickness of around 3 μm. To increase its elastic properties at cryogenic temperatures, the layer is cured for 30 minutes at 300 ° C.

3. For the electron beam lithography process, two PMMA resist layers are spin-coated and baked. Next, the desired pattern is exposed using standard electron-beam lithography (see Fig. 2.3). The used pattern consists of two thin wires (500 x 100 nm) positioned in the middle of the substrate, connected with a larger pattern to the contact pads. After development, the exposed pattern dissolves, making it ready for metal deposition.

4. Metal deposition, by thermally evaporating 120 nm Au, in a cryo-pumped system, at a back pressure of 10^{-7} mbar. To improve the sticking of the gold

to the polyimide a 1 nm chromium adhesion layer is used. Subsequently, we perform lift-off in heated acetone. This removes the PMMA, leaving a well defined gold wire on the substrate.

5. Finally, the central constriction is made free-hanging by Reactive Ion Etching with an O_2/CF_4 plasma. This etching procedure only affects the polyimide layer, and we stop after etching ≈600 nm. The final result is shown in Fig. 2.4.

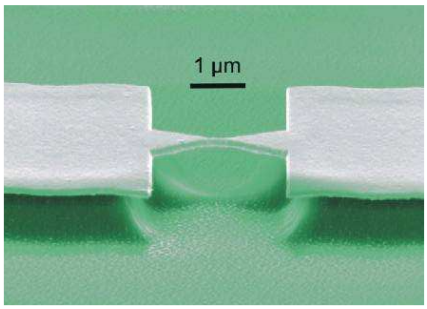

Figure 2.4: *Scanning electron micrograph of break junction. One can observe the free hanging gold bridge, on top of the polyimide layer.*

2.3 The insert

For the bending of the substrate at cryogenic temperatures, the junction is mounted into a specially designed insert (see Fig. 2.5) [6]. The lower part of the insert, called the sample chamber, can be submerged in a vessel with liquid helium, such that the temperature can be lowered down to ≈4 K. The upper part of the insert is called the socket head and is kept at room temperature.

The MCBJ sample can be bent by the movement of the pushing rod. The pushing rod is situated directly underneath the sample and can be displaced by a brushless motor (Faulhaber). This motor is controlled by the computer, using the serial port of the PC and a motion controller. However, between the motor and pushing rod, a bronze/stainless steel differential screw is used to make slow movements possible and, secondly, to convert the rotational motion of the motor into vertical displacement of the rod (depicted in Fig. 2.5b). We note here that the screws are smeared with carbon powder, for a smoother rotation. Furthermore, the effective pitch of the differential screw is 100 μm per turn with

a maximum of 30 turns. Hence, by using a gearbox (1:246) and a motor with high positional resolution we obtain sub-micrometer resolution in the pushing rod position z. The pushing rod can be moved with a speed which can be varied between 0.01 μm s^{-1} and 5 μm s^{-1}.

Before cooling the sample chamber to liquid helium temperature, the interior of the dipstick is pumped to avoid contamination on the sample surface. We use a turbomolecular pump and the minimum pressure that can be reached is approximately $1 \cdot 10^{-6}$ mbar. After cooling, the cryopumping effect gives a ultra high vacuum inside the sample chamber ($< 10^{-9}$ mbar). The cryopumping effect can be further enhanced by increasing the surface area of the interior of the sample chamber. This was done by placing a small volume (± 5 cm^3) of Norit activated carbon on the bottom of the sample chamber. This is especially to get rid of impurities when doing long during experiments ($\approx$ weeks). An example of such impurities is the presence of hydrogen. Since hydrogen has a high vapor pressure, even at 4.2 K ($\approx 10^{-6}$ mbar), it is one of the few elements which is not being immediately frozen to the walls of the insert.

2.4 The electronics

Data acquisition and voltage sources

Much effort has been put into optimizing the electronics. Basically, all measurements are done two terminally, by biasing the voltage while measuring the current. The setup is drawn schematically in Figure 2.6, of which the main part is the home built VI measurement system. This system decouples the voltage source from the mains voltage, using a 9V battery (often called a "floating" voltage source). This gives a more stable voltage signal to the sample, less affected by voltage spikes. Second, an IV convertor transfers the current, from the sample, into a voltage. Both the voltage applied and current measured are done relative to a reference wire, which follows the same path as the sample wires. This wire is then grounded at a single grounding point, thereby avoiding the occurrence of any ground loops. Furthermore, any electrical noise picked up by the sample wires, is also picked up by the reference wire, and will therefore not show up in the measurements.

The conductance is measured using a National Instruments Data Acquisition Card (DAQ-6221). This card is directly inserted into a PCI-slot of the computer, and transfers the analog signal from the IV convertor, into a 16 bits digital signal.

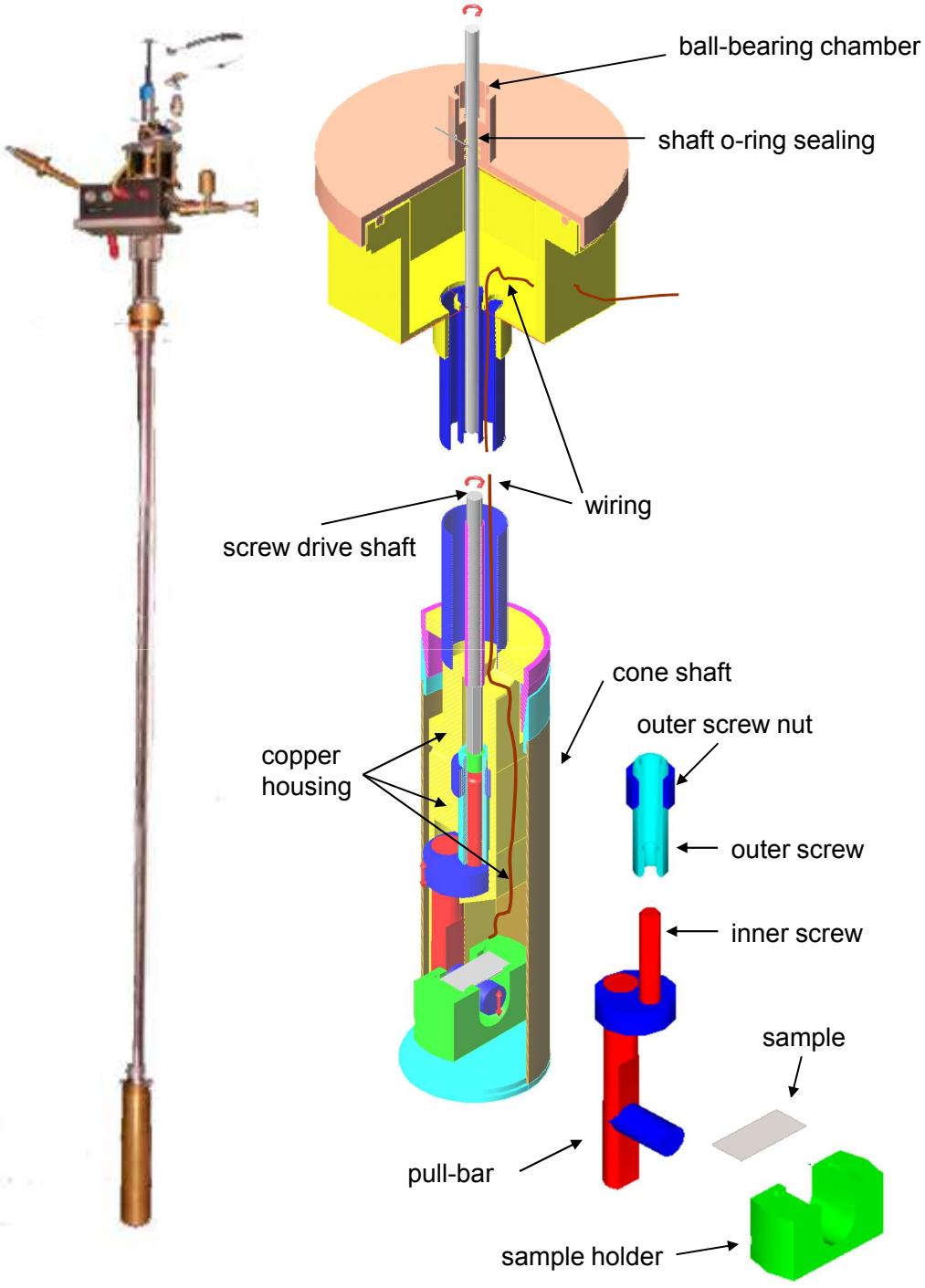

Figure 2.5: *Left: picture of the insert, including the brushless motor (on top) and the vacuum can (below). Right: schematic drawing of the interior of the insert. Below, the different parts of the differential screw are shown.*

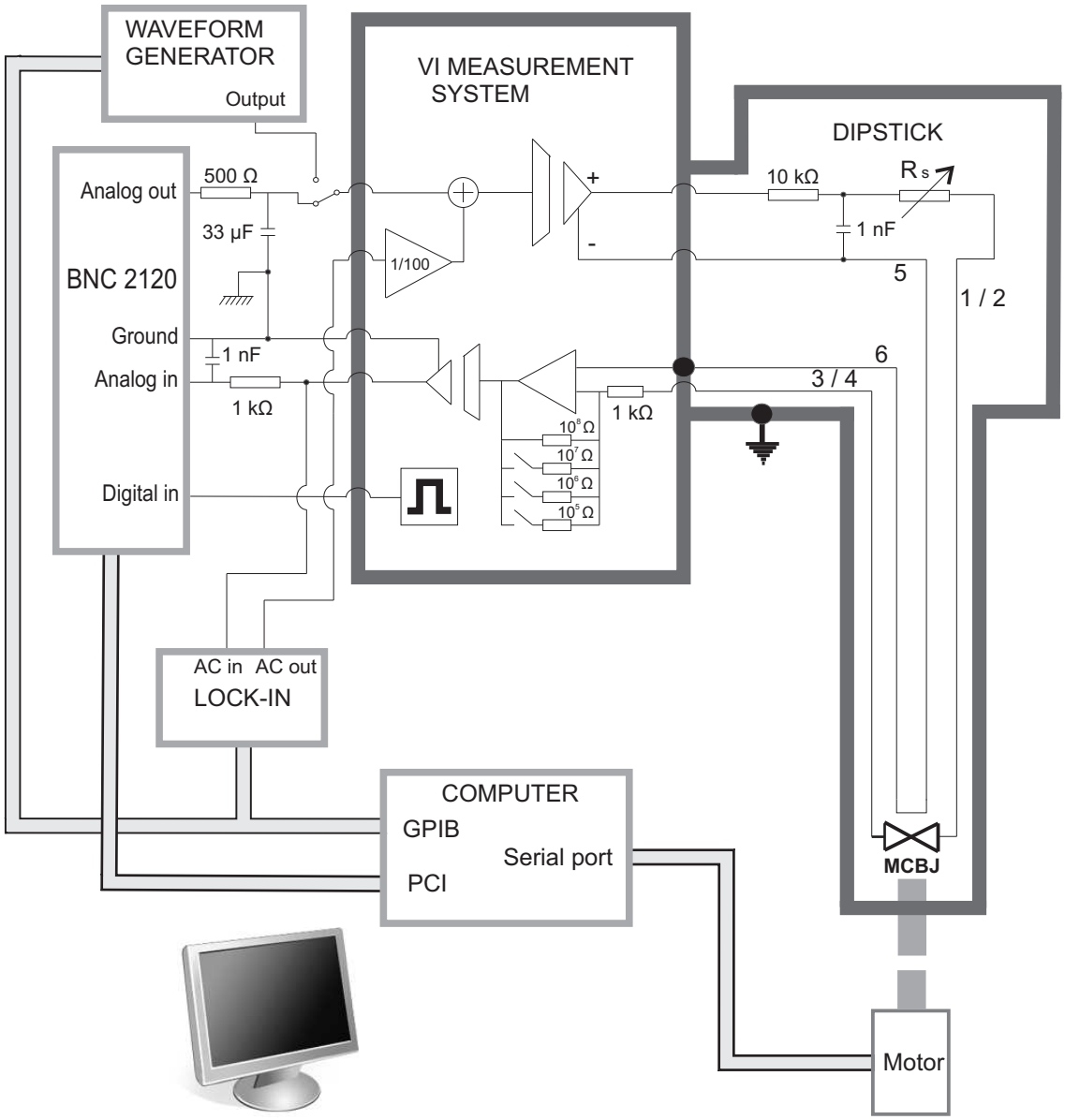

Figure 2.6: *Schematic layout of the electrical circuit used for our measurements. The central part is the VI measurement system, which transfers all signals between the sample (right below), and the rest of the equipment (shown left). See main text for more information.*

In between the VI measurement system and the computer, a connector box (BNC-2120) has been placed, where we can connect up to 16 analog input signals, 2 analog output signals, and 24 digital inputs. These signals can be measured at a maximum speed of 250.000 Samples/s.

The DC voltage is applied from one of the analog outputs of the DAQ, after leading it through a strong RC filter (cut-off frequency 10 Hz, -3dB). For fast IV measurements, we use the waveform generator for high frequent triangular voltage sweeps. Also, with this device, one can define its own waveforms, making it ideal for creating fast voltage pulses. Note that its frequency is limited by the bandwidth of the floating voltage source, which is around 15 kHz (-3dB). After this voltage source, the voltage signal is filtered for a second time, using a RC filter of 16 kHz (-3dB). However, for measuring the sample response, the most important limitation is the bandwidth of the IV convertor.

Bandwidth of the IV convertor

The maximum bandwidth for recording our measurements depends on the ability of the op-amp, to give feedback to the 'virtual' ground. This is difficult to calculate, since the IV convertor is far more complicated than drawn in Fig. 2.6. Hence, we determined the bandwidth by taking a measurement while replacing the sample with a resistor box. When switching the resistance, the current should change in steps with an infinitely small time step. Therefore, maximum 1 data point should appear in between these steps. The measurement was taken at 250 kS/s, with a 10 MΩ resistance for the IV convertor. Doing so, we observed 5 datapoints in between each step. In other words, measuring with 50 kHz gives a proper measurement, while measuring with a higher sample rate returns datapoints which are averaged over a longer time scale. Therefore, all measurements are done with maximum 250 kHz, of which 5 points are used to average the signal for a higher signal-to-noise ratio, resulting in a 50 kHz sample rate.

Automatic scaling IV convertor

To further increase the signal-to-noise ratio, the IV convertor is equipped with an automatically rescaling IV convertor. This is helpful when the conductance changes over many orders of magnitude. An example of such a measurement is when recording histograms, where the conductance is measured while opening and closing the junction. For these measurements, the conductance typically varies from 0-10 G_0. Using the automatic scaling, the feedback resistance of the

IV convertor changes automatically between 10^5, 10^6, 10^7 and 10^8 Ohm. This occurs when the current exceeds 3 μA, 300 nA and 30 nA. To avoid any oscillating behavior, the convertor changes back at a different value, namely 2.7 μA, 270 nA and 27 nA. The switching takes less than 1 ms, and the state of the IV feedback resistance is indicated by a digital TTL signal. This signal is then measured using one of the digital input channels of the DAQ. Since we measure both the regular output of the IV convertor and the digital TTL signal at the same time, the conductance can be measured accurately over many orders of magnitude. For example, using a 50 mV bias, the conductance can vary 7 orders of magnitude, while fast measurements can still be done with a noise level less than 1 % of the signal.

The only drawback here is that the switching gives a small voltage pulse to the sample wires. This voltage pulse is in the order of 50 mV, with a decay time of around 100 ns. Although this pulse does not affect the measurements on the bare gold electrodes, the hydrogen measurements are more sensitive and can be affected by this pulse. Therefore, the auto scaling is switched off during the hydrogen experiments.

2.5 Measurement control system

For measuring the current, and controlling the bias voltage and motor displacement, a large number of software programs were developed, using LabVIEW 7.1 (National Instruments) [10, 11]. This makes it possible to fully automatize the measurements. For example, for measuring IV curves in a fast way, we measure the input voltage and output current at the same time, both triggered by a TTL pulse. Immediately after, the electrodes are separated by a certain distance, after which another IV curve is recorded. When repeating this process over the entire tunneling regime, a full characterization of the metal-molecule-metal junction is obtained.

2.6 Characterization of the setup

2.6.1 Conductance in the contact regime

Since all measurements in this thesis are performed on gold junctions, it is crucial to know its properties, both in the contact regime and the tunneling regime. In this paragraph, two measurements are shown which are characteristic for gold

nanowires. First, the conductance in contact is discussed. When pulling a gold wire, the conductance decreases, according to Sharvin's rule. However, just before the wire breaks in two, the minimum cross section of the wire only holds a single atom. As already introduced in chapter 1, a single gold atom has a transmission of nearly 1, giving a conductance of $2e^2/h$. This is indeed what is observed in the measurements. An example is shown in Fig. 2.7, where a conductance trace is shown while opening and closing the junction. While pulling, the smallest cross section of the contact decreases in steps (since the number of atoms in this cross section decreases stepwise). Just before breaking, the conductance has a value close to 1 G_0, indicating a single gold atom contact.

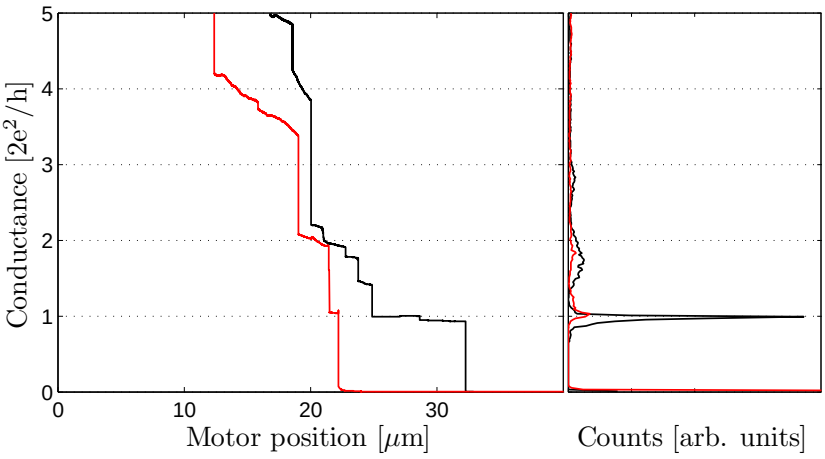

Figure 2.7: *Left: Typical conductance traces during the opening (black line) and closing (red/grey line) of the wire, as a function of motor position. In this conductance regime, the conductance mostly depends on the number of gold atoms in the minimum cross section of the contact. Hence, the conductance decreases in steps, until the wire breaks (below 1 G_0). Note the presence of a conductance plateau around 1G_0, due to the formation of atomic chains. Right: Histogram, obtained by counting the number of datapoints in a certain conductance window, for 300 traces. The highest peak, between 0.85 -1.02 G_0 and maximum 1 G_0, is attributed to the smallest possible cross section, a single gold atom. Since the transmission of a single channel can only be $\leq$ 1, the peak at 1 G_0 is strongly asymmetric. Data are measured at 4.2K and $V_{bias} = 50mV$. Data by Marius Trouwborst and Frank Bakker, 2007, unpublished*

Interestingly, around 1 G_0, the decrease in conductance goes slower than for any other conductance value. This is related to the formation of atomic chains, as first shown by Yanson *et al* [6] and discussed in section 1.4.3. For a number

of metals, including gold, the binding energy of gold atoms situated in a chain, is higher than the binding energy of atoms situated in the bulk [8, 9]. Therefore, when stretching a single atom contact, it can be energetically favorable that atoms are "pulled out" from the electrodes, instead of breaking the wire. When this occurs, the atoms form a chain with a cross section of a single gold atom. This remarkable phenomenon is stronger in metals like Au and Pt, where chains are observed up to 8 atoms long. During the formation of these chains, the conductance does not change dramatically. Instead, the conductance stays close to 1 G_0, resulting in a relatively long plateau around 1 G_0, as observed in the conductance traces. Finally, we note that the formation of atomic chains can be limited by training the junction, as will be discussed in chapter 4.

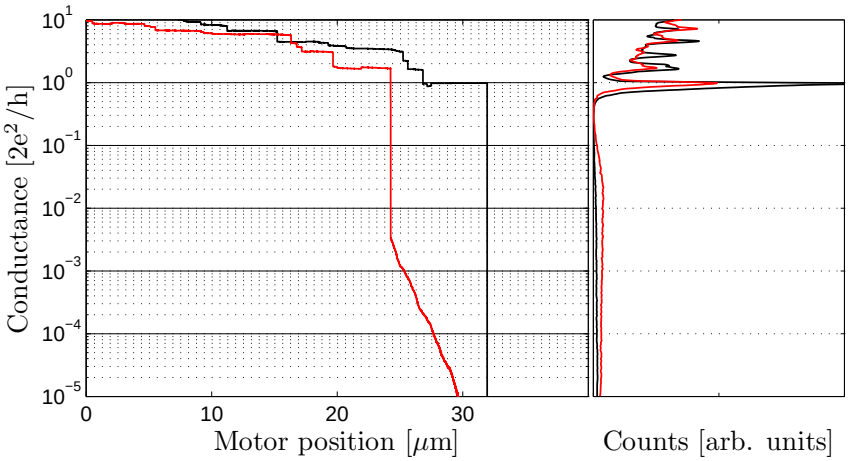

Figure 2.8: *Left: Typical conductance traces during the opening (black line) and closing (red/grey line) of the wire, plotted on a logarithmic scale. Just after breaking, both elastic and plastic deformation takes place, causing a Jump out of contact (as discussed in chapter 4.1. Right: Histogram of 1100 opening and closing traces. Note the flat background of the closing traces (red), in between* 10^{-5}-10^{-2} G_0*, showing the exponential decay of the conductance as a function of distance. Data are measured at 4.2K and* $V_{bias} = 100mV$*. Data by Marius Trouwborst and Frank Bakker, 2007, unpublished.*

2.6.2 Conductance in the tunneling regime

Having discussed the conductance in the contact regime, we now continue to the regime where the electrodes are separated by a small distance $< 5\mathring{A}$. A typical measurement is shown in Fig. 2.8, where an opening and closing trace is

plotted. Right after breaking, both plastic and elastic deformation takes place, causing a jump towards a low conductance value. This is called the Jump Out Contact (JOC), and will be discussed in chapter 4. The electrodes are now separated by a vacuum gap, with a barrier height equal to the workfunction of the metal. When again closing the junction, the conductance increases exponentially with distance (resulting in a straight line on a logarithmic scale). This is due to the fact that, at these small electrode separations, electrons can quantum mechanically tunnel from one electrode to the other. This tunnel current has an exponential dependence on the electrode separation, with a slope directly related to the barrier height or workfunction (as discussed in section 1.3). The exponential decay can also be observed when taking a (logarithmic) histogram from a large number of traces. In between 10^{-5}–10^{-2} G_0, the number of points are constant (straight vertical line in the right figure). Above $> 10^{-2}$ G_0, the number of counts decreases, due to the Jump to Contact (JC) (as will be discussed in chapter 4).

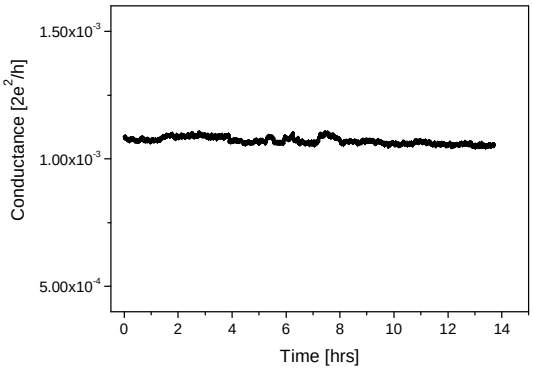

Figure 2.9: *Tunnel conductance measured as a function of time. Sample rate = 1 Hz, averaging time per data point is 500ms.* $V_{bias} = 20\ mV$.

2.6.3 Drift of the electrodes

One of the remarkable properties of the lithographically defined break junctions, is the negligible drift during the measurements. Due to the small and symmetric geometry, the system is hardly influenced by mechanical vibrations and is very stable in time, especially in comparison with Scanning Tunneling Microscopes (STM). To characterize the drift, we open the junction into the tunneling regime, stop the electrode motion at a certain tunnel gap, and measure the tunnel conductance as a function of time. The result is shown in Fig. 2.9. When we

assume that the noise is resulting from changes in the tunnel gap, we can write down the drift in $\mathring{A}$. With the help of Eq. 1.15 and Fig. 2.9, we find that the drift of our setup is below 0.2 pm/hr, which is equal to the value found by Ref. [3].

2.6.4 Mechanical backlash of the setup

Finally, we present a measurement on the mechanical backlash of the system [12]. Due to expansion of the metals during the cooling down of the system, there are small margins in the connection between the nut and rotation rad and the differential screw. Therefore, when the motor is turned in an opposite direction, the pushing rod does not follow immediately. Instead, the motor first has to move 4 μm, before the electrodes react (see Fig. 2.10). This is called the mechanical backlash. Since the backlash is constant during the measurements, the opening and closing traces can be shifted by this value when plotting the data.

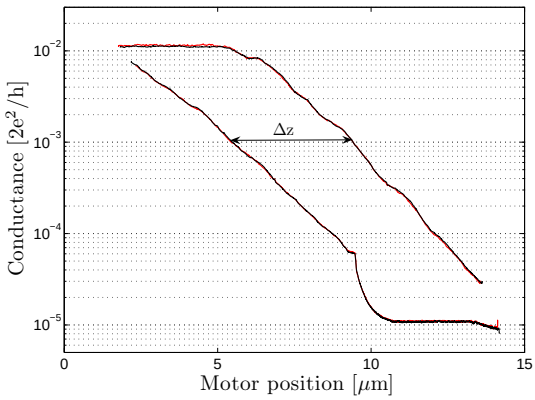

Figure 2.10: *Measurement of the tunnel current, while changing the motor position. Two successive traces are plotted, showing the perfect reproducibility when making traces. Due to the mechanical backlash, the electrode distance does not change when turning the motor in another direction. Only after 4 μm, the electrodes start responding. The small structure in the exponential line is due to mechanical imperfections of the differential screw.*

References

[1] J. Moreland and J.W. Ekin, J. Appl. Phys. **58**, 3888 (1985); J. Mooreland and P.K. Hansma, Rev. Sci. Instr **55**, 399 (1984); P.K. Hansma, IBM J. Res.

Develop. **30**, 370 (1986).

[2] J.M. Krans, C.J. Muller, I.K. Yanson, Th.C.M. Govaert, R. Hesper and J.M. van Ruitenbeek, Phys. Rev. B. **48**, 14721 (1993).

[3] J.M. van Ruitenbeek, A. Alvarez, I. Pineyro, C. Grahmann, P. Joyez, M. H. Devoret, D. Esteve and C. Urbina, Rev. Sci. Instrum. **67**, 108 (1996).

[4] *Mechanics of lithographically defined break junctions*, S.A.G. Vrouwe, E. van der Giessen, S.J. van der Molen, D. Dulic, M.L. Trouwborst, B.J. van Wees, Phys. Rev. B **71**, 035313 (2005).

[5] N. Agraït, A.L. Yeyati and J.M. van Ruitenbeek, Physics Reports **377**, 81 (2003).

[6] *A low temperature break junction setup*, S.A.G. Vrouwe, Master thesis, Rijkuniversiteit Groningen (2005).

[7] A.I. Yanson, G. Rubio Bollinger, H.E. van den Brom, N. Agraït and J.M. van Ruitenbeek, Nature **395**, 783 (1998).

[8] G. Rubio-Bollinger *et al*, Phys. Rev. Lett. **87**, 26101 (2001).

[9] S.R. Bahn and K.W. Jacobsen, Phys. Rev. Lett. **87**, 266101 (2001).

[10] *Automatizing of break junction setup with the aid of LABVIEW*, F.L. Bakker, FIT-stage verslag, Rijksuniversiteit Groningen (2006).

[11] *Mechanical properties of single gold atom contacts*, F.L. Bakker, Master thesis, Rijksuniversiteit Groningen (2007).

[12] *Low temperature mechanically controllable break junction setup; a characterization*, P. Ivo, Master thesis, Rijksuniversiteit Groningen (2006).

Chapter 3

Calibration of lithographically defined break junctions

Abstract

In this chapter, both experimental and theoretical results are presented on the calibration of the break junctions. The calibration factor, or attenuation factor, is defined as the ratio between the change in electrode separation and the bending of the substrate. It is shown that this attenuation factor depends on the details of the break junction geometry, and the softness of the polyimide layer in particular. Furthermore, experimental results are presented on the calibration of the junctions. This calibration was done by three different methods: using the tunnel slopes, measuring the average plateau length and measuring Gundlach oscillations.

3.1 Introduction

For a good understanding of the experimental results on break junctions, it is crucial to know the electrode separation. For example, from the relation between conductance and electrode separation, one can deduce important values like the workfunction of the electrodes (giving information on the presence of impurities), and the strength of the gold-molecule bond.

For an estimation of the calibration ratio, one can derive an expression for the attenuation factor using elastic beam theory, as first deduced by Van Ruitenbeek *et al* [1]. For the calculation, two approximations are made. First, since the

This chapter is based on Refs. 6 and 7 on p. 147.

substrate thickness is much larger than the thickness of the polyimide and gold layer, the latter two are expected to have no influence on the bending properties (see Fig. 3.1). Second, since deformations remain small, there is no deviation on the original geometry when bending the substrate.

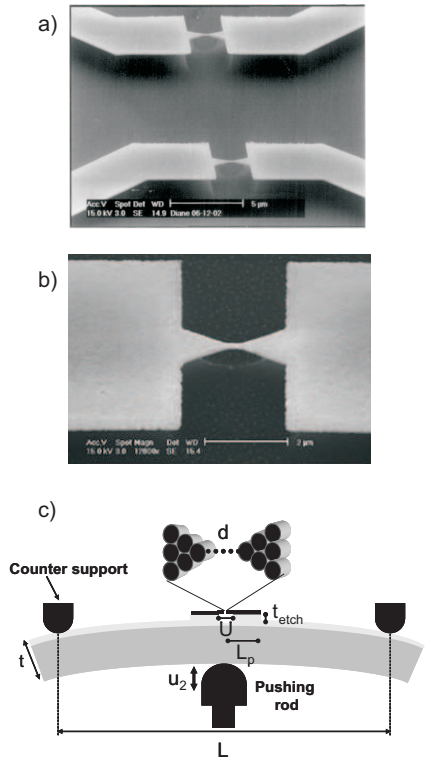

Figure 3.1: *(a) Scanning electron micrograph of two free gold strips, fabricated on a single substrate. Note that L_p is defined as the distance from the middle of the gold bridge to the kink in the lead. (b) Scanning electron micrograph of the free-hanging bridge. (c) Schematic drawing of the sample in a three-point bending set-up. The elongation of the bridge can be tuned by the pushing rod. Concerning the different parameters: The length of the free-hanging bridge is U, and the thickness of the substrate, polyimide and etch depth is given by t, t_p and t_{etch} respectively. Finally, the electrode separation d can be modified by changing the pushing rod distance u_2.*

As shown in Fig. 3.2, one can now write down the relation for the bending moment $M(x)$, as a result from the pushing rod, giving a load P to the substrate.

$$M = 1/2P(1/2L - x_1) \tag{3.1}$$

As drawn in Fig. 3.2b, the stress σ_{11} and strain ε_{11} are linearly related to the position x_2. This is described by Hooke's law, $\sigma_{11}(x_2) = E\varepsilon_{11}(x_2)$, where E is the Young's modulus. When combining this relation with Eq. 3.1, the bending moment can be expressed as:

$$M(x_1) = \frac{EI\varepsilon_{\max}(x_1)}{t/2} \tag{3.2}$$

where $\varepsilon_{\max}$ is the strain at the surface of the strip ($\varepsilon_{\max} = \varepsilon(x_2 = t/2)$).

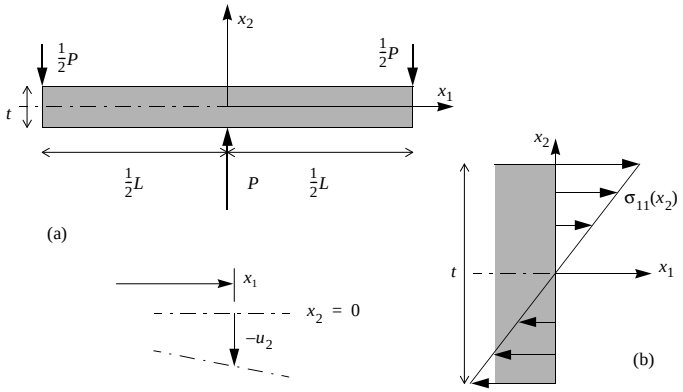

Figure 3.2: *(a) The strip used for the modeling. When bending the strip, by applying a load P, the middle of the strip moves in the x_2 direction. (b) Bending of the strip results in a linear variation in tensile stress σ_{11} over the cross-section. Note that in the middle of the strip ($x_2 = 0$), no stress takes place.*

Next, the plane moment of inertia is considered, which is typically $I = wt^3/12$, where w denotes the width of the beam. Now, the curvature can be calculated, which is $d^2u_2/dx_1{}^2 = -M/EI$. Integration along x_1 then leads to the deflection

$$u_2 = \frac{PL^3}{48EI}$$

at the center of the strip ($x_1 = 0$). For the displacement in the x_1 direction, previous equations are combined, leading to

$$u_1(x_1) = \frac{tPL^2}{8EI}\left(\frac{x_1}{L}\right)\left[1 - \left(\frac{x_1}{L}\right)\right] = \frac{6tu_2}{L}\left(\frac{x_1}{L}\right)\left[1 - \left(\frac{x_1}{L}\right)\right] \tag{3.3}$$

for points on top of the strip surface. Finally, when assumed that the electrode separation equals the separation at $x_1 = U/n$, the relation for the electrode displacement u_1 becomes

$$u_1 = \Delta U/2 = \frac{6tu_2U/2}{L^2} \tag{3.4}$$

when $U \ll L$. This directly leads to the attenuation factor, r, defined as the ratio between the electrode separation d and substrate bending u_2:

$$r = \frac{\Delta d}{\Delta u_2} = \frac{6tu}{L^2} \tag{3.5}$$

This is the formula, as introduced in chapter 2. For the geometry of the junctions presented in Fig. 3.1, the value for r is $1.7 \cdot 10^{-5}$. However, as we will show in the next paragraphs, this value is smaller than the real attenuation factor.

3.2 Modeling

Although Eq. 3.5 is widely used, it ignores the fact that the polyimide layer has different mechanical properties than the substrate material. In fact, the equation assumes that the displacement of the tip of the junction is the same as that of the point $x_1 = U/2$ on the substrate surface. Ie, the displacements on top of the polyimide are equal to the displacements on top of the substrate. However, for a more precise relation for the attenuation factor, one should incorporate the polyimide layer and its mechanical properties. To do so, the break junction geometry was modeled using a three dimensional finite element analysis. Its results are published in Ref. [2], and are briefly discussed here. For the analysis, the junction is modeled as shown in Fig. 3.3.

For the modeling, one half of the junction is considered, while focusing on the displacements of both the polyimide film and gold layer. The bottom layer of the polyimide follows the displacements of the substrate, which is given by Eq. 3.5. Furthermore, we assume that the substrate is infinitely wide, and for the other values we use the geometry shown in Fig. 3.1. This gives for half of the bridge length $U/2$ to be 1.2 μm, for the width of the Au lead 3 μm, for the length of the bridge L_p is 5 μm, and the polyimide thickness t_p is equal to 3 μm. The elastic (Young's) modulus of Au is 75 GPa, for the polyimide 2GPa, while the Poisson ratio is 0.4 for both materials. For the modeling, the pushing rod displacement is set to 2.8 mm, although other values for the displacement gave identical results.

The result is shown in Fig. 3.4. Interestingly, while Eq. 3.5 assumes that the contours of equal displacement are vertical lines, Fig. 3.4 shows dramatic

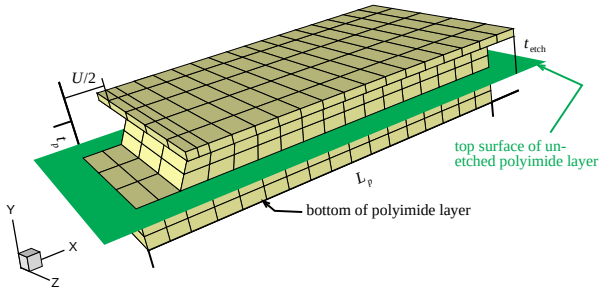

Figure 3.3: *Schematic of the junction model used for the three-dimensional finite element analysis. The shaded surface indicates the depth to which the polyimide layer has been etched,* t_{etch}*. The thickness of the layer below the gold surface is given by* t_{p}*.*

deviations, especially towards the tip. In fact, where Eq. 3.5 predicts a tip displacement of $\Delta U/2 = 0.024$ μm, the calculated displacement from the model is $\Delta d/2 = 0.056$ μm. Thus, for this geometry, Eq. 3.5 should be multiplied with a correction factor $\zeta = 2.3$.

To investigate the origin of this effect, we have explored other geometries by varying the etch depths t_{etch} and the length of the gold film L_p. The results are shown in Fig. 3.5, where the correction factor is given for various values of t_{etch} and L_p. Especially the junction length is found sensitive for the attenuation factor.

To conclude, by modeling the break junction, the effect of the softness of the polyimide layer was investigated. It is found that the polyimide gives a strong

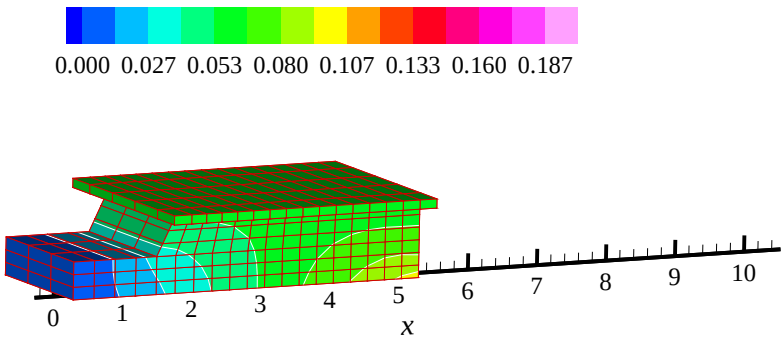

Figure 3.4: *Contours of equal displacement for the break junction (in* μm*). Constants:* L_p*= 5* μm*,* $t_{etch} = 0.75$ μm *and* u_2 *is 2.8 mm.*

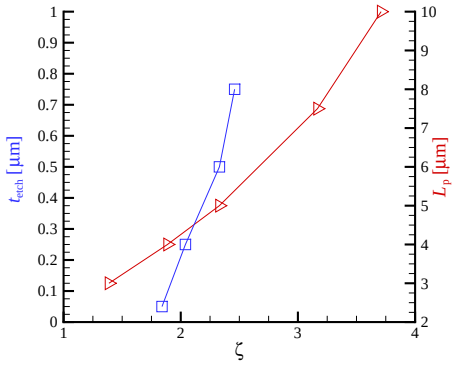

Figure 3.5: *Correction factor ζ, as deduced from the model, for different values of the etch depth t_{etch} (squares, at fixed length $L_p = 5$ µm) and for different values of the junction length L_p (triangles, at fixed etch depth $t_{etch} = 0.5$ µm).*

deviation on the attenuation factor, depending on the exact geometry of the break junction, and the junction length L_p in particular. To correct for this effect, the formula for the attenuation factor has to be multiplied by a correction factor ζ:

$$r = \frac{\Delta d}{\Delta u_2} = \frac{6tu}{L^2} \cdot \zeta \tag{3.6}$$

where ζ varies between 2 and 4, for junction length of 4 to 11 μm respectively. For our sample geometry, with t_{etch} is 650 nm and L_p equals 5 μm, we estimate ζ to be in between 2.5 and 2.7 (with the help of Fig. 3.5)

3.3 Experiments

To show the validity of Eq. 3.6, we have performed a number of experiments to obtain the attenuation factor. In the past years, four different calibration methods have been developed: using the slope in the tunneling regime, measuring Gundlach oscillations, measuring the plateau lengths and the interferometric calibration method [2, 12]. Here, the first three are discussed.

3.3.1 Slope in tunnel regime

Introduction

The most straightforward way to calibrate the electrode separation, is to use the exponential dependence of the conductance on the electrode separation. As introduced in chapter 1, we can write for the tunnel conductance:

$$G \propto exp\left(\frac{-d}{\hbar}\sqrt{8m\phi}\right) \tag{3.7}$$

where ϕ is the work function of the material and d the distance between the contacts. The workfunction of gold is known from literature and depends on the crystal orientation. For example, the workfunction, as measured on a flat gold surface, is 5.3 eV for Au[111] and 5.5 eV for Au[100]. We will discuss this variation in the next paragraph, but, for now, we assume a workfunction of 5.4 eV. According to Eq. 3.7, when plotting the logarithm of the tunnel conductance as a function of motor position, one obtains a straight line with slope equal to:

$$\frac{\Delta \log G}{\Delta d} = \frac{-\sqrt{8m\phi}}{\hbar \cdot ln10} = -1.04 \text{ Å}^{-1} \tag{3.8}$$

In other words, when increasing the gap by 1 $\mathring{A}$, the conductance will drop approximately 1 decade. So, using this relation, one can directly calculate the attenuation factor.

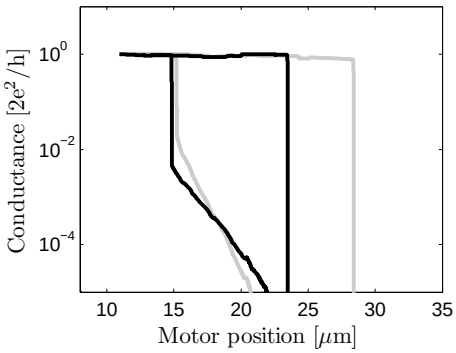

Figure 3.6: *Two opening and closing traces measured right after each other. After breaking, the conductance jumps towards a low conductance value (Jump out Contact, see chapter 4). When closing the junction, the conductance increases exponentially, resulting in a straight tunnel slope, until the Jump to contact. The average slope is -0.45 μm^{-1}, while the two curves differ 25 % from this value. The origin of the x-axis is arbitrarily.*

Experiments on the tunneling slope

As mentioned above, the exact workfunction of a flat gold surface slightly depends on the crystal orientation. However, since the workfunction is actually a bulk

value, larger variations can occur when the electrodes are two atomically sharp wires, as the case in our experiments.

An example of these variations is given in Fig. 3.6, where two successive tunnel traces are shown. In between the two traces, the junction is closed up to 1 G_0, thereby changing the atomic configuration of the apex. Although the tips are only slightly modified, this can lead to a 30% variation in the tunnel slope and will be further discussed in the next chapter [4]. Hence, to obtain the average tunnel slope, a larger number of traces is needed. We have done so on 1100 traces, where the slope was calculated in the conductance range $2 \cdot 10^{-5}$ and $2 \cdot 10^{-4}$ G_0. In this conductance range, the tunnel slope is constant and shows no deviation when changing the distance (as will be shown in the next paragraph). The results are plotted in Fig. 3.7, giving an average slope of -0.41 μm^{-1}. Finally, using Eq. 3.8, we obtain the attenuation factor, which is $\mathbf{(4.0 \pm 1.0)} \cdot 10^{-5}$ for this junction.

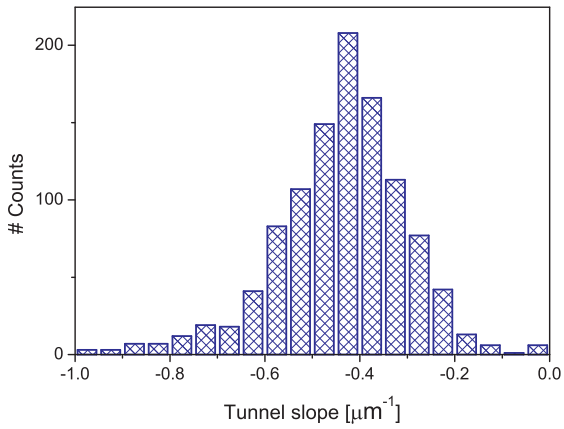

Figure 3.7: *Histogram of slopes in the tunnel regime, obtained from 1100 closing traces. The slope was determined by fitting the data in the conductance range between* $2 \cdot 10^{-5}$ *and* $2 \cdot 10^{-4}$ G_0. *In between each trace, the junction is closed to 20* G_0. *Data is taken with* V_{bias}*=100 mV.*

Dependence of the tunnel slope with electrode distance

Before continuing to the other calibration methods, we like to discuss here the dependence of the tunnel slope, as a function of the electrode distance. In the last paragraph, we assumed the tunnel slope to be constant, independent of the

electrode separation. However, for many samples we observed a strong deviation in tunnel slope, especially towards smaller electrodes gaps. For example, when focusing on the traces of Fig. 3.6, the black line shows a gradual decrease in tunnel slope when closing the contact. This effect especially shows up when plotting conductance histograms, on a logarithmic scale (see Fig. 3.8). Since the tunnel slope is inverse proportional to the number of counts in the histogram, the tunnel slope for a large number of traces can be compared. Clearly, the tunnel slope has a minimum around 10^{-2} G_0, giving the largest number of counts in the histogram. In contrast, the tunnel slope around 10^{-5} G_0 is 20 % higher than the slope around smaller 10^{-2} G_0 (5000 versus 6000 counts). We emphasize that this is not an artifact of the electronics, but purely related to the tunnel current.

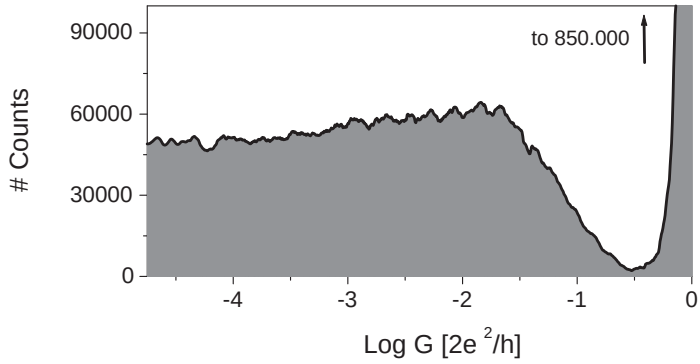

Figure 3.8: *Conductance histogram, plotted on a logarithmic scale, for 1100 closing traces. The decrease in counts around* 10^{-1} G_0 *is due to the adhesive forces between the electrodes, resulting in the so called jump to contact (as further discussed in section 4.1). The number of counts around* 10^{-2} *is 20 % higher than the number of counts around* 10^{-4} G_0 *and is probably related to the lateral approach of the two electrodes. Data is taken with* V_{bias}*=100 mV. The data is plotted with 170 bins / decade.*

There are two possible explanations for this deviation on the tunnel slope. First, the image potential can decrease the barrier height. Lang *et al* performed calculations on an STM geometry, where they found a dramatic decrease of the barrier at small electrode separations; 3.5 eV at 6 $\AA$ can decrease to 0.6 eV at 3 $\AA$ [24]. However, its effect on the tunnel slope is not trivial, since the absolute conductance should *increase* due to the lowering of the barrier. We note here that this is in contrast to the calculations by Oleson et al, where only a decreasing tunnel slope was assumed [7]. Nevertheless, simulations by Laloyaux *et al* show a

lowering of the tunnel slope of 20 % at electrode separations of 3 $\mathring{A}$ [8]. Although this could explain our data, the image potential is expected to play only a minor role at atomically sharp wires, as used in the break junctions.

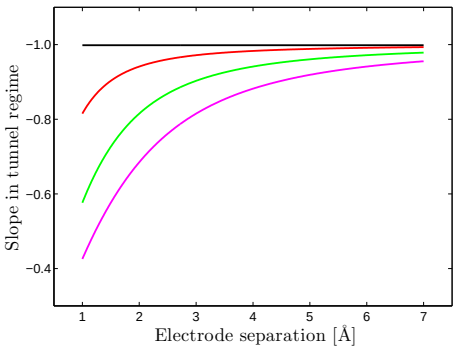

Figure 3.9: *Normalized deviation of the tunnel slope if the outer atoms of the electrodes are not in line with the direction of the electrode movement. The effect is calculated, assuming stiff electrodes, by setting the atoms out of line by 0 Å (upper line), 0.5 Å, 1 Å and 1.5 Å (lower line).*

A more likely explanation of the variation in tunnel slope, is the so called lateral approach of the electrodes. Till now, we have assumed that the apex atoms of the electrodes are in the same line as the movement of the electrodes. However, a small deviation from this line is more realistic. To make a rough estimation of this effect, we modeled the electrodes by assuming an infinitely stiff apex, which is misaligned by a small distance. The result is shown in Fig. 3.9, for a misalignment of 0 to 1.5 $\mathring{A}$. As expected, the effect is minimum on large electrode separations. However, at separations < 4 $\mathring{A}$, the tunnel slope decreases, similar to the observations of Fig. 3.8. Hence, when the tunnel slope is measured at these small electrode separations, one can find tunnel slopes smaller than expected. This could explain the smaller workfunctions often reported in literature [9].

3.3.2 Plateau length histogram

The second calibration method we discuss is the plateau length histograms. As introduced in section 1.4.3, the conductance plateaus around 1 G_0 are much longer than the plateaus at other conductance values (see Fig. 3.10). These plateaus are related to the formation of chains of atoms [10]. In general, the length of these chains is equal to an integer number of gold atoms. Hence, the plateau length

is equal to an integer number times the bond length of a single atom. Since the bond length of a gold atom in a chain is well known from literature (2.5 ± 0.2 $\mathring{A}$), this value can be used for the calibration of the break junction.

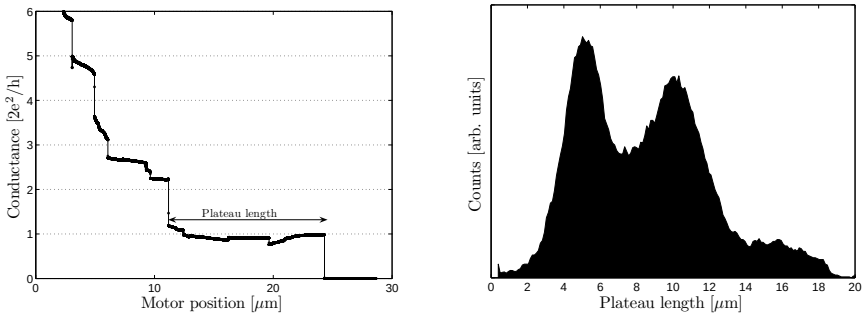

(a) Definition of the last plateau length.

(b) Distribution of lengths for the last conductance plateau.

Figure 3.10: *(a) Definition of the plateau length: The plateau length is defined as the length of the trace, starting at the first data point where $G < 1.2G_0$ and ending at the last data point where $G > 0.7\ G_0$. (b) From the distribution of the plateau lengths of 1100 traces we obtained the attenuation factor. A smoothing function which averages over 15 bins is applied to the data. The bin size is 0.11 μm. All data are taken at 4.2 K with $V_{bias} = 100\ mV$. In between each trace, the junction was closed up to 20 G_0.*

The plateau length was measured for 1100 traces, and plotted in a histogram. From Fig. 3.10 (b), clearly two peaks can be observed. The distance between the two peaks, 4.9 μm, is assumed to be equivalent to the expected bond length of 2.5 $\mathring{A}$, resulting in an attenuation factor of $\mathbf{(5.1 \pm 1.5)} \cdot 10^{-5}$. We emphasize that, when measuring a larger number of traces (>10.000), more peaks will show up in the histogram, thereby increasing the accuracy of the calibration measurement.

3.3.3 Gundlach oscillations

Theory on Gundlach oscillations

The third calibration method concerns the so called Gundlach oscillations [11]. This method is based on field-emission resonance, i.e. tunneling in the Fowler-Nordheim regime [13]. Thus, this regime is entered when applying bias voltages higher than the work function of the metal (see Fig. 3.11).

In this case, the electrons with the highest energy no longer "see" a potential barrier, but are directly injected into the other electrode. However, when calcu-

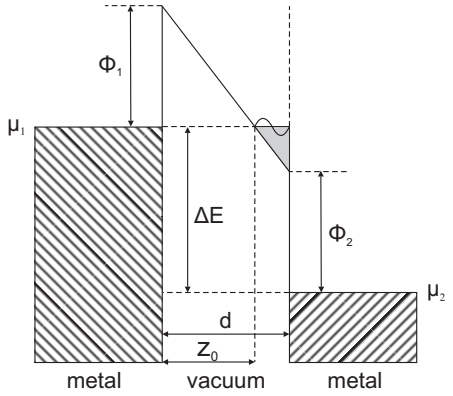

Figure 3.11: *Energy band diagram for the Fowler-Nordheim regime. When the bias voltage exceeds the workfunction of the metal, $\Delta E = eV > \Phi_2$, a part of the barrier becomes classically available. This gives rise to a new interface, as denoted by z_0. In between this interface and the right electrode, a part arises where the electron wavefunctions can interfere (gray triangular shape). This interference pattern influences the total transmission coefficient, and can be tuned by the bias voltage.*

lating the electron wavefunctions, one finds transmission coefficients smaller than 1. This is due the fact that an interfere pattern arises at the interface (gray area in Fig. 3.11). Hence, the transmission will have a oscillating dependence on the bias voltage, called Gundlach oscillations [11].

The differential conductance can be calculated, as first obtained by Kolesnychenko *et al.*, resulting in the following expression [12]:

$$\frac{dI}{dV} \sim A(V)cos(\zeta(V)) \tag{3.9}$$

where ζ is given by:

$$\zeta(V) = \frac{4\sqrt{2m}}{3\hbar}\frac{(eV-\phi_2)^{3/2}}{eF} \tag{3.10}$$

and F is the electric-field strength in the vacuum gap. The differential conductance has a maximum when the argument ζ equals $2\pi n$. Furthermore, the triangular shape of the energy at the interface can be kept constant, when keeping the electric field constant. In this regime, this can be done by simply keeping a constant current. Now, one can write for the bias voltage V as a function of peak number n:

$$eV = \phi_2 + \left(\frac{3\pi\hbar}{2\sqrt{2m}}\right)^{2/3} F^{2/3}n^{2/3} \tag{3.11}$$

From a plot of V versus $n^{2/3}$ one obtains the work function ϕ_2 as the intercept at the voltage axis. Furthermore, from the slope of the curve σ, the electric field F can be calculated using $F = 1.087\sigma^{3/2}$ (as deduced from Eq. 3.3.3). The distance between the contacts will be related to the electric-field F. An expression for the distance d between the electrodes can be found:

$$d = \frac{1}{eF}(eV + \Delta\phi) \tag{3.12}$$

where $\Delta\phi$ is the difference in work function between the two contacts. The fact that both the work function and the calibration factor can be obtained from a single measurement, makes Gundlach oscillations a powerful method. Note that we can investigate the presence of impurities on the surface, by comparing the obtained work function.

Measuring Gundlach oscillations

A typical Gundlach calibration is shown in Fig. 3.12. During the experiment, we apply a feedback loop to the voltage, to keep a constant current of 1.00 ± 0.01 nA. Meanwhile, the differential conductance and the bias voltage was measured, as a function of the motor position, using a standard Lock-in (AC signal is 100 mV). As shown in Fig. 3.12, the differential conductance is maximum just above the workfunction of gold (around 5.4 eV), above which the interference gives the oscillating behavior. When plotting the position of the maxima of the peaks, as a function of peak index $n^{2/3}$, one obtains a linear relation at higher voltages (as shown in the inset of Fig. 3.12). The slope of this curve directly returns the electric field, while the interception of this line at the voltage axis equals the work function. For this measurement, the electric field is 2 V/nm, and the workfunction equals 5.6 ± 0.2 eV. Note that the electric field can differ for each measurement, and is in the order of 2 to 4 V/nm. Due to these high electric fields, atomic reorganization can take place, thereby destroying the measurement. Hence, we found that it is not always possible to use this calibration method.

Finally, the attenuation factor can be obtained from the measured motor position, as a function of bias voltage. For higher voltages (or larger electrode distances), this relation is linear. Using the slope, and with the help of Eq. 3.3.3, the attenuation factor can be calculated (assuming $\Delta\Phi$ =0). For this sample, the attenuation factor is found to be $\mathbf{(4.2 \pm 0.5)}\cdot 10^{-5}$.

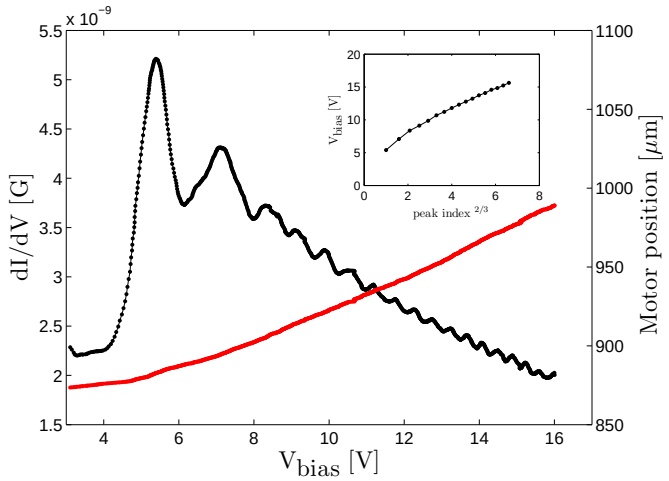

Figure 3.12: *(dotted curve) Oscillating differential conductance as a function of applied bias voltage. During the measurement we measured the differential conductance and the bias voltage versus the motor position, while keeping the current constant. (line) The motor position plotted as a function of the applied bias voltage. The attenuation factor can be obtained from the relation between the motor positions and the bias voltage. This relation is fitted at higher voltages where the response is almost linear. (inset) The peak index is plotted versus the position of the maxima at the voltage axis. For higher peak index, one can make a linear fit and find the work function of the material from the interception at the voltage axis (see text). The electric field strength in the gap can be obtained from the slope of the fit.*

3.3.4 Comparing different techniques

To investigate the variation in attenuation factors between different samples, we calibrated 5 different junctions. The attenuation factors we have found, using different techniques, are listed in Table 3.1.

From the obtained results we can conclude the following. The Gundlach calibration technique is the most accurate technique and can be used to acquire both the attenuation factor and the work function. Also, a single measurement is enough to obtain the calibration ratio, as shown by the perfect reproducibility of the measurements (sample D). In contrast, for calculating the tunnel slope, a large number of traces has to be measured. Changes in the atomic configuration of the apex, can give a deviation in the tunnel slope up to 30 %. Interestingly, when considering the Gundlach experiments, only slight variations have been found in the workfunction (see Table 3.2). The measured values (4.9 to 5.6 eV), are close to the literature values for the workfunction of gold (5.3 to 5.5 eV) [12].

Table 3.1: *Attenuation factors for different calibration techniques for five samples. Each letter corresponds to a different sample. Numbers listed in the table must be multiplied with* 10^{-5} *to obtain the attenuation factor. For sample D, we have performed two independent Gundlach experiments, by closing the junction in between the measurements. Regarding the tunnel slope measurements, the slope is measured in between* $2 \cdot 10^{-5}$ *and* $2 \cdot 10^{-4}$ G_0*, on a total number of traces given in between the brackets.*

Sample	**Plateau length**	**Tunnel slope**	**Gundlach oscillations**
A	-	-	4.2 ± 0.5
B	-	4.5 ± 1.1 (85)	4.5 ± 0.5
C	-	3.9 ± 0.9 (360)	3.3 ± 0.3
D (1)	-	4.1 ± 1.0 (120)	4.0 ± 0.4
D (2)	-	4.1 ± 1.0 (120)	4.0 ± 0.3
E	5.1 ± 1.5 (1100)	3.9 ± 0.9 (1100)	-

Finally, we return to the modeling results on the break junctions. As derived in section 3.2, the formula for the attenuation factor should be multiplied with a factor 2.6, leading to an attenuation factor of $4 \cdot 10^{-5}$ (for break junctions with length $L_p = 5$ μm). This value is in excellent agreement with the values we have found experimentally. Concerning the Gundlach experiments, we obtained an average attenuation factor of $4.0 \cdot 10^{-5}$.

Table 3.2: *Work functions for five different samples, as obtained from the Gundlach measurements. Each letter corresponds to a different sample.*

Sample	**Work function [eV]**
A	5.6 ± 0.2
B	5.1 ± 0.2
C	5.5 ± 0.3
D (1)	5.2 ± 0.2
D (2)	4.9 ± 0.3

3.4 Conclusions

When calculating the attenuation factor of break junctions, one should include deviations due to the softness of the polymide. This was found with the help of a finite-element analysis, where large deviations were found on the attenuation factor. This factor depends on the exact geometry of the break junction, and the size of the polymide strip in particular. In practice, the attenuation factor is 2 to 4 times larger than the value derived from elastic beam theory. We have shown the validity of the model, by calibrating different junctions using the tunnel slopes, plateau length histograms and Gundlach oscillations.

References

[1] J.M. van Ruitenbeek, A. Alvarez, I. Pineyro, C. Grahmann, P. Joyez, M. H. Devoret, D. Esteve and C. Urbina, Rev. Sci. Instrum. **67**, 108 (1996).

[2] *Mechanics of lithographically defined break junctions*
S.A.G. Vrouwe, E. van der Giessen, S.J. van der Molen, D. Dulic, M.L. Trouwborst, B.J. van Wees, Phys. Rev. B **71**, 035313 (2005).

[3] Yu. Kolesnychenko, O.I. Shklyarevskii, and H. van Kempen, Rev. Sci. Instrum. **70**, 1442 (1999).

[4] The same variation is also found by Ref. 5, on "notched wire" break junctions.

[5] A.I. Yanson, PhD thesis, Leiden University 2001.

[6] N.D. lang, Phys. Rev. B **37**, 10395 (1988).

[7] L. Olesen, M. Brandbyge, M. R. Sørensen, K. W. Jacobsen, E. Lægsgaard, I. Stensgaard and F. Besenbacher, Phys. Rev. Lett. **76**, 1485 (1996).

[8] Th. Laloyaux, I. Derycke, J.P. Vigneron, Ph. Lambin and A.A. Lucas, Phys. Rev. B. **47**, 7508 (1993).

[9] G. Rubio-Bollinger, P. Joyez and N. Agraït, Phys. Rev. Lett. **93**, 116803 (2004).

[10] A.I. Yanson, G. Rubio Bollinger, H.E. van den Brom, N. Agraït and J.M. van Ruitenbeek, Nature **395**, 783 (1998).

[11] K.H. Gundlach, Solid State Electron **9**, 949 (1966).

[12] H.B. Michaelson, J. Appl. Phys. **48**, 4729 (1977).

[13] R.H. Fowler and L. Nordheim, Proc. Roy. Soc. A. **119**, 173 (1928).

[14] C. Untiedt, A.I. Yanson, R. Grande, G. Rubio-Bollinger, N. Agraït, S. Vieira and J.M. van Ruitenbeek, Phys. Rev. B **66**, 085418 (2002).

Chapter 4

Single atom adhesion in optimized gold nano junctions

Abstract

We study the interaction between single apex atoms in a metallic contact, using the break junction geometry. By carefully 'training' our samples, we create stable junctions in which no further atomic reorganization takes place. This allows us to study the relation between the so-called jump out of contact (from contact to tunnelling regime) and jump to contact (from tunnelling to contact regime) in detail. Our data can be fully understood within a relatively simple elastic model, where the elasticity k of the electrodes is the only free parameter. We find $5 < k < 32$ N/m. Furthermore, the interaction between the two apex atoms on both electrodes, observed as a change of slope in the tunnelling regime, is accounted for by the same model.

4.1 Introduction

Many macroscopic phenomena find their origin on the nanoscale, since they are ultimately due to the interaction between single atoms. A good example is formed by friction and wear, which have been studied for centuries, but still inspire fascinating research. For example, several groups have recently explored methods to minimize friction in nanoelectromechanical systems (NEMS), where no liquid lubricants can be applied [1]. In this chapter, we focus on the ultimate miniaturization of the problem and investigate adhesion and elasticity on the atomic scale.

This chapter is based on Ref. 2 on p. 147.

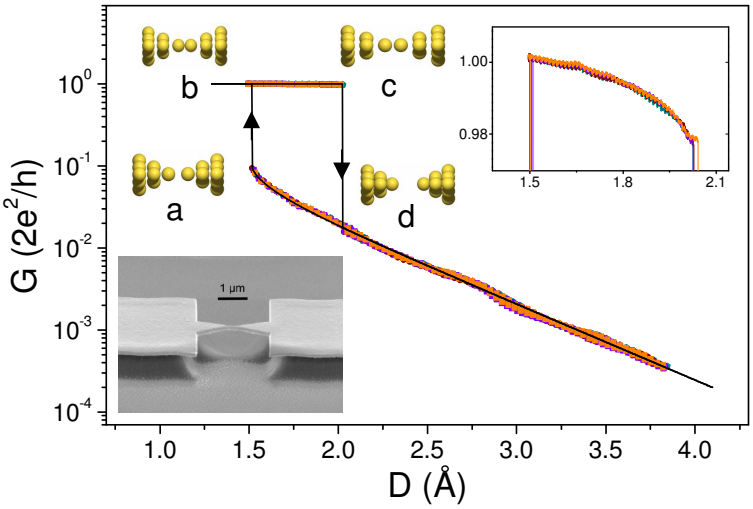

Figure 4.1: *Points: conductance G vs. distance D for four successive G_0-loops (V_{bias} = 50 mV). The jump to contact occurs at D=1.5 Å; the jump out of contact at D=2.0 Å. Black line: fit to model in Fig. 8.6 (k=15.7 N/m). For the other parameters we use literature values: $F_0 = 1.5nN$, $d = 2.5Å$, and $E_b = 0.7eV$. The work function, $\phi = 5eV$, was measured independently. Inset graph: zoom of G vs. D in contact regime (linear scale). Picture: scanning electron micrograph of a lithographic break junction.*

The interaction between single atoms can be studied by carefully extending a notched metallic wire, while monitoring its conductance G. As the wire is thinned out, G decreases, until its value is dominated by a few atoms forming a constriction [2]. When pulling is continued, an abrupt rupture of the wire is observed (see Fig. 4.1, point c to d). Upon closing the contacts, a second jump occurs for many metals, including gold (see Fig. 4.1, point a to b) [3, 4]. These jumps are known as the 'jump out of contact' (JOC) and 'jump to contact' (JC), respectively. By carefully studying these discontinuities, one can in principle obtain detailed information on the adhesion forces between two single atoms. However, the details of the hysteretic loop in Fig. 4.1 are still not fully understood. In fact, no relation between the JC and JOC has been observed so far. The reason for this is that the breaking process is generally accompanied by plastic deformation, i.e., the atoms first reorganize before rupture [5]. Therefore, during closing and opening, the electrodes have a different atomic configuration. The most intriguing example of plastic deformation is the formation of atomic chains prior to breaking [6].

Here, we explore junctions in which no plastic deformation occurs during breaking and making of the single atom contact. This is achieved by properly 'training' each device first. Figure 4.1 displays G during the opening and closing of a 'trained' Au wire. Note that the single gold atom conductance is characterized by a value close to the conductance quantum $G_0 = 2e^2/h$. As can be seen from the absence of conductance steps in the contact regime, no atomic reorganization takes place. Moreover, the curves in Fig. 4.1 are perfectly reproducible for tens of subsequent runs. Being able to exclude plasticity, we infer that the two jumps (JC and JOC) in Fig. 4.1 are related to the adhesive forces between the single atoms forming the junction. The remarkable reproducibility of the 'trained' junctions allows us to test a generic potential energy model. In fact, we show that the whole making and breaking process can be fitted by a single fit parameter: the elasticity of the electrodes.

4.2 Experimental details

For our study, it is crucial to minimize drift and vibrations in the electrodes during the measurements. This is achieved by using a mechanically controllable break junction (MCBJ) at 4.2 K [7]. The wires are patterned with electron beam lithography, after which we evaporate 1 nm of Cr and 120 nm Au at $2 * 10^{-7}$ mbar. Finally, the area below the wire is etched with a CF_4/O_2 plasma, to create a free hanging gold wire [inset in Fig. 4.1]. The MCBJ is cooled down to 4.2 K and broken by bending the substrate. Thus, clean and stable gold electrodes are obtained in cryogenic vacuum. Opening and closing of the junction is done with an effective speed of 0.5 $\mathring{A}/s$, while the conductance, at a 50 mV bias, is monitored. Measurements at 1-300 mV gave similar results [8]. We emphasize the impressive stability of the electrodes, resulting in a drift below 0.3 pm/h. Our break junctions are calibrated using Gundlach oscillations [9, 10]. We find an attenuation factor $r = (5.4 \pm 0.6) \cdot 10^{-5}$ [11, 12], and a work function $\phi = 5eV$.

4.3 Training the apex of the electrodes

The details of our 'training' method are as follows. When closing the electrodes, we stop immediately as soon as the electrodes are in contact, i.e. at $G \approx G_0$,

preventing further disorder. Subsequently, we break the wire, extend it 1-2 $\mathring{A}$ into the tunnelling regime and close it again until the jump to contact. Repeating this procedure rearranges and orders the tip atoms. In this way, the atoms are able to probe (energetically and spatially) different positions, allowing them to find the most stable configuration. Remarkably, after typically >10 sweeps, JC and JOC occur at two *exactly* reproducible positions. In Fig. 4.1, four subsequent traces are shown with perfect repeatability. In fact, the maximum variation in the closing and opening points was less than 5 pm over 50 sweeps. Although these loops (which we call 'G_0-loops') have already been observed by other groups [4, 13], we are the first to optimize the training method to investigate JC and JOC in well-defined geometries. We have measured 734 different G_0 loops, on 8 different samples, to study the variation in the contacts. To obtain a new G_0-loop, we first rearrange a contact by closing up to $> 10G_0$, before training the contact for a different G_0-loop. For each G_0-loop, we automatically record the four conductance values G_a, G_b, G_c en G_d (at points a,b,c and d in Fig. 4.1, respectively). The fact that 85% of the conductance values G_c is above $0.9G_0$ emphasizes the good definition of our junctions. Recently, Untiedt *et al.* studied JC (no 'training' method was employed) [14]. A statistical analysis was made of many closing traces and correlations were found between the conductance values just before and just after JC (G_a and G_b). For gold, they observed maxima in density plots below 1 G_b and around 1.6 G_0. Conductances below 1 G_0 were attributed to a dimer configuration, whereas higher conductances were related to monomer and double bond configurations. We have also observed the peak around 1.6 G_0 for untrained junctions. However, upon breaking G dropped in steps to lower conductances, making it impossible to create stable 'G_0-loops' for this configuration. Furthermore, for our trained contacts, more than 80 % of our G_b values have a conductance below 1.02 G_0. Therefore, we conclude that training of the contacts results predominantly in the dimer configuration, as sketched in Fig. 4.1. Also from molecular dynamics simulations, dimers are expected to be the most stable geometry [14, 15].

4.4 Modeling the electrode system

Since for the trained contacts all plastic deformation is removed, we can employ an elastic model to describe the hysteretic loop in Fig. 4.1. The basic configuration is shown in the inset of Fig. 8.6, where a dimer is depicted in between two elastic

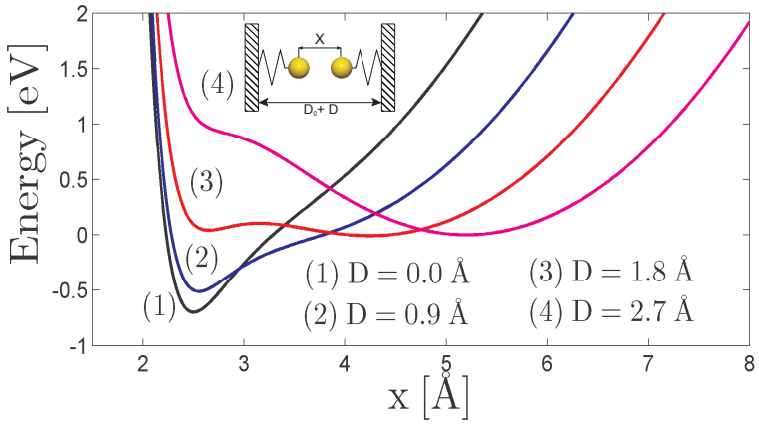

Figure 4.2: *Total energy as a function of the inter-atomic distance x of a gold dimer, for different electrode separations D (see inset; D_0 denotes an offset distance). Two contributions are included: one due to the springs (spring constant k) and one due to the dimer (described by the 'universal' binding curve). Depending on D, the total energy may have two minima. For the atom to jump in and out of contact, a barrier has to be overcome. Hence, opening and closing occurs at different positions, explaining the hysteresis in G_0 loops. Note: same parameters as in Fig. 4.1.*

electrodes. To describe the force between the two atoms, we use the so called 'universal' binding curve, which is given by [16, 17, 18]

$$E(x) = -\alpha(x - x_0)e^{-\beta(x-x_0)} \tag{4.1}$$

where x is the interatomic distance. The parameters α, β and x_0 are related to the equilibrium bond distance $d = x_0 + 1/\beta$, the binding energy $E_b = -\alpha/\beta e$ and the slope at the inflection point $F_0 = \alpha/e^2$, with $e = 2.718$. These values are known from literature, i.e., $d = 2.5 \pm 0.2\mathring{A}$ [10], $F_0 = 1.5 \pm 0.3nN$ for the break force [19] and $E_b = 0.7 \pm 0.2eV$ for the binding energy [13]. For the bonding energy of the dimer to the rest of the electrodes (the "banks"), we take the potential energy of a spring ($ku^2/2$). Hence, we are left with only one free parameter, the spring constant k, which is directly related to the hysteresis of the G_0-loop. In Fig. 8.6, the total energy is plotted versus the interatomic distance x, for different electrode distances D. Depending on D, two minima are present. When starting with a closed contact in equilibrium, i.e. D=0 $\mathring{A}$, the equilibrium interatomic distance equals $x_{eq} = 2.5\mathring{A}$ (minimum of curve 1). As the electrodes are pulled apart, e.g., by 1.8 $\mathring{A}$ (curve 3), the two atoms are separated by only 0.2

$\mathring{A}$. The rest of the displacement is invested in stretching the spring. Increasing D further (towards curve 4), the first minimum disappears and the system jumps to the second minimum (at $x_{eq} \approx 5.3\mathring{A}$); this is JOC. The atoms of the dimer get separated by typically 2-3 $\mathring{A}$. Upon closing the junction, a linear relation between x_{eq} and D is initially seen. However, at small separations, the spring stretches somewhat due to the attractive forces of the opposing atoms, i.e. x_{eq} moves faster than D[13, 20]. This gives a deviation from exponential tunnelling, as observed in Fig. 4.1. The effect is maximal just before JC, which takes place in between curves 3 and 2, and covers a distance of $\approx 1\mathring{A}$. To apply our model to the tunnelling part of the G_0-loops, we assume that the work function, ϕ, does not depend on x_{eq}, so that $G \propto exp(-2x_{eq}\sqrt{2m\phi}/\hbar)$. Taking $G = G_0$ for $D = 0$, we have the tools to fit the data in Fig. 4.1. The corresponding trace is shown in Fig. 4.1. It gives a perfect fit, not only to the exact position of JC and JOC, but also to the deviation from exponential tunnelling. For this G_0-loop, the fit parameter k assumes a value $k = 15.7$ N/m.

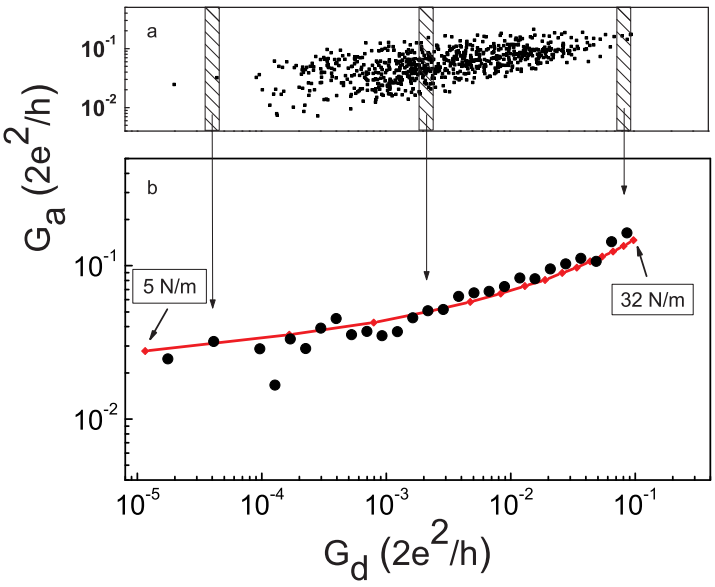

Figure 4.3: *(a) Conductance G just before JC (G_a) vs. G just after JOC (G_d) for 734 different G_0-loops. (b) Average G_a as a function of G_d. Averaging is done within regular bins of G_d, as indicated in a). The line is a fit to the model, assuming a varying spring constant $5 < k < 32$ N/m. The other parameters are the same as in Fig. 4.1 and 8.6.*

4.5 Statistics on the jumps to and out of contact

In total, we studied 734 G_0-loops, which could all be fitted with the model. In Fig. 4.3, the conductance G_a (just before JC) is plotted versus G_d (just after JOC), for all G_0-loops measured. Remarkably, the graph shows a relation between these points. This is especially visible in Fig. 4.3b, where the average G_a is displayed versus G_d. We compare these data points to our model. By varying the elasticity k from 5-32 N/m, with all other parameters fixed to literature values, one obtains the line drawn in Fig. 4.3. Clearly, the data points are well described by the model, using only k as a variable. Note that the range of k-values is in agreement with Ref. [13]. Moreover, $>$ 90 % of our k values (per electrode) are in the range 7-26 N/m. This variation is substantially smaller than the spread found in Ref [13]. We relate the spread in k to the following phenomena. First, breaking a gold wire is only possible along certain crystal orientations ([111], [100] and [110]) [21]. For each orientation, the apex atom is bonded differently to the second layer of the electrode. In fact, the apex atom has 3, 4 and 5 nearest neighbors for the Au [111], [100] and [110] direction, respectively. This is expected to have substantial influence on the elasticity of the electrode. However, this picture is not yet complete. The work by Olesen implies that k is only partly determined by the nearest neighbors of the apex atom [22]. In fact, the most significant contribution to k arises from elastic displacements in the rest of the metal tips. Hence, k is related to the precise structure of the electrodes on a larger scale, which varies with each G_0 loop. Every time we close the junction up to 10 G_0, we most likely introduce defects in the atomic layers further into the contact [23], which influence the elasticity of the electrodes. A final source of variation is the so-called "lateral approach" of the electrodes. For the model in Fig. 8.6, we assumed that the apex atoms are perfectly aligned. However, small misalignments (0-1 $\AA$) may occur in reality. We extended the 1D model to a 2D model by assuming springs in both x and y directions. This yields a variation in k of up to 10 %. We stress that the other parameters in our model cannot explain the data in Fig. 4.3. Only the spring constant gives a relation along the direction shown. The variation in the vertical direction (Fig. 4.3a), however, can be explained by small deviations in E_b. As indeed shown by Ref. [16], E_b is sensitive to the local atomic configuration. We find that a spread of 25 % in E_b explains the variation in G_a. Such a spread is consistent with the results of Ref. [13]. We conclude that our relatively simple model does not only explain the occurrence of JC and JOC, but also their relationship. Finally, we emphasize

that without 'training', atomic reorganization upon opening and closing destroys the interdependence between G_a and G_d.
Remarkably, our model fits the data in Figs. 4.1 and 4.3 very well, despite the fact that we assume a constant barrier height ϕ for all x_{eq}. This contrasts computations by Lang which predict a strong decrease of the apparent barrier at electrode distances $< 4\mathring{A}$ [24]. Such barrier lowering would primarily be due to the image forces and local effects related to the electric charges on the electrodes. Olesen *et al* carefully examined the tunnel curves of Ni, Pt and Au by scanning tunnelling microscopy (STM) and found no deviations from exponential behavior. This was explained by assuming that barrier lowering is exactly cancelled by adhesion between tip and sample [22]. The fact that we can fit our G_0-loops using an elastic model only, shows that the influence of image forces in break junctions (which feature two sharp tips) is relatively small.

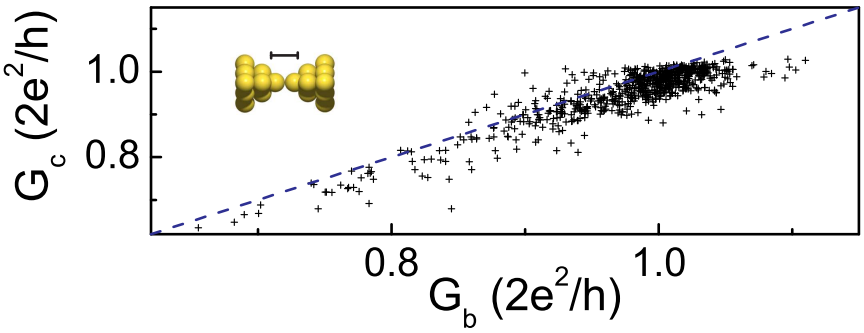

Figure 4.4: *(a) Conductance just before JOC (G_c) vs. G just after JC (G_b) for 734 different G_0-loops. The dashed line represents $G_c = G_b$. Inset: schematic junction; scale bar: barrier length for tunnelling.*

4.6 Conductance channels in a single atom contact

Having described three quarters of the G_0-loop (JOC, tunnelling and JC), we focus on the contact regime. In Fig. 4.4, G_c is plotted versus G_b. In all cases, we have $G_c \leq G_0$, as expected for the conductance of a single atom contact. In contrast, the values of G_b go well above 1 G_0. On average, G_b is 0.025 G_0 higher than G_c. This is exactly as expected, if a second conductance channel is

considered. As calculated by Ref. [15], the small distance between the second layers of the two electrodes allows for tunnelling with a conductance of at most 0.03 G_0. When stretching the contact, however, the tunnel gap increases and the transmission of the second channel tends to zero. This is why it is not visible in G_c, where the contact is fully extended.

4.7 Conclusions

In summary, we have created highly ordered gold electrodes, using a "training" method. Upon opening and limited closing, our junctions show no plastic deformation, allowing us to study the jump out of contact, tunnelling curves and jump to contact in detail. Individual breaking and making loops can be perfectly fitted with an elastic model, having the spring constant of the electrodes, k, as the only free parameter. Hence, by suppressing plastic deformation effects, we are able to measure and model adhesion on the single atomic level.

This work was financed by the Nederlandse Organisatie voor Wetenschappelijk onderzoek, NWO, via a Pionier grant, and the Zernike Institute of Advanced Materials. We thank Simon Vrouwe, Siemon Bakker and Bernard Wolfs for technical support and Jan van Ruitenbeek for useful discussions.

References

[1] M. Dienwiebel *et al*, Phys. Rev. Lett. **92**, 126101 (2004); A. Socoliuc *et al*, Science **313**, 207 (2006);

[2] N. Agraït, A. Levy-Yeyati and J.M. van Ruitenbeek, Phys. Rep. **377**, 81 (2003).

[3] J.K. Gimzewski and R. Møller, Phys. Rev. B **36**, 1284 (1987).

[4] J.M. Krans *et al*, Phys. Rev. B **48**, 14721 (1993).

[5] G. Rubio, N. Agraït and S. Vieira. Phys. Rev. Lett. **76**, 2302 (1996).

[6] A.I. Yanson *et al*, Nature **395**, 783 (1998).

[7] J. Moreland and J.W. Ekin, J. Appl. Phys. **58**, 3888 (1985).

[8] C. Sirvent *et al*, Physica B **218**, 238 (1996).

[9] O.Yu. Kolesnychenko *et al*, Physica B **291**, 246 (2000).

[10] C. Untiedt *et al*, Phys. Rev. B **66**, 85418 (2002).

[11] S.A.G. Vrouwe *et al*, Phys. Rev. B **71**, 035313 (2005).

[12] M.L. Trouwborst *et al*, to be published.

[13] G. Rubio-Bollinger, P. Joyez and N. Agraït, Phys. Rev. Lett. **93**, 116803 (2004).

[14] C. Untiedt *et al*, Phys. Rev. Lett. **98**, 206801 (2007).

[15] M. Dreher *et al*, Phys. Rev. B **72**, 075435 (2005).

[16] S.R. Bahn and K.W. Jacobsen, Phys. Rev. Lett. **87**, 266101 (2001).

[17] J.H. Rose, J. Ferrante and J.R. Smith, Phys. Rev. Lett. **47**, 675 (1981).

[18] J.M. Krans, PhD thesis, Leiden University (1996).

[19] G. Rubio-Bollinger *et al*, Phys. Rev. Lett. **87**, 26101 (2001).

[20] W.A. Hofer *et al*, Phys. Rev. Lett. **87**, 236104 (2001).

[21] V. Rodrigues, T. Fuhrer and D. Ugarte, Phys. Rev. Lett. **85**, 4124 (2000).

[22] L. Olesen *et al*, Phys. Rev. Lett. **76**, 1485 (1996).

[23] I.K. Yanson *et al*, Phys. Rev. Lett. **95**, 256806 (2005).

[24] N.D. Lang, Phys. Rev. B **37**, 10395 (1988).

Chapter 5

Molecular heating in hydrogen-gold junctions

Abstract

In this chapter, we present conductance measurements on hydrogen-gold junctions. By fast data acquisition, a strong hysteretic behavior is observed, starting exactly at the hydrogen vibration frequency. We show that this is related to a substantial heating effect, triggered by vibrational excitations of the hydrogen molecule. Hence, our results give new insights in the influence of molecular vibrations on the conductance properties of molecular junctions.

5.1 Introduction

One of the most important issues in molecular electronics is the coupling between the molecule and the metallic electrode. The coupling does not only determine the conductance of the molecular system, but also the local temperature of the system. Theoretical studies have shown that molecules could heat up by several hundreds of Kelvin, under bias voltages below 1 V (see for example Ref. [1]). Only recently this has been confirmed experimentally on C60 molecules. These molecules can thermally degrade when brought into resonance by a bias voltage [2].

In this chapter we present an experimental study of heat dissipation in a system where molecular hydrogen is contacted between two gold electrodes. By first

This chapter is based on Ref. 3 on p. 147

vibrationally exciting the molecules, and subsequently measuring the response time for releasing this vibrational energy, interesting effects appear. Surprisingly, response times of 200 ms are observed, for the system to return to equilibrium. These relatively large response times are explained by a substantial heating effect, triggered by inelastic excitations of the hydrogen molecules. We will start, however, with a short overview on the vibrational spectra of molecules, contacted in between two electrodes.

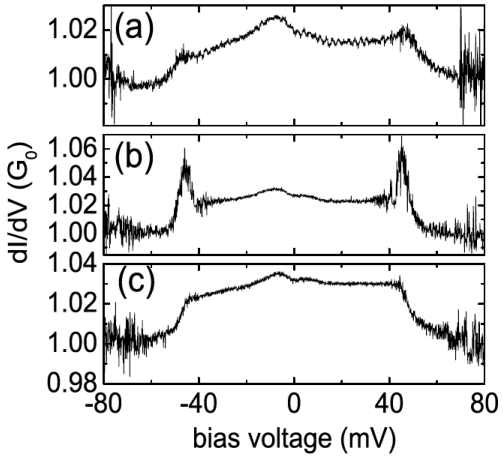

Figure 5.1: *Differential conductance spectra on a single deuterium molecule, contacted by platinum electrodes. The electrodes were moved apart 0.1 Å and 0.2 Å in figure (b) and (c) respectively, as compared to figure (a). In all figures, the step in conductance can be observed, around the hydrogen vibration frequency. In figure (b), an extra feature occurs, a spike in dI/dV. Measurement is taken at 4.2 K by Thijssen et al, Ref. 4.*

5.2 Literature: vibrational spectra of molecules

5.2.1 Spikes in the differential conductance

As first shown by Smit *et al*, the vibration mode of a single hydrogen molecule can be clearly observed by point contact spectroscopy [3]. When the applied voltage is equal to $\hbar\omega$ (where ω is the vibration frequency), the reflectivity of the contacts is enhanced, leading to a step down in the differential conductance [16]. An example is given in Fig. 5.1(a), showing a decrease in dI/dV around 40 meV (measurement by Thijssen *et al*) [4]. However, at the same time, another effect can show up, leading to a spike in dI/dV (as shown in Fig. 5.1(b)). We emphasize

that this effect can be much larger than the conductance step (> 100% versus typically <5 % for PCS), and can result in a peak or dip feature in the differential conductance. These anomalies are the key ingredient of our experiments.

Interestingly, the spikes are observed on a large variety of molecular systems. For example, peaks or dips in dI/dV have been reported on STM and MCBJ systems, with Au, Ag, Pt, Ni, NiAl, or Cu as the metallic contact. Also, the anomalies have been observed on a large number of molecules, like O_2, C_2H_2, CO, H_2O, H_2, D_2 and pyrrolidine molecules [5, 6, 7, 9]. An example is shown in Fig. 5.2, where a pyrrolidine molecule (C_4H_8NH) on a copper [001] surface is measured with a STM. A strong dip in dI/dV was observed around 400 mV, which was ascribed to the vibration energy of the molecule; when the hydrogen atoms in the molecule are substituted for deuterium, the energy of the vibration decreases, as expected by the higher mass of D_2 (lower graph). This relation has also been observed by Thijssen *et al.* For H_2 on gold, the spikes were always observed around 41 meV, while for D_2 the spikes were found around 29 meV (as shown in Fig. 5.4(a)). This $\sqrt{2}$ difference is exactly as expected, since the vibration frequency scales with the mass by $\sqrt{k/m}$. Furthermore, spikes can only be observed for certain vibration modes. In the case of H_2 and D_2, only the transversal vibration mode shows the anomalies, and no spikes are observed for the longitudinal modes [4]. Finally, two other examples from Thijssen *et al*, are the measurements on Co-Pt and $Au - H_2$, as shown in Fig. 5.3. We note that for both systems, both dips and peaks are observed, depending on the contact.

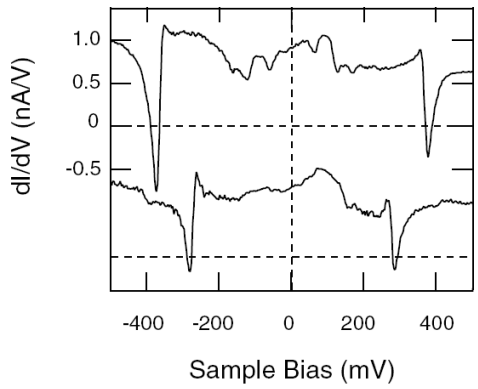

Figure 5.2: *Upper graph: dI/dV spectrum, taken with an STM, for a pyrrolidine molecule on a Cu[001] surface, taken at 7 K. Lower graph: Spectrum taken on a similar molecule, where the hydrogen is substituted with Deuterium. Note that the spectra are obtained by averaging over > 100 scans, which also averages out the fluctuations around the dip in conductance. Picture from Ref. 7.*

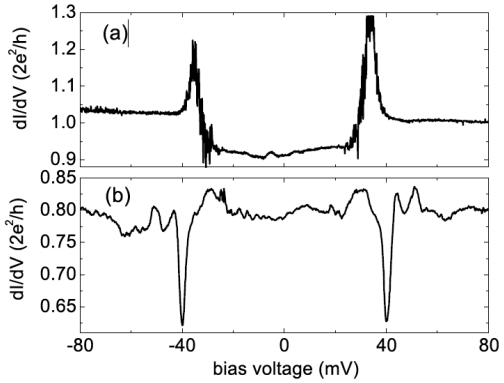

Figure 5.3: *Upper graph: dI/dV spectrum of a CO molecule, contacted with Pt electrodes. Lower graph: dI/dV spetrum of a $Au - H_2$ contact. Both figures are measured with a MCBJ at $\approx 4.2K$. Picture from Ref. 5.*

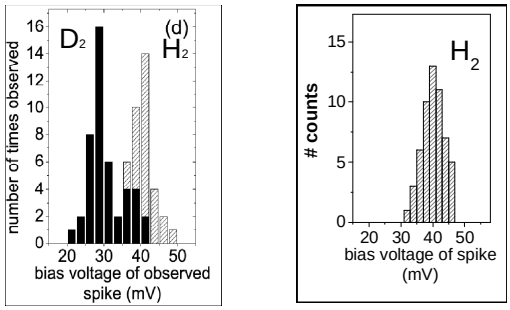

(a) (b)

Figure 5.4: *(a) Histogram, as measured by Thijssen et al, on the position of the spike, for different contacts. For hydrogen, the average position is 41 meV, and when the measurements are repeated on D_2, the position is shifted to 29 meV. This is exactly a $\sqrt{2}$ difference, as expected by the mass ratio. Picture from Ref. 4. (b) Position of spikes, as measured by us, on 6 different samples. The average voltage is 40.5 mV. Clearly, the average position of the peak is equal to the H_2 vibration frequency (41 meV).*

To summarize the observations, we describe the four characteristic features of the spectroscopic anomalies. First, the position of the peak is equal to the position of the (regular) conductance step. This shows that the spike is related to molecular vibrations. A second observation is the increase of electrical noise, at the conductance spike. Third, the observed features can be a peak or a dip in the conductance. And finally, the appearance of the peak strongly depends on

the exact morphology of the contact, and on the distance between the electrodes (as shown in Fig. 5.1).

5.2.2 Literature: proposed explanation for the spectroscopic anomalies

Although the exact mechanism which drives the anomalies is not yet understood, in the past years, a number of models were suggested to fit the corresponding data [4, 6, 9]. For all models, a two level system is suggested, which explains the increase in noise around the conductance spike. The idea is as follows: When the molecule is vibrationally excited, the molecular energy increases, resulting in a larger spatial freedom of the molecule. Hence, it can hop to a neighboring (lattice) position. Since this second position can have a higher or lower conductance than the first position (at V$< V_{\hbar\Omega}$), a peak or dip can be observed in the differential conductance respectively. Furthermore, the cross-over between these two conductance levels can be gradual, when assuming that the molecule hops back and forth in between the two levels. This then results in an apparently smooth transition, when the hopping process is faster than the bandwidth of the electronics. Finally, we note that, even though the two level models can fit the data, the exact physical origin of the relaxation rates (from one level to the other) is not yet understood.

5.3 Experimental details

For our measurements, we focus on the spikes in dI/dV, on $H_2 - Au$ chains. The procedure is as follows: First, the break junction is opened in cryogenic vacuum, at 4.2 K, and the electrode tips are "trained" (see chapter 4). Subsequently, high purity hydrogen gas (99.999 %) is introduced into a space of $\approx$1 cm^3 volume (at a pressure of $\approx$1 mbar). This space has two valves; 1 connected to the hydrogen vessel and pump, and one valve connected to the insert. Hence, after repeatedly flushing the space with hydrogen gas, the content of the space is brought into the insert. This ensures us to have only a small number of molecules ($<$1 μmol) in the chamber. Next, we wait for one hour for the hydrogen molecules to cool down. Subsequently, the junction is closed and slowly opened again to stimulate the formation of $H_2 - Au$ chains (the pulling is done with a speed of $\approx$5 pm/s). Meanwhile, IV curves are recorded, real time, by sweeping the voltage using a triangular waveform of 1 Hz (amplitude is in between 90 and 100 mV). Hence,

steps in the IV curves can be easily recognized, giving enough time to stop the pulling of the electrodes, and to start characterizing the contact. Two examples are plotted in Fig. 5.5, showing a peak and dip feature around 40 mV. For a statistical analysis on many different contacts the wires are broken, subsequently brought into contact again (to conductance values of $> 5\ G_0$), before starting the pulling process over again. In total, we have measured 56 different contacts, on 6 different samples. From all the measurements, we collected the position of the spikes into a histogram, as shown in Fig. 5.4. The average position of the peaks is 40.5 mV, which is the typical value for the hydrogen vibration frequency (around 41 mV, as shown in Fig. 5.4(a)). The zero bias conductance of the contacts varied in between 0.001 and 1 G_0, which are typical conductance values for $H_2 - Au$ chains [11] (see Fig. 5.6). Furthermore, most of the measurements ($\approx$ 85 %) showed a peak in conductance, at $eV = \hbar\omega$, while the rest showed a dip feature.

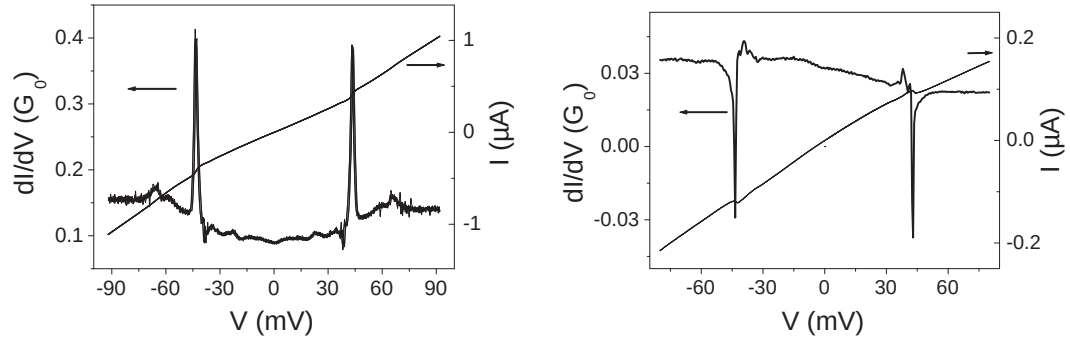

(a) (b)

Figure 5.5: *Two examples of spikes in the IETS spectra, measured on a $H_2 - Au$ contact (relatively slow measurement). Both the current as the differential conductance are plotted, which are measured simultaneously. Note the negative differential conductance for the right plot. Dwell time is 500 ms, $V_{ac} = 0.5$ mV, step size is 0.5 mV. Temperature is $\approx$ 4 K.*

5.4 Hysteresis effects in $Au - H_2$ junctions

5.4.1 Hysteresis in IV measurements

Let us now return to Fig. 5.5. Clearly, the observed spikes in dI/dV have a much larger amplitude than the regular vibrational steps in dI/dV (typically

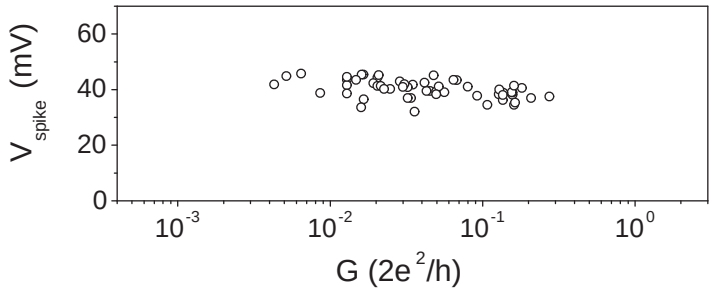

Figure 5.6: *Position of the spikes as a function of zero bias conductance of the contact (in total, 56 different contacts are measured).*

$\geq$200% versus $\leq$5%). To measure the small steps in dI/dV, one uses a standard lock-in technique, to average out any electrical noise. However, this technique needs a relatively long averaging time for each data point. In contrast, the dips and peaks have a much larger amplitude, and can already be observed from the IV measurements. This makes it possible to acquire the data directly by IV measurements, using a much faster data acquisition. Hence, we have the unique opportunity to investigate the decay times of vibrational excitations of single molecules.

A typical example of such a measurement is shown in Fig. 5.7. Here, the current is recorded, while sweeping the voltage with different time scales. Surprisingly, we find that time plays an important role in the conductance spikes. For the lower trace, measured over 10 s (0.1 Hz), no hysteresis is observed. However, when sweeping the voltage faster, a hysteresis effect shows up, exactly at the vibration frequency. In other words, the system needs time to fall down from the upper to the lower conductance state. Remarkably, when the voltage is sweeped even faster, in 100 ms (10 Hz), the system has not enough time to relax to the lower conductance state, and stays in the upper state. These unexpected results are the main focus of this chapter.

We emphasize that the hysteresis effect is not an artifact of our electronics. This is simply shown by the fact that the system responds immediately at the turning points (at V $=\pm$ 100 mV), and the observation of two level fluctuations (as will be shown in section 5.6). Finally, we stress that the method of fast data acquisition has not been used before on these measurements, which explains that we are the first to observe the hysteresis effect. Even the lower curve, showing almost no hysteresis and measured with 0.1 Hz, is recorded faster than typically used for PCS measurements (for PCS, one uses acquisition rates of minimum 20

s (0.05 Hz) for a full trace) [5].

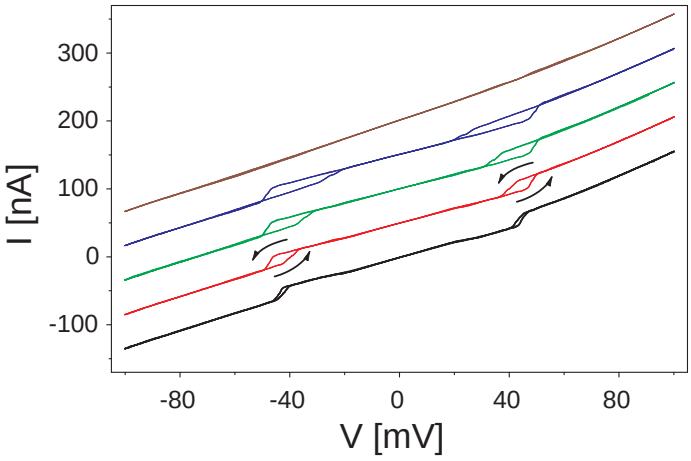

Figure 5.7: *Hysteresis while sweeping the voltage with 0.1 Hz (lower curve), 1 Hz, 2 Hz, 3 Hz and 10 Hz (upper curve). For clarity, the upper traces are shifted by 50 nA each. Sample rate is 10.000 data points per second, with an averaging time of 100 µs for each data point. Temperature is ≈ 4 K. Each trace consists of 3 voltage sweeps, showing the perfect reproducibility.*

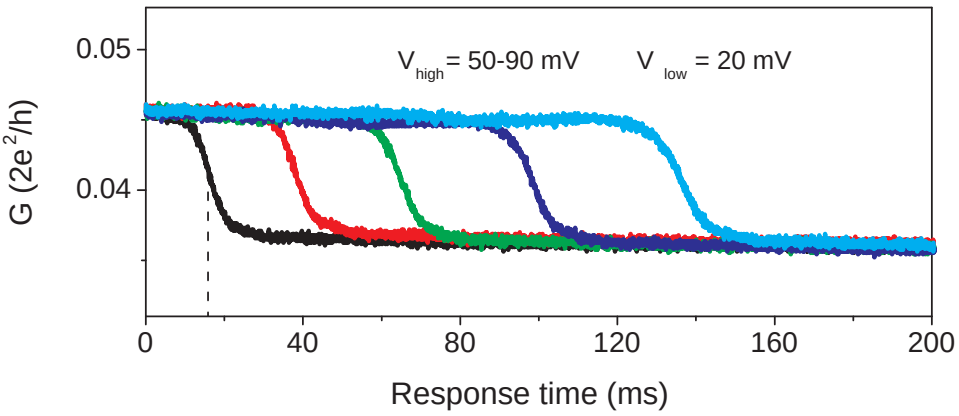

Figure 5.8: *Response of pulsing the voltage around the conductance step. At t=0, the voltage is dropped from a initial voltage ($V_{high} > V_{\hbar\omega}$), to a low voltage ($V_{low} < V_{\hbar\omega}$). For this measurement, V_{low} is constant and is set to 20 mV. The initial voltage is 50 mV (first curve), 60, 70, 80 and 90 mV (last curve).*

5.4.2 Pulse response

To further investigate the hysteresis, we use voltage pulses to record the response times. An example of such a measurement is shown in Fig. 5.8. Here, the voltage was set to a certain voltage above the anomaly, defined as V_{high}. The conductance is now in the upper state. After 1 second, long enough to reach equilibrium, the voltage was instantly dropped to a certain voltage below the anomaly, in this case 20 mV (defined as V_{low}). Meanwhile, the conductance is measured, as a function of time. Let us first consider the trace with V_{high} =50 mV. The time scale is defined as the time after the voltage drop (to $V = V_{low}$). Clearly, the system does not respond immediately. Only after about 10 ms, the conductance starts to drop to the lower state. This relatively large hysteresis time is an indication of an heating effect close to the contact. Remarkably, when these measurements are repeated for different initial voltages, strong differences are observed in the response time. This occurs even though the initial voltage is well above the vibration frequency.

To compare the effect for different contacts and initial voltages, the typical decay times were measured. This decay time is defined as the time where the conductance has dropped halfway (as depicted by the dotted line, which gives a decay time of 16 ms). We have plotted these decay times, for 4 different contacts, as shown in Fig. 5.9(a). Clearly, the process has an onset around 40 meV and the decay times strongly increase at higher voltages. Apparently, a heating process is initiated around the vibration frequency of the hydrogen molecule. This effect is even more pronounced in Fig. 5.9(b). Here, the results are shown on a similar measurement. However, now V_{high} is constant, and V_{low} is systematically varied. Close to the vibration frequency, the response time increases dramatically. Apparently, the observed heating effect is somewhat broadened towards lower voltages. Here, we note the similarity of the two plots 5.9(b) and 5.4(b). Both curves have approximately the same broadening around 40 mV.

Let us now focus on the relation between the decay times and applied bias voltage (as depicted in Fig. 5.9(a)). Actually, since the exact conductance value varies for each data point, also the injected current differs for each voltage pulse. Hence, to compare the data, one could divide the decay times by the total injected current. This result is given in Fig. 5.10(a). Interestingly, the decay times, corrected for the injected current, have a linear relation with the applied voltage. Moreover, the origin of the linear relation is equal to the position of the spectroscopic anomaly (and so the energy of the vibration mode). Thus, when taking into account the different vibration energies of each contact, one can plot the

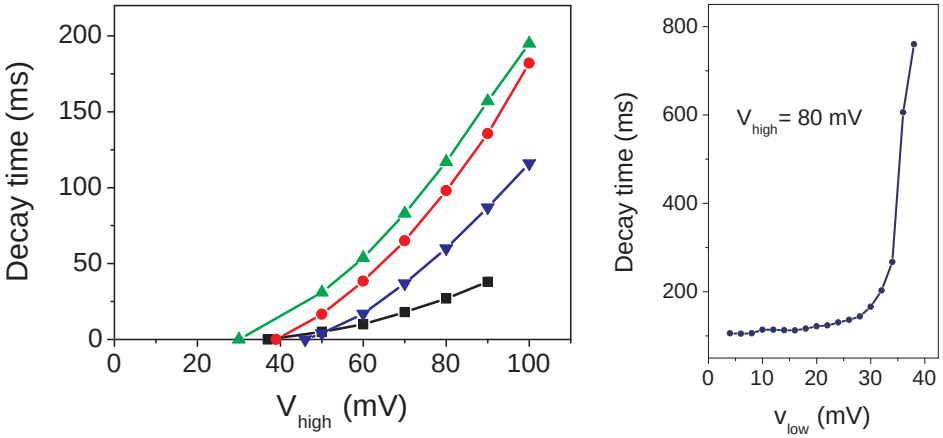

(a) (b)

Figure 5.9: *(a) Decay times as a function of the initial voltage, for 4 different contacts (V_{low} = 20 mV.) The contacts have a conductance of, from lower to upper curve, 0.015, 0.044, 0.048 and 0.058 G_0 (at 50 mV). (b) Decay times as a function of the final voltage. The initial voltage, V_{high}, was set to 80 mV. For this sample, the spike in dI/dV occurred at 39 meV.*

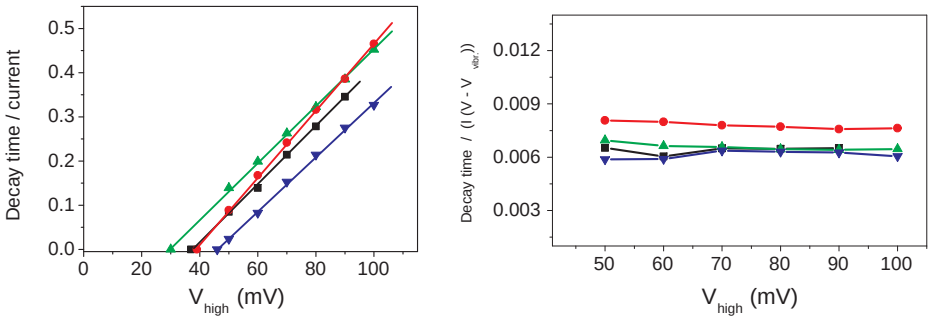

(a) (b)

Figure 5.10: *(a) Decay times, divided by the total injected current during the pulse, including linear fits (Same data as in Fig. 5.9(a)). (b) Same data as in Fig. 5.9(a), but now divided by $I \cdot (V - \hbar\omega/e)$.*

decay times divided by the relation $I \cdot (V - \hbar\omega/e)$. This results in an almost constant decay, independent of the conductance of the contact (varying in between 0.015 G_0 and 0.058 G_0), or the energy of the vibration mode (between 30 and 46 meV) (see Fig. 5.10(b)). This important result can be used for understanding the observed hysteretic behavior of the hydrogen-gold junctions, and will be further discussed in section 5.6.

5.5 Temperature dependency of the conductance spikes

In the previous section, we suggested a heating effect to explain the observed hysteresis. To investigate the relation with the bath temperature (temperature of the electrodes), the temperature of the insert was varied systematically. This was done by slowly lifting the insert above the helium level, thereby warming up the entire insert. The result is plotted in Fig. 5.11. Surprisingly, the position of the anomaly shifts towards higher voltages, with increasing temperature (up to 80 mV at 8 K.). A similar effect was observed by Kubatkin *et al*, on C60 molecules in between gold electrodes [10]. Here, a step in the current was measured, which shifted from 40 mV (at 4 K) to 90 mV (at 8 K). Cooling down from 4 K to 2 K did not change the position of the step. Instead, the position of the step saturated close to 40 mV. Since their results are similar to ours, and hydrogen can easily show up as an impurity, we suggest that their data could also be related to molecular hydrogen.

We emphasize that it is difficult to draw conclusions from the observed temperature dependency. When raising the temperature, many different effects occur, like electron and phonon heating of the gold electrodes, a strong increase of partial pressure of the hydrogen, and decreasing electrode separation. Nevertheless, it is interesting that the shape of the hysteresis is not effected by the temperature. Finally, we note the similarity between our observations and the STM experiments by Gupta *et al* [6]. Here, a step in current was observed for H_2 on a Cu surface, which shifted towards higher voltages when increasing the hydrogen pressure in the system. However, it is difficult to separate the two effects of hydrogen pressure and electrode temperature. Especially in an STM setup, high gas pressures can cause a strong thermal coupling between the STM tip and other (room temperature) parts of the cryostat. This can result in a higher temperature of the STM tip, in comparison with the surface temperature.

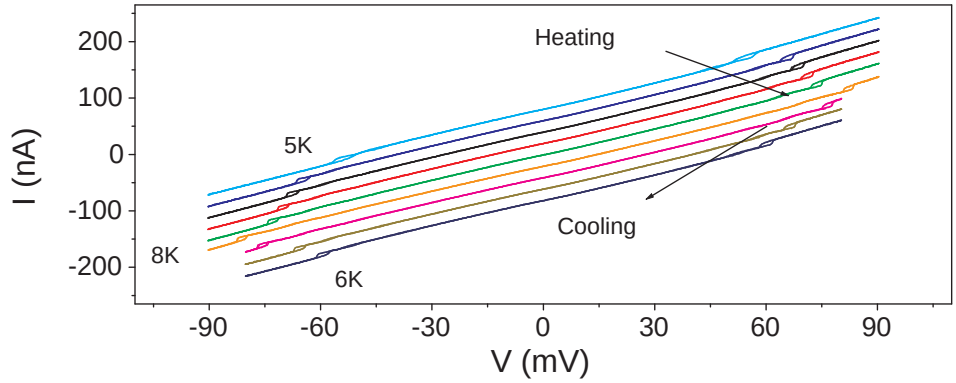

Figure 5.11: *IV measurements on a hydrogen gold junction, as a function of temperature. By heating the system to 8 K (middle curve), the step in current shifts towards higher voltages. When cooling down again, the anomaly returns to its initial value. For clarity, the curves are shifted with 20 nA each, relative to the middle curve. We estimate the measurement error for the temperature to be 2 K, due to uncertainties for the thermal coupling between sample and insert. Measurement is done by sweeping the voltage with 1 Hz and a sample rate of 10kS/s, with an averaging time of 100 µs for each data point.*

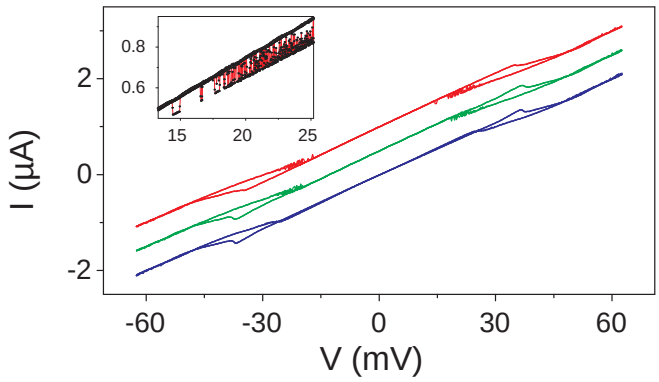

Figure 5.12: *Example of IV measurement, showing the origin of the peak structure. Measurement taken with 0.6 Hz (lower curve), 1 Hz and 1.4 Hz (upper curve) (curves are shifted 500 µA each for clarity). At faster voltage sweeps, clear two level fluctuations appear when decreasing the voltage. Inset: zoom in of the upper curve.*

5.6 Discussion of the experimental results

In section 5.4, we showed that the IV characteristics of $H_2 - Au$ junctions have a strong hysteretic behavior, at voltages above the vibration energy of the hydrogen molecule. Apparently, at $V \geq \hbar\omega/e$, a large amount of energy is put into the system, which needs a ms time scale to flow away into the electrodes. This observation is consistent with a heating effect. To quantify the observed hysteresis, we recorded the decay times for the system to return to equilibrium, as a function of the applied voltage. We found that the decay times are proportional to $I \cdot (V - \hbar\omega/e)$, where $\hbar\omega$ is the vibration energy of the molecule. Since I is proportional to V, by G, the relation can be rewritten as $G \cdot (V - \hbar\omega/e) \cdot V$. Furthermore, the number of electrons which are inelastically scattered is proportional to $G \cdot (V - \hbar\omega/e)$. This suggest that the decay times are proportional to the number of inelastically scattered electrons times the energy of each electron. However, a basic analysis of Inelastic Electron Tunneling Spectroscopy (IETS), would result in an energy of the inelastic electrons equal to $\hbar\omega$. Hence, a more advanced theoretical analysis is needed, for understanding the observed relation for the decay times. In this context, we note that we did not take into account any cooling effects. Since the molecular system is in equilibrium at the end of the voltage pulse, both heating and cooling effects should be taken into account.

To make it even more intriguing, we note here that the heating is related to a much faster two level process (as also proposed by others, and introduced in section 5.2). Even though most of the measurements show a smooth transition around $V_{\hbar\omega}$, an exceptional measurement is plotted in Fig. 5.12. When the voltage is sweeped relatively slow (lower curve), a smooth transition can be observed around 36 mV, with hysteresis. However, when sweeping faster as for the upper curve (resulting in less heating), two level fluctuations appear when going down in voltage. These two level fluctuations are also observed in measurements where the hydrogen is not contacted, but separated by a tunnel barrier (as will be shown in chapter 7). In the next section, we discuss two possible mechanisms which could give a qualitative explanation of our observations: a heating effect of the gold electrodes, or phonon heating of the hydrogen molecule(s).

5.7 Possible mechanisms

5.7.1 Heating of the electrodes

One could suggest that the observed current step is triggered by a critical temperature of the electrodes. In fact, the temperature of the gold lattice is expected to increase at high current densities. This was shown experimentally by Kolesnychenko *et al* [12]. Here, it was observed that the metal electrodes expand under large current densities (at power dissipations above 1 μW). When suddenly dropping the current, the electrodes cool down with a millisecond time scale (as shown on W break junctions). These relatively long cooling times were attributed to heating of the entire electrodes.

Nevertheless, we claim that electrode heating can not be the (main) responsible mechanism for our observations. The first argument is that the power dissipation during our measurements is relatively small (in the order of 10 nW). As shown by Kolesnychenko *et al*, any increase in electrode temperature can be observed directly by thermal expansion of the electrodes. For this purpose, we have performed reference measurements on bare gold tunnel junctions. In agreement with Ref. [12], the conductance of the tunnel junctions did not rigorously change for power dissipations up to 100 nW. Hence, the tunnel distance did not decrease by more than 1 pm. When we assume a heating length of 1 μm and a thermal expansion coefficient of 10^{-5} K^{-1}, an electrode expansion of 1 pm would coincide with a temperature increase of only 0.1 K. Clearly, this can not explain our observations.

The second argument is that the current step is always positioned around 40 mV, independent on the current density through the contact (see Fig. 5.6). This is also shown in Fig. 5.13, where IV measurements are plotted for different stretching configurations of the contact. Although the current density increases by more than 200%, the position of the step in current hardly changes. This proofs that the anomaly is not triggered at some critical electrode temperature. Furthermore, the temperature profile is not expected to change dramatically when an extra inelastic path opens (like the hydrogen vibration mode). Only a small number of electrons will be scattered inelastically ($\approx 5\%$). Hence, the total current will only slightly increase. Finally, the phonon coupling between a hydrogen molecule and the gold atoms is expected to be negligible (due to the large mass difference between the different atoms) [15]. Moreover, even in the hypothetical case of large phonon coupling, the temperature profile will only change locally. In

this case, the inelastic current would be dissipated close to the molecules, instead of within an distance equal to the inelastic mean free path (which is in the order of 200 nm). The heat conduction over such a small distance is expected to be a fast process. Especially at temperatures below 20K, where the thermal diffusivity of metals is orders of magnitude higher than at room temperature [12]. Thus, the cooling times are expected much faster than the observed ms decay time. To conclude, we claim that the observed heating effect can not be explained by an increase in temperature of the electrodes.

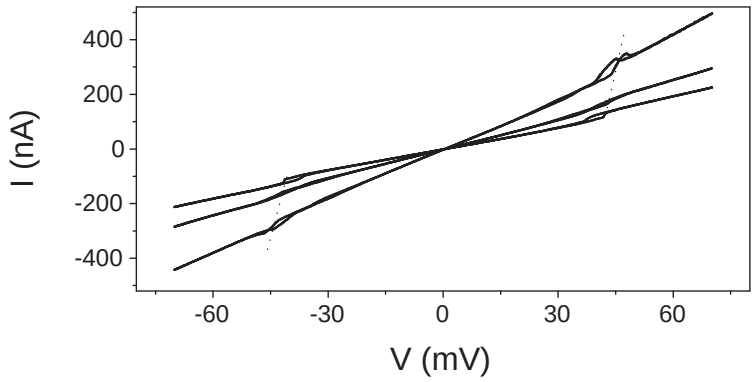

Figure 5.13: *Example of IV measurements, while stretching the junction. Although the zero bias conductance increases by more than a factor of 2, the position of the step in current changes only by 5% (from 41 to 43 mV). Hence, the vibration frequency is rather independent on the conductance of the junction. The voltage is swept with 1 Hz, and the junction is stretched relative to the lower curve, by 0.4 Å (middle curve) and 0.8 Å (upper curve).*

5.7.2 Molecular heating by vibrational excitations

In the previous section we discussed that the observed heating effect must be directly related to the hydrogen molecules. Therefore, we start with a discussion on the number of molecules which are involved in the heating process. In this context, we emphasize that the two level system is always observed around the hydrogen vibration frequency of 40 mV (independent on the sample, hydrogen exposure or conductance of the contact). This can not be explained by some critical energy of a much larger system. Instead, the critical voltage of 40 mV suggests that a small number of molecules (possibly even a single molecule) is responsible for the switching. Another indication for a small number of molecules

is that we have also measured IV curves with 2 or 3 current steps, each with their own onset voltages (but close to 40 mV).

On the other hand, we have observed extremely long decay times of more than 100 ms. While the lifetime of a vibrational excitation of a H_2 molecule on a metal surface is expected smaller than 1 ns. This indicates a large number of molecules.

Therefore, we suggest the following model. Let us assume a hydrogen molecule contacted between two electrodes, and that this system is surrounded by many other hydrogen molecules. When applying a bias voltage equal to $\hbar\Omega/e$, inelastic excitations will cause a vibration of the hydrogen molecule. Interestingly, this can result in a strong temperature increase of the molecule, exactly at a voltage $\hbar\omega/e$ (as shown in Fig. 5.14) [1, 8]. Subsequently, the molecule can release its vibrational energy by creating an electron hole pair, or by phonon coupling to the environment. As mentioned before, the phonon coupling between a hydrogen molecule and the gold electrodes is negligible, due to the large mass difference between H_2 and Au [15]. In contrast, the phonon coupling between identical molecules is expected to be a highly efficient process. Interestingly, this could result in heating of the entire cluster of hydrogen molecules. When now decreasing the bias voltage below the vibration energy, the entire cluster has to cool down. This thermal process could explain the observed decay times of typically 100 ms.

The process described above could even suggest a phase transition of a small cluster of molecules [6, 19]). In fact, the temperature during our measurements ($\approx 4K$) is close to the melting point of molecular hydrogen ($14K$). Moreover, the two level system disappears at temperatures above $25K$, which is equal to the desorption temperature of hydrogen (as observed experimentally). Thus, it is very well possible that (part of) the cluster of hydrogen molecules undergoes a phase transition, by heating of the cluster. This heating effect could be triggered by inelastic excitations of the molecules.

So let us discuss such a phase change in more detail. Obviously, there are two possible phase transitions. At voltages above $\hbar\Omega/e$ a transition could occur towards the liquid phase or a transition towards the gas phase. In the second case, the molecules would evaporate from the electrodes. However, there are indications that the gas phase is not reached during our experiments. First of all, we have observed that the contacts are not stable at much higher voltages. At voltages above 150 mV, the contacts show irreversible changes in the conductance. Since these changes are not observed for bare gold electrodes, the hydrogen molecules are expected to be still adsorbed on the electrodes (at voltages below 150 mV).

A second indication is formed by the reproducibility of the hysteresis and the relation of the decay times with bias voltage (as depicted in Fig. 5.10(a)). If the molecules would evaporate, the decay times would be given by some typical diffusion time for the molecules to return to the electrodes. This diffusion time would be independent on the initial voltage, something which is not observed. To conclude, we suggest that the observed heating process is probably related to a phase transition of the hydrogen molecules, from the solid phase to a liquid phase. To return to the solid phase (at voltages below $\hbar\Omega/e$), the entire cluster of hydrogen molecules has to cool down. This can be a time consuming process, thereby explaining the observed hysteresis effect.

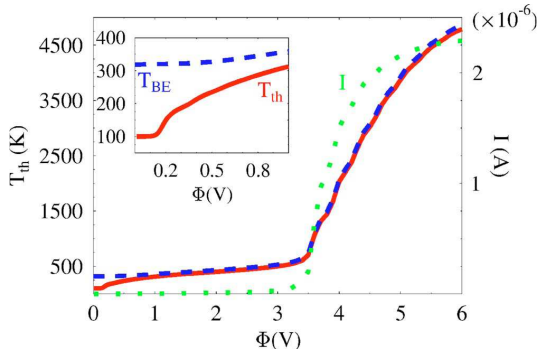

Figure 5.14: *Calculated molecular temperature, as a function of voltage over a molecular junction. For the modeling, one molecular level is included (at 2 eV above the Fermi energy), and 1 vibrational level at 0.2 eV. The temperature of the leads is set to 100 K. Note the sudden increase in temperature at voltages just above the vibration energy (see inset). Fig. from Ref. 1.*

5.7.3 Comparison with STM experiments

As already discussed in the introduction, spikes in dI/dV have also been observed in STM experiments by Gupta *et al* and, more recently, by Temirov *et al* [6, 19]. Here, hydrogen gas was admitted into a STM chamber, with a pressure around 10^{-8} mbar (leading to a much higher hydrogen exposure compared to our experiments). Interestingly, in contrast to our break junction experiments, the spikes already occurred at voltages of 10 mV. This difference in onset voltages could be explained by the experimental differences. For example, for our break junction experiments, the molecules are contacted in between the electrodes. In contrast, for the STM experiments, the electrodes are separated by a tunnel

gap, where the surface and STM tip are covered by the molecules. Hence, it is possible that for the STM measurements, the two level system starts by heating of an entire cluster. Indeed, the phonon excitation energy of a small cluster of molecules can can be as low as 10 meV [20]. Moreover, when considering a phase transition of the molecules, one would expect a strong relation with the hydrogen pressure in the system (especially for larger hydrogen exposures). This could result in a broad range of onset voltages for the two level system. We will return to this discussion in chapter 7, where we present experiments similar to the STM measurements.

5.7.4 Proposed two level system

In this section, we speculate about an alternative explanation for the two level system. This is done with the help of the measurement plotted in Fig. 5.15. Here, a H_2-Au contact is characterized by slowly pulling the electrodes. At first, two different conductance levels are observed, above and below $eV = \hbar\omega$. However, by stretching the junction, the system is left in the high conductance state, even at zero bias voltage. Thus, the change in conductance can be triggered in two ways, by vibrational heating or by stretching of the electrodes. This behavior is consistent with a spatial change of the molecule. Let us focus on a contact like the one drawn in Fig. 5.16(a). For simplicity, we assume a single molecule, although more molecules are expected in the vicinity of the contact. The molecule is connected to two gold electrodes, in a configuration perpendicular to the direction of the current flow. However, when stretching the electrodes, the hydrogen molecule will change to a parallel configuration (as drawn in Fig. 5.16(b)). As shown by DFT calculations by Barnett *et al*, this configuration indeed has a higher conductance [11, 21]. One can argue that this second configuration can also be reached by vibrational excitation of the molecule. For example, when considering the so called hindered rotation mode, the molecule has the tendency to rotate from the perpendicular towards the parallel configuration. At sufficient vibrational energy, this could result in a spatial change of the molecule, from a perpendicular to a parallel configuration. Furthermore, as shown by Barnett *et al*, the energy difference between the two states strongly depends on the stretching of the contact. And finally, the long decay times could then be explained by the weak phonon coupling between the light molecule and the much heavier gold atoms. Hence, cooling down of the molecule could be a relatively slow process.

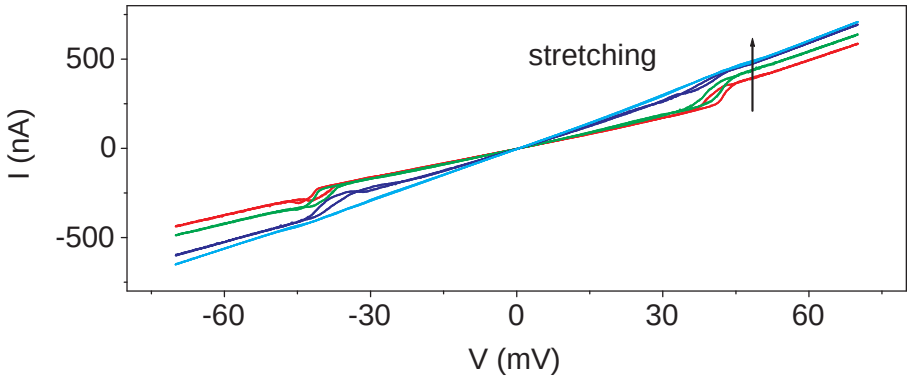

Figure 5.15: *Example of step in the current, while pulling the electrodes. When stretching the junction, the step disappears and the junction is left in the same conductance state as the level at higher bias, before stretching. Note that the zero bias conductance* ***increases****, while stretching the junction. This can be characteristic for a* $Au - H_2$ *chain [11]. In total, the junction is stretched 0.7 Å. The voltage is swept by 1 Hz.*

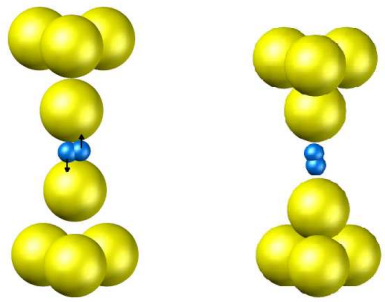

Figure 5.16: *Schematic model for the proposed two level system, showing the molecule at low voltage (a), and when vibrationally excited (b). In the initial state, the molecule is contacted in a configuration perpendicular to the direction of the current flow. In contrast, when the molecule is vibrationally excited, the molecular energy increases, possibly leading to a change from contact (a) to contact (b). The same change in configuration is expected when stretching the electrodes. Note that much more molecules could participate in the process.*

5.8 Conclusions

To conclude, we have investigated the vibration spectra of hydrogen molecules, contacted in between gold electrodes. By fast data acquisition, a large hysteretic behavior is observed, starting exactly at the hydrogen vibration frequency. Large hysteresis times up to 200 ms were observed, for the system to return to equilibrium. Our observations are an indication of a substantial heating effect of the hydrogen molecule(s), due to inelastic electron scattering. In detail, the hysteresis times were found to have a linear relation with $I \cdot (V - \hbar\omega/e)$, where ω is the vibration frequency of the hydrogen molecule. To understand this relation, and the relatively large hysteresis times, a more advanced theoretical model is needed. Possibly, the heating effect can be explained by a phase transition of a cluster of molecules near the contact, due to the efficient phonon coupling between identical molecules.

Finally, we emphasize the following: the observed peaks in dI/dV (related to molecular vibrations) are very similar to the ones one can observe when bringing a molecule intro resonance. Both features start at a certain voltage, can be symmetric in the voltage and can have identical amplitudes. Hence, when the energies of the vibration modes and molecular levels are unknown, it is difficult to separate or identify the two different mechanisms.

5.9 Future experiments

It is an intriguing result that the position of the conductance spike shifts upwards with increasing temperature (Fig. 5.11). It is unclear why this shift occurs. To investigate a shift in vibration frequency, we propose the following experiment. As plotted in Fig. 5.10(a), the vibration frequency can be measured indirectly by extrapolating the response times. By repeating the measurement (of the decay times) at higher temperatures, one can investigate whether the vibration frequency changes with temperature.

A second experiment we propose, is to repeat the fast IV measurements on other (organic) molecules. It is well known that the conductance of an organic molecule changes when brought into resonance [22, 23]. At the same time, it is expected that the molecular temperature strongly increases when a molecular level starts to participate (as shown in Fig. 5.14). Hence, it is possible that also for these molecular systems, millisecond decay times can be observed. We are

aware of one example from literature, also showing ms decay times. This was observed for the so called BPDN-DT switch [24]. The IV characteristics of this molecular switch were found to be strongly dependent on the measurement speed (at 100K).

References

[1] M. Galperin, M.A. Ratner and A. Nitzan, J. Phys.: Condens. Matter **19** 103201 (2007).

[2] G. Schulze *et al*, Phys. Rev. Lett. **100**, 136801 (2008).

[3] R.H.M. Smit, Y. Noat, C. Untiedt, N.D. Lang, M.C. van Hemert, J.M. van Ruitenbeek, Nature **419**, 906 (2002).

[4] W. H. A. Thijssen, D. Djukic, A. F. Otte, R. H. Bremmer and J. M. van Ruitenbeek, Phys. Rev. Lett. **97**, 226806 (2006).

[5] W.H.A. Thijssen, PhD thesis, Leiden university, (2007).

[6] J.A. Gupta, C.P. LutzDuprat, A.J. Heinrich and D.M. Eigler, Phys. Rev. B. **71**, 115416 (2005).

[7] J. Gaudioso, L.J. Lauhon and W. Ho, Phys. Rev. Lett. **85**, 1918 (2000).

[8] Y. Chen, Condmat 0803.4379v2 (2008).

[9] A. Halbritter, P. Makk, Sz. Csonka and G. Mihály, Phys. Rev. B **77**, 075402 (2008).

[10] S. Kubatkin, A.V. Danilov, S.E. Kubatkin, S.G. Kafanovb and T. Bjørnholm, Faraday discussions **131**, 337 (2005). More experimental data can be found on the W.W.W., as presentations by S. Kubatkin (Powerpoint).

[11] Sz. Csonka, A. Halbritter and G. Mihály, Phys. Rev. B **73**, 75405 (2006).

[12] O.Yu. Kolesnychenko, A.J. Toonen, O.I. Shklyarevskii and H. van Kempen, Appl. Phys. Lett. **79** 2707 (2001).

[13] S. Gao, M. Persson and B.I. Lundqvist, Phys. Rev. B **55** 4825 (1997).

[14] D. Djukic, K.S. Thygesen, C. Untiedt, R.H.M. Smit, K.W. Jacobsen and J.M. van Ruitenbeek, Phys. Rev. B. **71**, 161402 (2005).

[15] M. Paulsson, T. Frederiksen and M. Brandbyge, Phys. Rev. B **72**, 201101 (2005).

[16] O. Tal, M. Krieger, B. Leerink and J.M. van Ruitenbeek, Phys. Rev. Lett. **100** 196804 (2008).

[17] R.H.M. Smit, C. Untiedt, and J.M van Ruitenbeek, Nanotechnology **15**, S472 (2004).

[18] T.N. Todorov, Phil. Mag. B **77**, 965 (1998).

[19] R. Temirov, S. Soubatch, O. Neucheva, A.C. Lassise, and F.S. Tautz, New journal of Phys. **10**, 053012 (2008).

[20] M. Nielsen, Phys. Rev. B **7**, 1626 (1973).

[21] R.N. Barnett, H. Hakkinen, A.G. Scherbakov and U. Landman, Nano lett. **4**, 1845 (2004).

[22] C. Kergueris, J.P. Bourgoin, S. Palacin, D. Esteve, C. Urbina, M. Magoga and C. Joachim, Phys. Rev. B **59**, 12505 (1999).

[23] J. Reichert, H. B. Weber, M. Mayor and H.v. Löhneysen, Appl. Phys. Lett **82**, 4137 (2003).

[24] E. Lörtscher, J.W. Ciszek, J. Tour and H. Riel, Small **2**, 973 (2006).

Chapter 6

Switching with hydrogen molecules

Abstract

Vibrationally exciting hydrogen molecules, contacted between two gold electrodes, can lead to a strong heating effect (as shown in the previous chapter). In this chapter, we show that this same mechanism can also exhibit a time *in*dependent hysteresis. Depending on the electrode separation, a hysteretic effect can be observed, typically 3 mV in size and independent of the recording time. We use this feature to demonstrate a new type of memory, where the operating voltage is simply equal to the vibration frequency of the hydrogen molecule. Fast switching can be achieved ($< 20\ \mu s$), using voltages pulses as small as 2 mV.

6.1 Introduction

One of the main goals in molecular electronics, is to create a non-volatile memory device from individual molecules [1, 2, 3, 8, 5, 6, 7]. In theory, fast switching can be achieved, with large on-off ratios and low operating voltages. In this chapter we show that molecular hydrogen, contacted between two gold electrodes, can act as a memory device. By using the vibrational energy of the molecule, the system can be reversibly switched in between two different (conductance) states.

This chapter is based on Ref. 4 on p. 147

6.2 Experimental details

For our measurements on the hydrogen switch, we have used the same experimental method as described in the previous chapter (see section 5.3). Basically, the measurements are done on gold electrodes, at 4.2 K, in an insert which has a small amount of high purity hydrogen gas. The $H_2 - Au$ contacts which show a hysteretic behavior, are formed by slowly pulling the electrodes ($\approx 5pm/s$), while measuring the IV characteristics (real time).

6.3 Hydrogen switch

In the previous chapter, we have discussed the interesting IV characteristics of hydrogen-gold contacts. For these contacts, a step was observed in the current, at the hydrogen vibration energy (around 41 mV) [8, 9, 10]. At relatively low measurement speeds, this step mostly occurs at a well defined position, independent of the direction of the voltage sweep (increasing or decreasing voltage). However, as we will show below, in about 10 % of these contacts, two different steps are observed; one for increasing voltage and one for decreasing voltage, but now independent on time. An example is plotted in Fig. 6.1(a). Here, a contact is slowly stretched, while measuring the IV characteristics. We emphasize that we used here a low measurement speed of 100 ms per data point, much slower than the time scale of the heating effects discussed in the previous chapter. When now stretching the junction, a hysteretic effect appears, which is maximum after an electrode displacement of ≈ 2.6 $\mathring{A}$ (note the small change in conductance, since we are in the contact regime). However, in contrast to the hysteresis effect described in chapter 5, this hysteresis does *not* depend on time. This is especially visible in Fig. 6.1(b), where the IV is measured with an even longer time scale ($\sim$minutes). At 32 mV and 35 mV, the conductance instantly decreases or increases respectively. Repeating the same measurement with a ten times longer time scale, does not change the curve. Hence, the observed hysteresis is time independent. Interestingly, such a system can be perfectly used for a switch.

This can be done by applying an offset voltage, exactly in between the hysteresis (so at 34 mV for the contact of Fig. 6.1(b)). Subsequently, by applying a voltage pulse just above or below the hysteresis, the system can be switched to the upper or lower conductance state respectively. An example is plotted in Fig. 6.2(a). By applying 20 mV voltage pulses (here 20 ms long), the system is

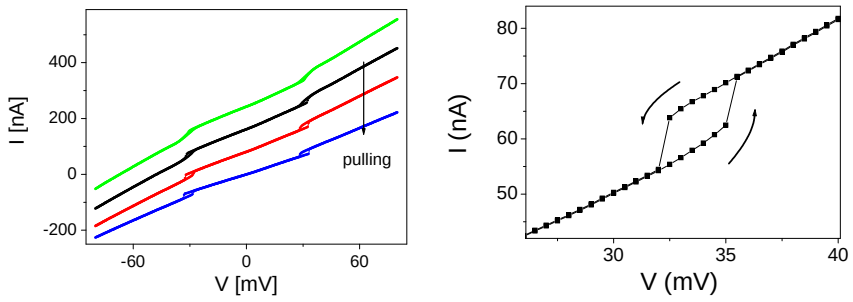

(a) (b)

Figure 6.1: *(a) IV measurements during pulling of the electrodes. Measurement is taken relatively slow, with a dwell time of 100 ms per data point. While stretching, a time independent hysteresis appears (in total, the junction is stretched 2.6 ± 0.2 Å). For clarity, the curves are shifted by 80 nA each. (b) Zoom in of an IV measurement (other contact than (a)), showing the time independent hysteresis. Measurement is taken with a long dwell time of 1s. per data point, step size is 0.5 mV.*

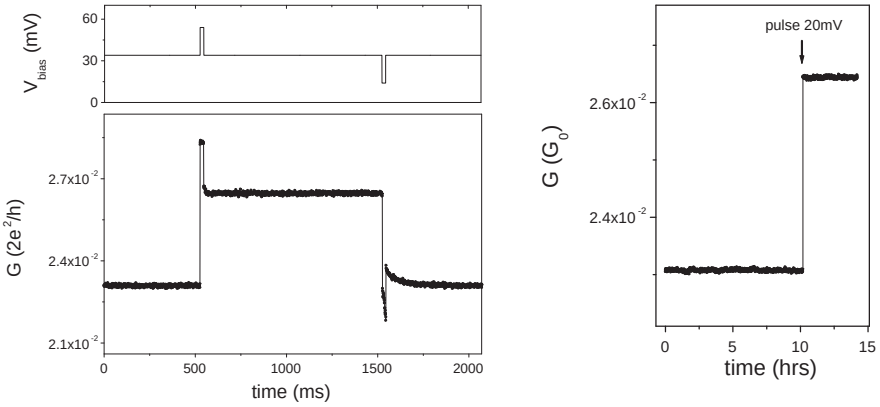

(a) (b)

Figure 6.2: *(a) Hydrogen switch (same contact as Fig. 6.1(b)). Upper graph: V_{bias} as a function of time. After 500 and 1500 ms, the voltage is pulsed with +20 mV and -20 mV respectively (duration is 20 ms). $V_{dc} = 34$ mV and sample rate is 5 kHz. Lower graph: Pulse response. With a positive pulse, the system switches to the high conductive state, and with a negative pulse to the low conductive state. Measurement is taken with 5000 data points per second, with an averaging time of 200 µs per data point. (b) Stability of the hydrogen switch. After 10 hours, the voltage is pulsed by +20 mV (20 ms) to switch to the upper conductive state. After 14 hours, the measurement is stopped.*

switched between the two states. The switch is remarkably stable in time. Even after 14 hours, no degradation is observed (as shown in Fig. 6.2(b)). Also, no degradation was observed after multiple switching events. This is shown in Fig. 6.3, where 4 mV, 20 ms pulses were used. Even after more than 5000 switching events, no differences were observed. We have measured this switching for many independent contacts, although the zero bias conductances were found in between 0.01 and 0.07 G_0. The switching voltages varied in between 32 and 46 mV, similar to the variation of Fig. 5.4(b). Furthermore, we found that the switching times strongly depend on the height of the voltage pulse. Switching times faster than the bandwidth of our IV convertor were found for voltage pulses >30 mV (so faster than 20 μs). Voltage pulses as small as 2 mV could be used, however, only with sufficiently long pulsing times. If too short, the system falls back to its initial state.

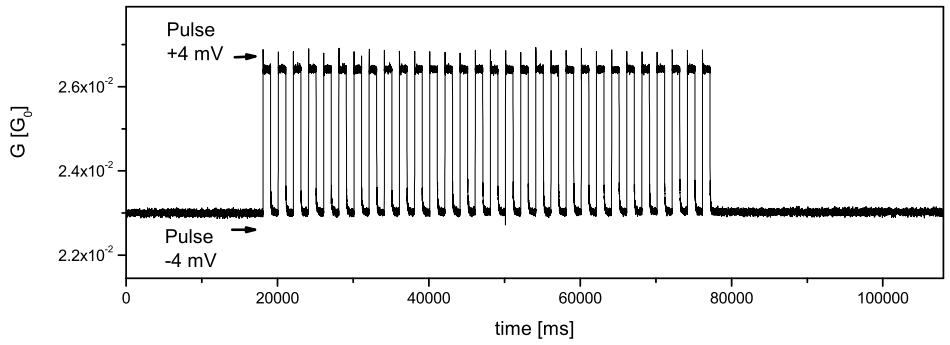

Figure 6.3: *Multiple switching events. The pulse height is ±4 mV, on top of a dc voltage of 34 mV (pulse duration is 20 ms).*

6.4 Physical mechanism

In chapter 5, we have shown that a $H_2 - Au$ contact shifts to a different conductance state, around the hydrogen vibration energy. This result was found consistent with a spatial change of the molecule(s), at a higher phonon temperature. The observations presented in this chapter are very similar, with the only difference that the step upwards and step downwards in current occur at a different voltage (now independent on the recording time). We emphasize that the switching upwards or downwards in current does not occur at some critical current. This can be concluded from observations on contacts where the current switches to lower values instead of higher values (not shown). Nevertheless, after

pulsing the voltage, the system does show a saturation (with a ms time scale) to the other conductance level (as can be observed after the second pulse in Fig. 6.2(a)). This is an indication that also for the switch, a similar heating effect is involved as for the contacts described in the previous chapter. Hence, we suggest that the switching occurs at the vibration energy of the hydrogen, and propose the following model:

It is well known that the exact value for the vibration frequency actually depends on the spatial freedom of the molecule in between the electrodes [8, 10, 11, 12]. Hence, the vibration frequency of the higher conductance state can be different than the vibration frequency of the lower conductance state. Interestingly, this can lead to the observed time independent hysteresis. This is schematically drawn in Fig. 6.4. At zero bias, the system is in conductance state 1, where the vibration frequency of molecule equals ω_1. When the voltage is increased above $\hbar\omega_1/e$, the vibrational temperature of the molecule instantly increases, and the molecule hops to a different position, with conductance G_2. Up to this point, the described process is similar to the contacts discussed in chapter 5). However, let us now assume that the vibration frequency of state 2 is higher than of state 1 (so $\omega_2 < \omega_1$). When we now decrease the voltage slightly below $\hbar\omega_1/e$, the vibrational temperature of the molecule does not change, and the system will stay in conductance state 2. Only by decreasing the voltage below $\hbar\omega_2/e$, the molecular system falls back to conductance state 1. Hence, this results in a time independent hysteresis, as observed in Fig. 6.1.

Finally, we emphasize that one could also explain the hydrogen switch by a phase transition (as introduced in the previous chapter). Let us assume that the hydrogen molecules are in a solid or liquid phase, below or above the vibration energy respectively. When the liquid is cooled below its transition temperature, it is expected that the molecules start to form crystals, finally leading to the frozen state. However, it is well known that this nucleation process does not necessarily occur at the melting temperature. For some systems, the nucleation process starts at lower temperatures, a process which is called undercooling. This could result in a hysteresis like the one shown in Fig. 6.1.

6.5 Conclusions

To conclude, we have demonstrated a new type of memory, based on molecular hydrogen contacted between two gold electrodes (at a temperature of 4 K). The

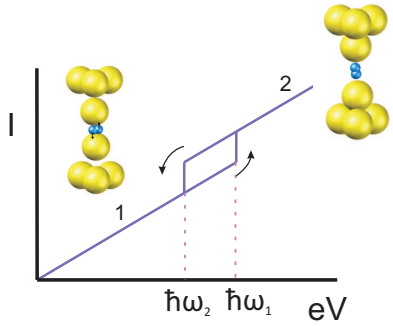

Figure 6.4: *Schematic drawing of the proposed mechanism for the hydrogen switch (note that many ore molecules are expected in the vicinity of the electrodes). At zero bias, the molecular system is in state 1, with vibration frequency ω_1. When the voltage is equal to $\hbar\omega_1/e$, the vibrational temperature of the molecule instantly increases, resulting in a spatial change of the molecule from state 1 to state 2. This conductance state 2 has a slightly lower vibration frequency than conductance state 1 ($\omega_2 < \omega_1$). Hence, to return to the low conductive state, the voltage has to be decreased down to $\hbar\omega_2/e$. Thus, the IV characteristics have a hysteretic effect, independent of the recording time.*

molecular system can be switched between two conductance values, using voltage pulses as small as 2 mV. Switching rates faster than the bandwidth of our electronics are observed ($>$ 50 kHz). The switching mechanism is attributed to the vibrationally energy of the contacted molecules, which could possibly result in a phase transition of the hydrogen molecules. Hence, our results give new insights in the switching properties of molecular junctions.

References

[1] E. Lörtscher, J.W. Ciszek, J. Tour and H. Riel, Small **2**, 973 (2006).

[2] J. He, Q. Fu, S. Lindsay, J.W. Ciszek, and J.M. Tour, J. Am. Chem. Soc. **128**, 14828 (2006).

[3] A. Szuchmacher Blum, J.G. Kushmerick, D.P. Long, C.H. Patternson, J.C. Yang, J.C. Henderson, Y. Yao, J.M. Tour, R. Shashidhar and B. R. Ratna, Nature **4**, 167 (2005).

[4] P. Liljeroth, J. Repp, G. Meyer, Science **317**, 1203 (2007).

[5] D. Dulic, S. J. van der Molen, T. Kudernac, H. T. Jonkman, J. J. D. de Jong, T. N. Bowden, J. van Esch, B. L. Feringa and B. J. van Wees, Phys. Rev. Lett.

91, 207402 (2003).

[6] J.A. Stroscio and R.J. Celotta, Science **306**, 242 (2004).

[7] V. Simic-Milosevic, M. Mehlhorn, K.-H. Rieder, J. Meyer, and K. Morgenstern, Phys. Rev. Lett. **98**, 116102 (2007).

[8] R.H.M. Smit, Y. Noat, C. Untiedt, N.D. Lang, M.C. van Hemert, J.M. van Ruitenbeek, Nature **419**, 906 (2002).

[9] W. H. A. Thijssen, D. Djukic, A. F. Otte, R. H. Bremmer and J. M. van Ruitenbeek, Phys. Rev. Lett. **97**, 226806 (2006).

[10] W.H.A. Thijssen, PhD thesis, Leiden university, (2007).

[11] D. Djukic, K.S. Thygesen, C. Untiedt, R.H.M. Smit, K.W. Jacobsen and J.M. van Ruitenbeek, Phys. Rev. B. **71**, 161402 (2005).

[12] R.N. Barnett, H. Hakkinen, A.G. Scherbakov and U. Landman, Nano lett. **4**, 1845 (2004)

Chapter 7

Two level fluctuations in hydrogen affected gold tunnel junctions

Abstract

In this chapter, conductance measurements on gold tunnel junctions are presented, in a hydrogen environment. Right after the addition of the hydrogen molecules, two level fluctuations (TLF) appear in the tunneling regime. These TLF are attributed to hopping of a molecule in between two positions, a process which is triggered by inelastic excitations of the molecule. Furthermore, we show that the potential landscape can be changed by varying the electrode separation. Hence, we can control the preferential conductance state in two ways: by vibrational heating and by tuning the electrode interaction.

7.1 Introduction: two level fluctuations

In the previous two chapters, we showed that a hydrogen-gold junction can heat up, at voltages above the vibration energy of the hydrogen molecule. This resulted in a change in conductance, which was attributed to a two level system where the molecule hops in between two different configurations in the contact. However, the two level fluctuations (TLF) were generally faster than the bandwidth of our electronics, leading to an apparently smooth transition to the other conductance

This chapter is based on Ref. 5 on p. 147

level. In this chapter, we present our results on hydrogen-gold junctions where the electrodes are separated by a tunnel gap. The hydrogen molecule is now not contacted, but adsorbed on the gold electrodes. Interestingly, in comparison to the case where the molecule is contacted, the two level fluctuations are now slower and can be resolved in time. A typical example is plotted in Fig. 7.1. Clear two level fluctuations are observed in the current, with an amplitude up to 100 %. Since these fluctuations are time-resolved, we have the opportunity to quantitatively investigate the two level system. By systematically changing the voltage and the electrode distance, we gain information on the exact physical mechanism of the TLF.

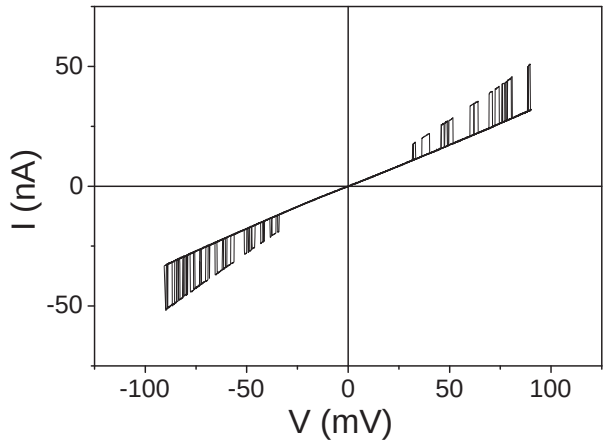

Figure 7.1: *IV measurement on hydrogen covered gold electrodes, separated by a vacuum gap. Clear two level fluctuations can be observed above 30 mV.* V_{in}*=0.1 Hz.*

7.2 Experimental details

For our measurements on the hydrogen affected tunnel junctions, we use a similar experimental method as described in the previous two chapters (see section 5.3). However, we now focus on junctions which are separated by a tunnel gap. The experimental details are as follows: To start with a clean gold system, the wires are cooled down to 4.2 K, after which the electrodes are broken. This gives clean gold electrodes, in cryogenic vacuum. The cleanliness of the electrodes is checked by measuring IV curves, real time, by sweeping the voltage each second from -200 to +200 mV, resulting in a smooth tunnel curve. Next, a small amount

of high purity hydrogen gas (99.999 %) is brought into the insert (≈1 cm^3, 1 mbar), although higher quantities lead to similar results. Within 5 minutes after admission of the hydrogen, two level fluctuations start to appear in the IV curves measured in the tunneling regime.

7.3 Two level fluctuations as a function of bias voltage

7.3.1 Inversion of the ground state

Let us return to Fig. 7.1. Clearly, the observed two level fluctuations strongly depend on the applied bias voltage. Below 30 mV no fluctuations are observed, whereas at higher voltages, the current starts to fluctuate in between two different conductance levels, with increasing frequency. However, besides the increasing frequency, also the occupation of the two conductance levels changes. This effect especially shows up in Fig. 7.2(a). With increasing voltage, the conductance of the system gradually changes from the high conductive state (with conductance σ_0) to the low conductance state ($G = \sigma_1$). Interestingly, we can use these plots to calculate the actual (fractional) occupation of each state. For a given bias voltage, the time-averaged conductance ($\overline{\sigma}$) is a function of σ_0 and σ_1, and can be described by:

$$\overline{\sigma} = n_0\sigma_0 + n_1\sigma_1 \tag{7.1}$$

where n_0 and n_1 are the fractional occupation numbers of the high and low conductance state respectively (note that $n_0 + n_1 = 1$). This gives us the opportunity to directly calculate the fractional occupation numbers, as a function of voltage. The result is plotted in Fig. 7.2(b). At bias voltages below 25 mV, the system is completely in the ground state ($n_1 = 0$). At higher voltages, the system slowly saturates to the lower conductance state. Apparently, the occupation of the conductance states strongly depends on the applied bias voltage, and can be completely inverted for low and high bias voltages. Furthermore, the sudden onset of the TLF indicates a vibrational level around 30 mV (we will return to this observation in the next section).

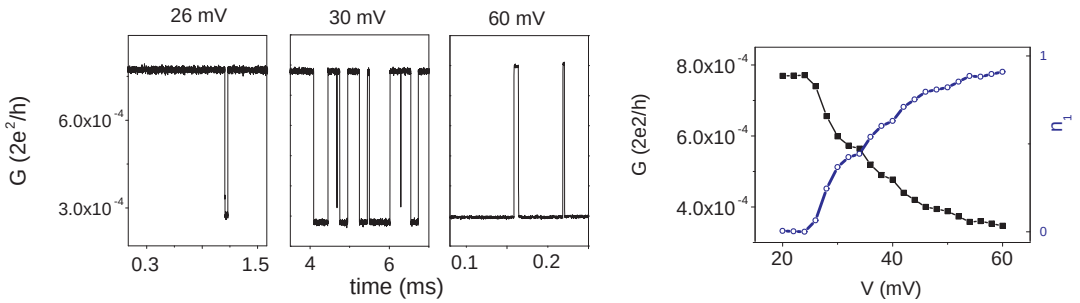

Figure 7.2: *(a) Conductance of a tunnel contact as a function of time, for 3 different voltages. The average conductance of the system changes in between 30 and 60 mV, from the upper to the lower conductance level. (b) Conductance and fractional occupation of the excited state, as a function of bias voltage. The fractional occupation of the lower conductance level slowly changes from 0 (at V <25 mV) to a value close to 1 at voltages > 60 mV.*

7.3.2 Transfer rates

A second method to characterize the TLF, is to investigate the residence times of each conductance level. When we assume that the two levels are independent and have no memory, the residence time probability density $P_{0,1}$ is given by a two state Markov process [2].

$$P_{0,1}(t) = R_{0,1} \exp(-R_{0,1}t) \tag{7.2}$$

where $R_{0,1}$ is the transfer rate of the specific conductance state. The residence time distributions for the two conductance levels, can indeed be well described by an exponential distribution, as shown in Fig. 7.3.

Subsequently, by repeating the analysis for different bias voltages, one can plot the transfer rates as a function of bias voltage. An example is plotted in Fig. 7.4(a). Interestingly, the transfer rates seem to follow a power law with the applied bias voltage. As we will show in the next section, this is a strong indication that the process is triggered by inelastic excitations of the molecule [1].

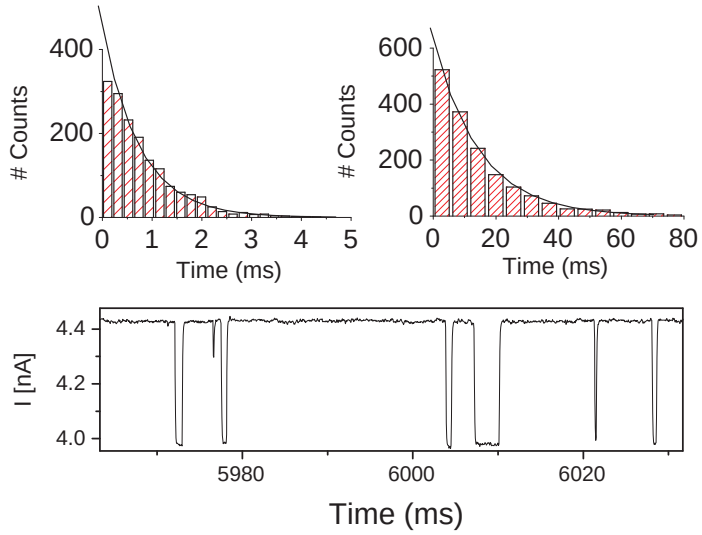

Figure 7.3: *Two level fluctuations, as a function of time. Lower graph: Current as a function of time, for V=90 mV. Sample rate is 20 kHz with an averaging time of 50 μs for each data point. Upper graphs: statistics of the residence times for the lower and upper conductance state respectively for the measurement plotted below (For the histogram, the current is recorded for 25 seconds). The line is a fit with a single exponential function.*

7.3.3 Vibrational heating model

One of the first atomic two level systems described in literature, is the xenon switch, as published by Eigler *et al* [3]. Here, a xenon atom could be reversibly switched between the STM tip and surface, by applying a voltage pulse. The transfer rates of the Xenon atom, were found to have a power law dependence on the current. To explain this result, a vibrational heating model was proposed, where an atom can overcome an energy barrier by multiple inelastic excitations [4, 5, 6]. This model is schematically drawn in Fig. 7.5, and is widely used for explaining two level fluctuations in molecular electronics [7, 8, 9, 10]. Basically, the model states that the energy of an atom or molecule can stepwise increase by vibrational excitations taking up energy from tunnel electrons. Thus, the molecule can climb a vibrational ladder, with probability $\Gamma_{\uparrow}$ (thereby taking up energy equal to $\hbar\omega$). Subsequently, by releasing energy to electrons or to substrate phonons, the molecule can step down in energy with probability $\Gamma_{\downarrow}$. This results in a probability R_n to reach the highest level n:

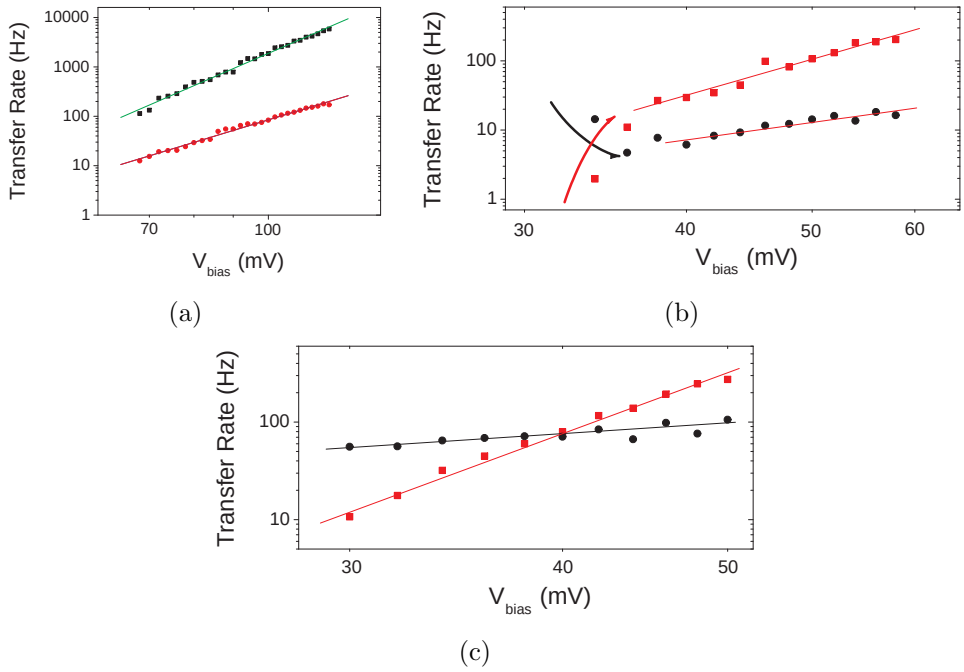

Figure 7.4: *Transfer rates as a function of bias voltage, for two different contacts (including linear fits). (a) Same contact as depicted in Fig. 7.3. Slopes of the lines are 6.7 and 4.7 for the upper and lower line respectively. (b) Transfer rates for the same contact as discussed in Fig. 7.2. Note the inversion of the ground state, around 35 mV. Slopes are 2.6 and 5.4. (c) transfer rates of the contact shown in Fig. 7.5(b), after stretching ≈8 pm. The most preferential conductance state changes around a bias voltage of 40 mV. Slopes are 1 and 6.3.*

$$R_n \simeq n\Gamma_\uparrow \exp(-\frac{(n-1)\hbar\omega}{k_B T_v}) \tag{7.3}$$

where $\hbar\omega$ is the vibration energy, k_B is the Boltzmann constant, and T_v is the vibrational temperature. Furthermore, when the atom or molecule reaches the highest level n, it has enough energy to cross the energy barrier, and hop to another position (to the other potential well). As depicted in Eq. 7.5, the transfer rate for barrier crossing strongly depends on the vibrational temperature T_v, which is given by:

$$T_v = \frac{\hbar\omega}{k_B \ln \frac{\Gamma_\downarrow}{\Gamma_\uparrow}} \tag{7.4}$$

Combining these two equation results in the following expression for the transfer rates:

$$R_n = n\Gamma_\uparrow \left(\frac{\Gamma_\uparrow}{\Gamma_\downarrow}\right)^{n-1} \tag{7.5}$$

Furthermore, by calculating the excitation and deexcitation rates , one finds that the ratio $\Gamma_\downarrow/\Gamma_\uparrow$ is a function of the number of injected electrons [5]. This results in a transfer rate proportional to I^n. Finally, since we are in the Ohmic regime of tunneling (voltage is much smaller than the workfunction of gold), the voltage is proportional to the current. Hence, we can write $R \propto V^n$, resulting in a power law dependence of the transfer rates, as a function of voltage.

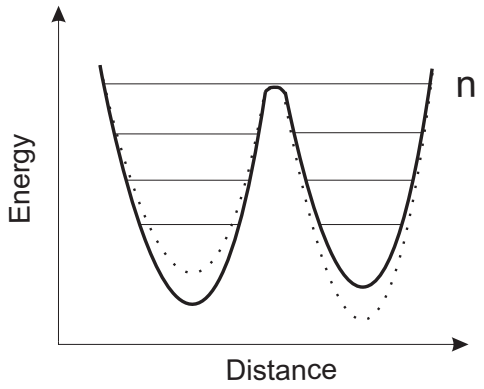

Figure 7.5: *Vibrational heating model. The molecule can overcome the barrier by stepwise climbing of the vibrational ladder. After n excitations, the molecular energy is higher than the energy of the potential barrier (solid line, with $E = n\hbar\omega$), and the molecule can cross the energy barrier. Dotted line: By changing the electrode separation, the potential landscape changes, thereby changing the ground state of the two level system.*

The power law is consistent with our observations, as plotted in Fig. 7.4. Hence, this indicates that the TLF are triggered by inelastic excitations of the hydrogen molecule. This is as expected, since the TLF are perfectly symmetric in the voltage, just like the observed heating effect at the hydrogen vibration frequency for contacted hydrogen molecules (as discussed in chapter 5). In this context, Fig. 7.4(b) is an important result. At voltages higher than 40 mV, the transfer rates follow the expected power law dependence on the voltage. However, a strong deviation from the power law is observed around 35 mV. Here,

the ground state suddenly changes from the high conductance state to the low conductance state. Interestingly, 35 mV is close to the typical vibration energy of contacted molecular hydrogen (around 40 mV). Hence, this graph shows the onset of the vibrational heating. Note that a similar onset around 30 mV is observed for the contact depicted in Fig. 7.2(b).

However, we emphasize that the vibrational heating model does not give a complete description of our observations. First of all, the model predicts that the slope of the power law equals the number of vibrational levels in the well. However, we observe strong differences in the slopes of power law for the upper and lower conductance states (as for Fig. 7.4). This would insinuate a strong difference in depth of the two potential wells. In contrast, the balance equation states that $R_1/R_2 = \exp[-(E_1 - E_2)/kT]$, where E_1 (E_2) is the depth of the potential well for state 1 (2). Thus, a crossing of the transfer rates for the upper and lower level would indicate that the depth of the potential well depends on the applied voltage. This is inconsistent with the linear slopes of Fig. 7.4(c). Hence, a more advanced theoretical model is needed for explaining our observations. We note here the calculations done by Halbritter *et al*, to explain the negative differential conductance as observed for contacted hydrogen molecules (as discussed earlier in section 5.2.2). They suggested a strongly asymmetric system for the two different conductance levels [11]. Our data presented in this section give new insight in this discussion.

7.4 TLF as a function of electrode distance

Finally, we investigate the TLF by changing the electrode separation. It is well known that the binding forces between the opposing atoms can have a large influence on the potential landscape around the apex [2, 12, 13]. Remarkably, these attractive forces can even change the fractional occupation of the two different conductance levels. A first example is plotted in Fig. 7.4. For Fig. 7.4(b), the inversion of the ground state occurs at a bias voltage of around 35 mV. However, by increasing the electrode separation by only 8 pm, the position of the ground state inversion shifts towards 40 mV. This effect is even more pronounced for the contact depicted in Fig. 7.6. Here, the conductance is measured at a bias voltage of 100 mV (well above the vibration energy of the molecule). By changing the electrode separation by 160 pm, the preferential conductance level is completely inverted. This process is schematically drawn in Fig. 7.5. By using the attractive

forces of the electrodes, one can change the potential landscape, and even change the ground state of the system (dotted line). We note here that a very similar effect was observed by Stroscio *et al*, where they investigated the dynamics of a Co atom on a Cu surface (using an STM) [2]. Also here, a TLF system was observed, where a Cu atom hopped back and forth between two lattice positions. By changing the electrode separation (and so the electrode interaction), one could strongly change the potential landscape, and even "select" the preferential conductance level.

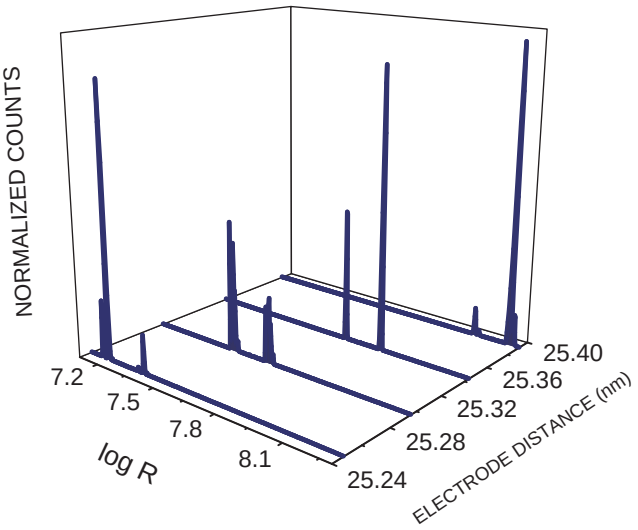

Figure 7.6: *Histogram of resistance values of TLF as a function of electrode distance. By decreasing the electrode separation by ≈160 pm, the fractional occupation is completely inverted. For close electrode separations, the low resistance level is now preferred above the high resistance level. Measurement taken with a bias voltage of 100 mV.*

7.5 Comparison with measurements on contacted molecules

In Fig. 7.2 and Fig. 7.4(c) a gradual transition towards another conductance level was observed, at increasing voltage. A similar transition was observed for contacted molecules (as discussed in chapter 5). However, for the contacted molecules, the complete transition occurred within a much smaller voltage window (< 5 mV), and the two level fluctuations were to fast to be resolved in time.

Furthermore, for the contacts discussed in this chapter, the onset of the TLF occur at voltages anywhere above 30 mV, while this is more restricted for the contacted molecules (30<V<50 mV). We suggest here that this could be related to a smaller energy barrier when the molecule is contacted between two electrodes. For larger energy barriers (for tunnel junctions), a higher vibrational temperature (and higher voltage) is needed for complete inversion of the conductance level. In contrast, for small energy barriers, a complete cross over to another conductance level can already occur right after the first inelastic excitations (at $V = \hbar\omega/e$). An example of a contact in the intermediate regime (contacted or tunnel junction), is plotted in Fig. 7.7. Here, the cross over to a higher conductance level occurs within 20 mV, while still two level fluctuation can be observed. Also, a hysteresis effect shows up, of the same time scale as discussed in chapter 5.

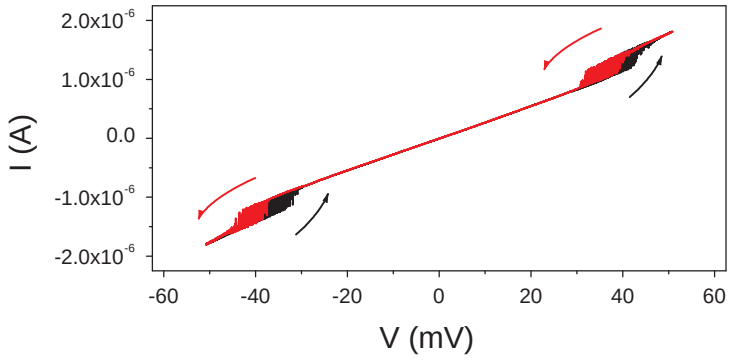

Figure 7.7: *TLF fluctuations at relatively high contact conductance of 0.3 G_0. The trace for increasing voltage is plotted in black, the trace for decreasing voltage in red/grey. The cross-over to the higher conductance level occurs in between 30 and 50 mV. The voltage is sweeped in 1 Hz. Note the hysteresis between the trace and retrace, of a ms time scale.*

7.6 Conclusions

To conclude, we have performed conductance measurements on gold tunnel junctions, in a hydrogen environment. Well resolved two level fluctuations are observed, which are attributed to hopping of a hydrogen molecule in between two different positions on the gold electrodes. The transfer rates were found to have a power law dependence on the voltage, which is indicative for vibrational heating. Moreover, the observations are independent of the polarity of the voltage,

thereby excluding any electromigration effects. Furthermore, the most preferential conductance level was found to be strongly dependent on both the voltage and electrode separation. Hence, our results give new insight in vibrationally induced two level fluctuations.

References

[1] J.A. Gupta, C.P. LutzDuprat, A.J. Heinrich and D.M. Eigler, Phys. Rev. B. **71**, 115416 (2005).

[2] J.A. Stroscio and R.J. Celotta, Science **306**, 242 (2004).

[3] D.M. Eigler, C.P. Lutz, and W.E. Rudge, Nature **352**, 600 (1991).

[4] S.W. Gao, M. Persson and B.I. Lundqvist, Solid State Common. **84**, 271 (1993).

[5] S.W. Gao, M. Persson and B.I. Lundqvist, Phys. Rev. B **55**, 4825 (1997).

[6] R.E. Walkup, D.M. Newns and Ph. Avouris, Phys. Rev. B **49**, 1858 (1994).

[7] A.J. Heinrich, C.P. Lutz, J.A. Gupta, D.M. Eigler, Science **298**, 1381 (2002).

[8] P. Liljeroth, J. Repp, and G. Meyer, Science **317**, 1203 (2007).

[9] C. Nacci, J. Lagoute, Xi Liu, and S. Fölsch, Phys. Rev. B **77**, 121404 (2008).

[10] J.I. Pascual, N. Lorente, Z. Song, H. Conrad and H.P. Rust, Nature **423**, 525 (2003).

[11] A. Halbritter, P. Makk, Sz. Csonka and G. Mihály, Phys. Rev. B **77**, 075402 (2008).

[12] J. Repp, G. Meyer, K. Rieder, and P. Hyldgaard, Phys. Rev. Lett **91**, 206102 (2003).

[13] J. Repp, G. Meyer, F.E. Olsson, M. Persson, Science **305**, 493 (2004).

Chapter 8

The role of joule heating in the formation of nanogaps by electromigration

Abstract

We investigate the formation of nanogaps in gold wires due to electromigration. We show that the breaking process will not start until a local temperature of typically 400 K is reached by Joule heating. This value is rather independent of the temperature of the sample environment (4.2-295 K). Furthermore, we demonstrate that the breaking dynamics can be controlled by minimizing the total series resistance of the system. In this way, the local temperature rise just before break down is limited and melting effects are prevented. Hence, electrodes with gaps < 2 nm are easily made, without the need of active feedback. For optimized samples, we observe quantized conductance steps prior the gap formation.

8.1 Introduction

Although most of the work in this thesis was done on mechanically controllable break junctions, we also focussed on another method to create nanogaps. The advantage of the break junctions, is the tunable electrode distance. However, the fabrication of such junctions is a time consuming process. Second, it is not possible to add a third (gate) electrode, which could be used to tune the number of molecular levels near the Fermi energy. In contrast, electromigration-induced tunnel devices can be made fast, and can easily be extended with a gate electrode, making this method one of the most promising techniques [1, 2, 3].

This chapter is based on Ref. 1 on p. 147.

Electromigration-induced nanogaps are produced by applying large current densities to gold wires. At high current densities j (typically $10^8 A/cm^2$), momentum transfer from the electrons to the gold atoms leads to drift of the atoms, in the direction of the electron flow. This mass flux can lead to the growth of voids in the wire, finally leading to the formation of gaps [4]. These gaps can have widths as small as a single nanometer, which makes them suitable for single molecular electronics [5, 6]. However, to obtain gaps smaller than 2 nm, it is crucial that the process is indeed dominated by electromigration. Joule heating, resulting in melting and surface tension effects, can be the cause of much bigger gaps and gold island formation [7, 8, 9].

It is a challenging problem to prevent excessive heating. The reason for this is that a high current density is only one of the requirements for nanogap formation. An additional condition is that the atomic mobility is high enough for substantial mass flux to occur. Since the mobility shows activated behavior, the local temperature plays a key role in electromigration. If the temperature of the sample environment is low (e.g., 77 K), Joule heating has to be substantial to induce the required local temperature. Below, we show, using a simple model and local temperature measurements, that gap formation typically takes place at a local temperature $T_{start} \sim 400$ K. This value is rather independent of the temperature of the sample environment (4.2 K, 77 K, or 295 K).
Unfortunately, the local temperature does not stay constant once the breaking process has started. While the slit is being formed, the current density and, hence, the local Joule heating increases. As a consequence, the local temperature diverges just before break down. In fact, temperatures can be reached up to the melting point of gold, leading to ill-defined junctions. This problem can be solved by using an active feedback system, where the speed of the electromigration process is kept constant [7, 8, 9, 10, 11]. In this way, the temperature is limited, giving better control on the final gap size. In this article, we discuss a simple model to describe the local temperature rise just before break down. We test this model by doing local temperature measurements during the electromigration process. We show that excessive heating can be prevented, by limiting the series resistance of the system. This makes a feedback system unnecessary. By optimizing our sample design, we have increased the number of junctions with gaps < 2 nm from 15 to > 90 percent. Furthermore, constrictions of only one or a few atoms can easily be achieved, leading to conductance steps of typically $2e^2/h$.

8.2 Theory: electromigration in metals

Electromigration is commonly described as a mass flux under the influence of a high current density. However, a full description of the electromigration problem is not trivial. To give some insight, we refer to thermodynamics of irreversible processes. This theory considers *all* fluxes and forces involved [12]. In our case, there are three types of fluxes to be dealt with: the electron particle flux ($\mathbf{J_e}$), the flux of metal atoms ($\mathbf{J_m}$), and the energy flux ($\mathbf{J_u}$). These fluxes are induced by a set of three 'forces' (or potential gradients), $\mathbf{X}_j$. For the particle forces, we can write $\mathbf{X_j} = -\nabla\mu_{\mathbf{ec}}^{\mathbf{j}}$. Here, $\mu_{ec} = \mu + Ze\varphi$ is the electrochemical potential, with φ, μ and Z, the electrostatic potential, the chemical potential and particle charge (-1 for electrons), respectively. The other 'force' is due to a temperature gradient: $\mathbf{X_u} = \nabla(\mathbf{1/T})$. From thermodynamics of irreversible processes we have following set of equations:

$$\mathbf{J}_m = -L_{m,m}\nabla\left(\frac{\mu_{ec}^m}{T}\right) - L_{m,e}\nabla\left(\frac{\mu_{ec}^e}{T}\right) - L_{m,u}\left(\frac{\nabla T}{T^2}\right) \tag{8.1}$$

$$\mathbf{J}_e = -L_{e,m}\nabla\left(\frac{\mu_{ec}^m}{T}\right) - L_{e,e}\nabla\left(\frac{\mu_{ec}^e}{T}\right) - L_{e,u}\left(\frac{\nabla T}{T^2}\right) \tag{8.2}$$

$$\mathbf{J}_u = -L_{u,m}\nabla\left(\frac{\mu_{ec}^m}{T}\right) - L_{u,e}\nabla\left(\frac{\mu_{ec}^e}{T}\right) - L_{u,u}\left(\frac{\nabla T}{T^2}\right) \tag{8.3}$$

where the phenomenological constants L_{ij} relate all fluxes to all forces, whilst obeying the Onsager relations, $L_{ij} = L_{ji}$. The coupled equations above provide a general description of the system. This description includes electromigration as well as thermo-electric effects and thermodiffusion. The latter refers to a mass flux due to temperature gradients (which can, in turn, be due to Joule heating). Unfortunately, to solve the set of equations for a three-dimensional geometry is a formidable task. With a few assumptions, however, a simplified relation for the mass flux can be obtained. First, for materials with a high conductivity, we can ignore $\nabla\mu^e$. Second, we choose to neglect thermodiffusion. In the experimental part of this article, this assumption will be justified. Finally, we note that in practice all charge current is due to electron flux, so that $-\nabla\varphi = \rho j$ (with ρ the electrical resistivity). Hence, we obtain:

$$\mathbf{J}_m = -L_{m,m}^*(\nabla\mu^m - Z^* e\rho j) \tag{8.4}$$

where we defined $L^*_{i,j} = L_{i,j}/T$. Furthermore, we introduced an effective charge Z^*:

$$Z^* = Z - \frac{L^*_{m,e}}{L^*_{m,m}} \tag{8.5}$$

In words, the atoms behave as if they had a charge Z^* [12, 13, 14]. This effective charge is due to momentum transfer from electrons to atoms. Generally, $\frac{L_{me}}{L_{mm}} >> Z$, so the net force acting on the gold atoms will be in the direction of the electron flow.

8.3 Experimental setup

Two kinds of samples are fabricated on top of a 500 nm thick SiO_2 layer on Si. For the first, called 'terrace samples', we use shadow evaporation and a resist bridge to obtain different thicknesses for the leads and the constriction (see Fig. 8.1a). In the constriction, 15 nm Au is evaporated, while for the leads 150 nm Au on top of 2 nm Cr is used. To decrease the constriction length, an extra 50 nm Au is evaporated. This way, a constriction of about 250 × 100 nm (length × width) is obtained. Due to thick gold leads, the total resistance is only 30 Ω (including the wires of the measurement setup). For the second kind of samples, called 'bow tie samples', we define a constriction in the shape of a bow tie with a minimum width of 20 to 60 nm. In this case, the thickness of the gold in the leads and the constriction is the same, namely 17 nm. Furthermore, a 3 nm adhesion layer is used for most of the gold structure. By evaporating this layer at an angle, we make sure that the Chromium does not reach the constriction. Therefore, the very center of the constriction contains gold only.
Electromigration is performed by applying a slowly increasing voltage (Keithley 230) to the wire, while monitoring the current (Keithley 6517A). Measurements were done at room temperature (in air) and at both 77 and 4.2 K (in cryogenic vacuum). After break down, tunnel currents were determined. In our setup, zero-bias tunnel resistances up to 10^{12} Ω can be measured.

8.4 Results and discussion

8.4.1 Excessive heating during electromigration

A typical graph of an electromigration experiment is shown in Figure 8.1b. Here, breaking is performed for a 'terrace sample' (Fig. 8.1a) by slowly increasing the voltage by 2 mV/s, at 77 K. The initial total resistance (including wiring) is 36 Ω. At about 0.38 V, the current density has reached a value that causes substantial mass flux, starting the formation of a slit. At 0.4 V, the wire finally breaks down. Subsequently, a small tunnel current can be observed, indicating that the gap size is around 1 nm.

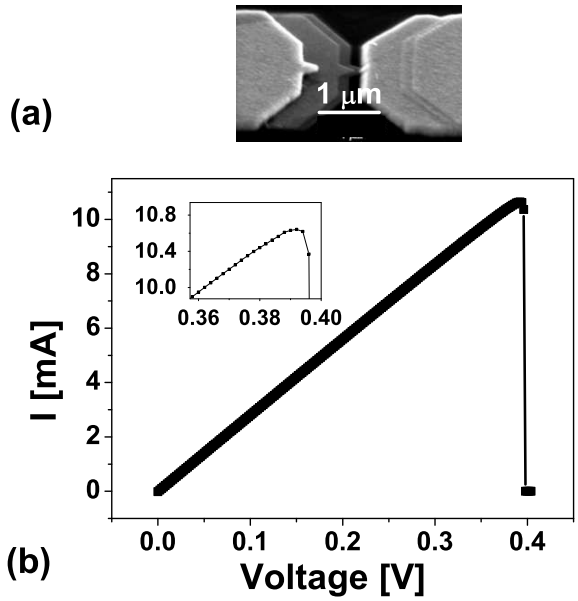

Figure 8.1: *a) Scanning electron micrograph of an electromigration sample, 'terrace' type, made with electron beam lithography. The thickness of the gold layer is 15 nm (middle), 50 nm, and 150 nm (leads). The constriction in the middle is about 100 nm in width. b) Representative breaking curve. The voltage is increased by 2 mV/s, while the current is observed. At 0.38 V, the electromigration process starts, leading to a decrease in current. At 0.4 V, after break down, a tunnel current can be measured of about 500 nA. Inset: magnification of region just before break down. Due to temperature increase and electromigration, dI/dV decreases slowly, until final break down occurs. Measurement at 77 Kelvin, the initial total resistance is 36 Ω.*

A very different result is obtained for the experiment in Fig. 8.2. For this mea-

surement, performed on a 'bow tie' sample, we added an extra series resistance. The total initial resistance equals 1780 Ω. Although the graph in Fig. 8.2a) looks similar to the one in Fig. 8.1b), there are some obvious differences. First, the breaking process is much more abrupt (see insets). Second, the voltage at break down is much higher (11 V vs. 0.4 V). The most dramatic difference is, however, that no tunnel current could be detected after break down. To investigate the gap in more detail, we used atomic force microscopy (AFM). In Figure 8.2b an AFM picture is shown of the 'bow tie' sample after the breaking process. The final gap size is approximately 100 nm, and the electrodes have clearly rounded off. Most likely this is due to local melting. Furthermore, there is a set of gold islands in between the electrodes. We note that the presence of such nanoparticles may lead to Coulomb blockade effects [16, 8, 15, 9]. From Figure 8.2b we conclude that the break down process has taken place in an uncontrolled manner, leading to high local temperatures (and fields). We shall show below, that the breaking dynamics is strongly correlated with the resistance in series with the constriction, R_s. We note that this resistance constitutes the main difference between the experiments in Figures 8.1 and 8.2. Minimizing R_s, results in a much better control of the final gap size, making a feedback system unnecessary.

To demonstrate the significance of R_s, we use a simple model for the constriction (a schematic drawing is shown in Fig. 8.3). We consider a slit of length l. Its width w(t) and height h(t) are decreasing functions of time, due to gap formation. The total resistance, R_{tot}, is the sum of the constriction resistance, $R_c(t) = \frac{\rho l}{h(t)w(t)}$, and a series resistance R_s. In a virtual experiment, we ramp up the voltage until electromigration begins at a bias $V = V_c$ (at $t \equiv 0$). A more accurate way of saying that 'electromigration begins' is to say that the flux of gold atoms, J_m, reaches a certain critical value J_m^c.[17] For this to happen, both the current density j and the mobility (related to $L_{m,m}^*$ in eq. (8.4)) need to be substantial. The mobility is strongly affected by the local temperature, which increases due to Joule heating via $p = \rho j^2$. Consequently, electromigration does not start, until a certain combination of current density j_c and local temperature T_{start} is reached. The latter is directly related to the local dissipation $p_c = \rho j_c^2$ (below, we discuss this in more detail) [18]. The voltage V_c and local dissipation p_c are related by $p_c = \frac{V_c^2}{\rho l^2}/(1 + \frac{R_s}{R_c(0)})^2$. Next, we consider the breaking process for $t > 0$, keeping the voltage constant at $V = V_c$. Due to electromigration a slit is formed in the constriction, leading to an increasing constriction resistance $R_c(t)$. Consequently, the local dissipation also increases, according to (in the diffusive regime):

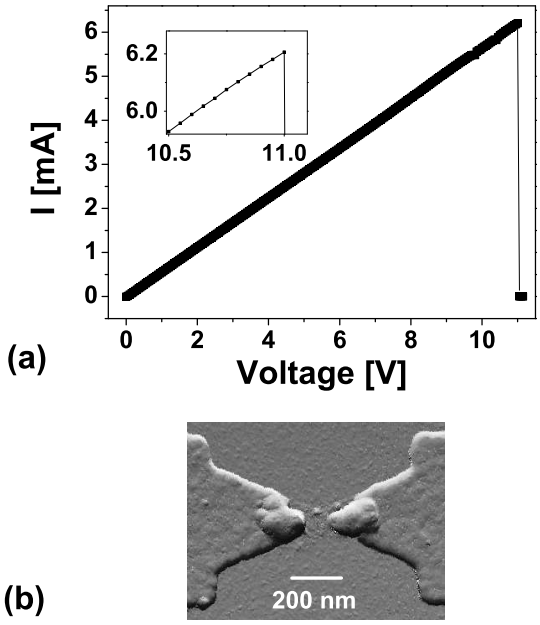

Figure 8.2: *a) I(V) measurement during an electromigration experiment ('bow tie' sample). The total resistance before electromigration is 1780 Ω. At 11 V, the sample breaks down abruptly. No tunnel current could be observed afterwards. Inset: Magnification of region just before breaking. Measurement at 295 K. b) AFM picture of the sample after breaking. As can be seen, the breaking mechanism for this sample was melting instead of electromigration. In between the electrodes, gold islands can be observed.*

$$p(t) = p_c \left(\frac{1 + \frac{R_s}{R_c(0)}}{1 + \frac{R_s}{R_c(t)}} \right)^2 \tag{8.6}$$

Let us first consider the limit with a small series resistance, $\frac{R_s}{R_c(0)} << 1$. In this case, the dissipated power is always equal to p_c, independent of the width of the constriction. Hence, the local temperature stays close to T_{start} and the gap grows slowly in time. In the other limit, $\frac{R_s}{R_c(0)} >> 1$, the situation is different. At the start of the process (t=0), the local power equals p_c. However, the dissipated power increases rapidly during the breaking process, especially when $R_c(t) >> R_c(0)$. In this limit, $p >> p_c$. Consequently, uncontrollable heating takes place. This can finally lead to melting of the electrodes [19]. We note that Eq. (8.6) only holds in the diffusive regime, where the mean free path of the electrons is much

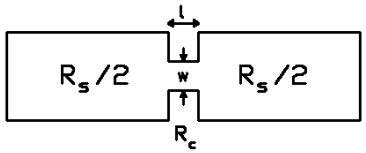

Figure 8.3: *Schematic presentation of an electromigration sample. The total resistance R consists of the constriction resistance R_c and series resistance R_s. Due to electromigration, the constriction will shrink in time, leading to a reduction of the width w and height h and an increase of R_c.*

smaller than the dimensions of the contact. Interestingly, as the electromigration process continues, the size of the constriction decreases. Provided that heating is limited, one expects a cross-over from the diffusive to the ballistic transport regime. We will return to this phenomenon in section C.

To have a better control of the final gap size, one has to limit the series resistance within the set-up as well as within the sample itself. For the latter we developed the 'terrace' samples that connect big leads to the constriction (see Fig. 8.1a). As compared to the 'bow tie' samples (see Fig. 8.2b), this geometry has three advantages. The most important one is to limit the dissipated power during electromigration, by the reduction of R_s. Another advantage is that the voltage needed to break the samples is limited. This is important, since, after break down all the voltage drop will be across the gap. This leads to a high electric field. It is well known that electric fields exceeding 2 V/nm, can cause a reorganization of the electrodes. Depending on the shape of the electrodes, this reorganization can result in a larger gap size [20, 21]. A third advantage of thick leads, is their use as heat sinks. In this way, the heat can easily flow away from the constriction. By the evaporation of 150 nm Au for the leads, we have a total resistance of typically 30 Ω (including the wiring of the measurement setup).

To show the effect of a series resistance experimentally, a variable resistance is inserted in series with the sample. This way, we can check the final gap size as a function of R_s. The result is shown in Fig. 8.4. We have investigated 142 samples, of both types. The wires were broken by slowly increasing the voltage until a gap occurs. Afterwards, the tunnel resistance at zero bias was measured, in order to make an estimation of the gap size. Zero bias resistances larger than 10^{12} Ω could not be measured, and are counted as "no tunnelling". As can be seen from Fig. 8.4, there is a strong relation between the gap size and the total initial resistance. Considering samples with large series resistances, from $2-8$ $k\Omega$,

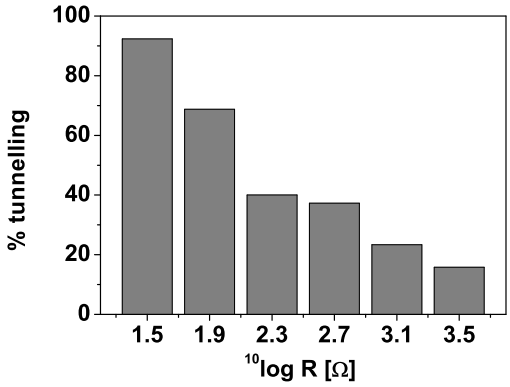

Figure 8.4: *Percentage of samples with a zero-bias tunnel resistance* $< 10^{12}$ *Ohm after electromigration, as a function of the initial series resistance. High initial series resistances lead to excessive heating, causing large gaps. The number of samples showing a tunnel current can be increased from 15 up to* > 90 *percent by limiting the series resistance. In total, 142 samples were measured. The number of samples per bar is 13/16/5/59/30/19.*

only 15 percent have nanogaps with a measurable tunnel current. Samples with low series resistances, however, give smaller gaps. Decreasing the value for the series resistance to about 30 Ω, gives nanogaps with a measurable tunnel current in more than 90 percent of the cases. From the tunnel current, an estimation can be made of the size of the gaps. These are in the range of 0 to 2 nm.

8.4.2 Local temperature during electromigration

For the model discussed above, we assumed that gap formation does not start until a certain critical temperature T_{start} is reached. To test if this is indeed the case, we performed measurements at 4.2, 77 and 295 Kelvin. We found no clear differences in final gap size. We did observe, however, that a higher critical power p_c is needed, when samples are broken at lower temperatures. This suggests that the local temperature at which electromigration is triggered, is more or less independent of the surrounding temperature. This is as expected, since the mobility of gold atoms is strongly dependent on the temperature (we will discuss this in more detail below).

In order to find the local temperature during electromigration, T_{em}, we fabricated four terminal devices. Knowledge of T_{em} is important, since, for molecular electronics, molecules are often put on the sample prior the breaking process. High temperatures could damage the molecules, right where the nanogap will be

formed.

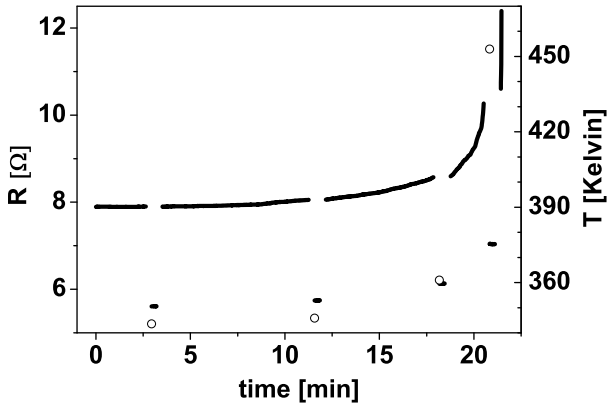

Figure 8.5: *Four-terminal resistance during electromigration. The voltage is set for an initial electromigration speed of 100 $\mu\Omega/s$, and kept constant afterwards. Due to electromigration, grain coalescence and heating, the resistance increases. Every couple of minutes, the resistance is measured at low voltage, and then V is set back to the initial value. From the change in resistance between low and high voltage, the average local temperature can be obtained (circles). The temperature of the environment is 77 K, while the temperature at which electromigration is initiated is 345 K. Just before break down, the temperature increases. The last temperature measured before break down is 450 K. The applied voltage is 0.72 V. The initial two-terminal resistance is 41 Ω, the four-terminal resistance is 5.8 Ω (at 77 K). The initial current density is $4\times10^8 A/cm^2$.*

To determine the local temperature, the samples were first cooled down to obtain the relation between temperature and (local) resistance (4.2 K < T < 295 K) [22, 23, 24]. The electromigration experiment is subsequently performed as follows. First, the voltage is increased till electromigration starts (defined as $dR/dt = 100\mu\Omega/\mathrm{s}$), and kept constant afterwards. An example is shown in Fig. 8.5. From here on, different processes will influence the local resistance. The most important ones are electromigration, heating and the coalescence of grains. To make an estimation of T_{em}, it is crucial to deduce only the resistance change due to heating. This was done by interrupting the measurement every couple of minutes, and determining the resistance at low voltage [23]. Finally, the average local temperature T_{em} is estimated from the resistance difference at low and high voltage and the (extrapolated) relation between temperature and resistance.

For the trace in Fig. 8.5, the initial four-terminal resistance was 5.8 Ω (at 77 Kelvin). Setting the voltage to start the breaking process, increases the resistance

Table 8.1: *Local temperature at which electromigration starts, T_{start}, for 5 different samples. Interestingly, T_{start} appears rather independent of the temperature of the sample surroundings, T_0. For data set C and E, the temperature is also measured just before break-down, T_{final}. This temperature depends strongly on to what extent the process is controlled. Data set C is taken from Fig. [8.5].*

Data set	$T_0[K]$	$T_{start}[K]$	$T_{final}[K]$
A	4.2	430 ± 40	–
B	4.2	440 ± 40	–
C	77	345 ± 10	455 ± 10
D	295	380 ± 40	–
E	295	420 ± 10	460 ± 10

drastically to about 8 Ω (due to heating). Subsequently, the resistance increases in time, and accelerates just before breaking. Furthermore, the local temperature increases, as predicted by eq. (8.6). We note that there is always some series resistance, so that heating cannot be taken away completely. However, when high series resistances are used, the temperature does not only reach higher values, it also diverges much faster. This is clearly shown in the insets of Figures 8.1b and 8.2a. In Fig. 8.1b, a slow increase in differential resistance is observed. In contrast, for Fig. 8.2b, gap formation goes all at once, and the breaking process cannot be resolved.

In Fig. 8.5, the local temperature increases from 77 K to 345 K, when the voltage is set to start the breaking process. The temperature determined just before break down, T_{final}, is about 450 Kelvin. In Table [8.1], four other data sets are shown, at different environment temperatures. The temperatures at which electromigration is triggered are close together, whereas the variation in the temperature of the environment is about 290 Kelvin. This is a strong indication that gap formation is indeed due to electromigration (at a critical temperature) and not due to thermodiffusion via a temperature gradient [24].
To understand why T_{start} is rather independent of the temperature of the sample environment, T_0, we introduce a simple model. To fit its parameters, we use the data taken at 77 K (Fig. 8.5). We rewrite Eq. (8.4), by noting that $\nabla\mu^m = \Omega d\sigma/dx$ is the driving force due to stress σ [14, 25]:

$$\mathbf{J}_m = -L^*_{m,m}(\Omega\Delta\sigma/L - Z^* e\rho j) \tag{8.7}$$

Here $\Delta\sigma$ is the stress built up over the length L. As long as $\Delta\sigma < \Delta\sigma_{max}$, the electromigration force is balanced by the stress gradient and the atom flux J_m is zero [14, 25]. This defines a critical current density $j_{min} = \frac{\Omega\Delta\sigma_{max}}{Z^*e\rho L}$, which is independent of temperature, since $Z^*\rho$ is temperature independent [26, 27]. Using the Einstein relation $D = L^*_{m,m}d\mu/dc$, where D and c are the diffusion constant and concentration respectively, we can write down the temperature dependence of the atom flux. For the chemical potential we have $\mu = kT\ln c$ [14] , and for the diffusion constant $D = D_0e^{-E_a/kT}$ so that we can write for the phenomenological coefficient: $L^*_{m,m} = \frac{D_0}{kT}ce^{-E_a/kT}$. Here, E_a is the activation energy of gold diffusion on the surface, which is 0.12 eV [28]. This leads to the following approximation for the atom flux due to the current density:

$$\mathbf{J}_m = \frac{\alpha}{T}(j - j_{min})e^{-E_a/kT} \tag{8.8}$$

where $\alpha \equiv cD_0Z^*e\rho/k < 0$. For our measurements we use temperatures in between liquid Helium and Room temperature and the applied voltage over the constriction is typically 20 mV or higher. In this range, the inelastic scattering length of the electrons does not exceed the contact size. Therefore, the effective temperature in the contact can be described by $T = T_0 + \beta j^2$, where β is a fit parameter.[29] We determine β from the first temperature point in Fig. 8.5: $T_{start} = 345$ K at $j = 4 \times 10^8 A/cm^2$. Furthermore, we estimate that j_{min} equals $j_{min} \approx 1 \times 10^8 A/cm^2$ [14].

Equation [8.8] implies a strong relation between temperature and mass flux, especially due to the activated behavior. Gap formation starts as soon as the mass flux is large enough, i.e., when J_m reaches a certain value J^c_m. We define this quantity, in arbitrary units, as $J^c_m \equiv 1$. Going back to Fig. 8.5 with $T_0 = 77$ K, we infer that for $j = 4 \times 10^8 A/cm^2$, we have $J_m = J^c_m = 1$. From this, we deduce the other parameter α. Knowing both α and β, we can plot J_m as a function of current density j for all three experimental temperatures T_0. This is shown in Fig. 8.6. For each T_0, we calculate the current density and temperature at which electromigration sets in, T_{start}, demanding $J_m = 1$. (For $T_0 = 77$ K, this is by definition at $j = 4 \times 10^8 A/cm^2$ with $T = 345$ K). For $T_0 = 4.2K$ and $T_0 = 295K$ we find that T_{start} equals 330 and 420 K, respectively. Hence, increasing the temperature of the environment by 290 K, increases T_{start} by only 90 K. Related to this is the fact that the critical current density increases with decreasing T_0. Although basic, the model is in rather good agreement with the values of Table [8.1].

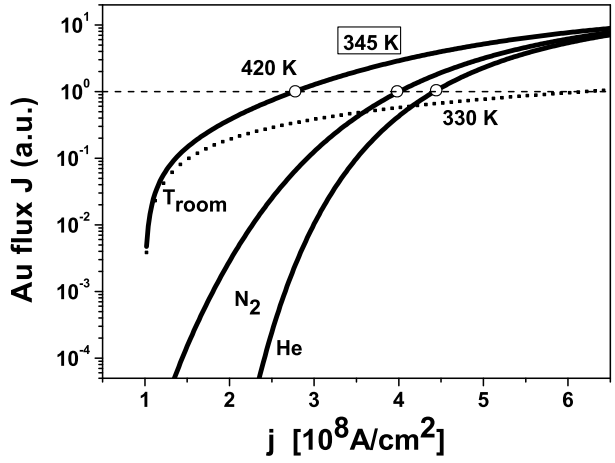

Figure 8.6: *Mass flux J_m (arbitrary units) versus current density j, for various surrounding temperatures T_0 (see eq. (8.8)). From Fig. [8.5], we know that electromigration starts (i.e., that $J_m = 1$) when $j = 4 \times 10^8 A/cm^2$ with a local temperature T_{start}= 345 K (rectangle). We use this to obtain the parameters α and β in eq. (8.8). With these, J_m versus j, can also be plotted for $T_0 = 4.2$ K and $T_0 = 295$ K, respectively. Taking Joule heating into account (solid lines), the temperature at which electromigration starts is 330 K for $T_0 = 4.2$ K and 420 K for $T_0 = 295$ K, respectively. Note that when Joule heating is neglected, electromigration can only set in at room temperature (dotted line). For 4.2 and 77 K, the critical mass flux ($J_m = 1$) cannot be reached for reasonable j.*

Do previously applied molecules get damaged at these temperatures? As we have shown above, the local temperature just before break down depends on the exact sample design. Also, the maximum temperature molecules can stand, strongly depends on the molecule. At 460 Kelvin, which is T_{final} in Table [8.1], most molecules used in molecular electronics, do not get damaged. However, care should clearly be taken. The electromigration process should be controlled either by optimizing the sample design, or by using active feedback. If not, the local temperature increases dramatically as the wire gets thinner and may reach values up to the melting point of gold.

8.4.3 Quantized conductance

As we have shown, decreasing the series resistance gives a better control of the final gap size. Another interesting consequence of controlled electromigration, is

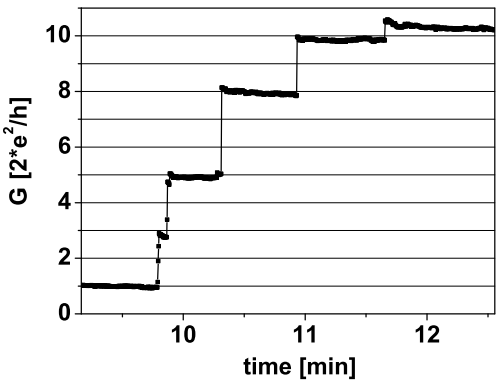

Figure 8.7: *Quantized conductance during the electromigration procedure at constant voltage. The voltage is set for an initial electromigration speed of 100 $\mu\Omega/s$, starting the breaking process. The resistance increases due to electromigration until, after 9 minutes, a conductance of 1 $\times$ $2e^2/h$ is observed. After another minute, the configuration starts to reorganize, leading to a stepwise increase in conductance. Measurement at room temperature with $V = 0.73$ V and $P = 1 \times 10^{-6}$ mbar.*

the possibility to observe the transition between the diffusive and the ballistic regime [7]. If slit formation is a well-defined process, at some point the constriction gets smaller than the inelastic scattering length. In this case, conduction becomes ballistic. This is indeed what we observe in a number of cases. During the breaking process, the sample conductance does not go smoothly to the tunneling regime, but locks in at plateaus equal to integer values of the conductance quantum $2e^2/h$ [30, 31]. An example is shown in Fig. 8.7. Here, we start with a resistance of about 45 Ω, increase the voltage until we see a change in conductance and, from there on, keep the voltage constant. Slowly, the conductance goes down, to finally stop at $1\times2e^2/h$. At this point, the electromigration process stops automatically, due to the almost perfect transmission of the gold atoms. The corresponding current density is about 57 μA/atom. This is close to the maximum value described elsewhere [32], and is much larger than the maximum current density in the diffusive regime. Nevertheless, the electrodes reorganize due to atomic diffusion. Slowly, the contact evolves from a single atom contact to a wider contact with conductance values of 3, 5, 8 and 10 G_0 [33]. At much higher voltages, it is still possible to break the constriction and obtain a tunnel resistance. We note that we have only observed quantized conductance in samples with minimized R_s. If the power is unlimited, the high temperature prohibits

the formation of a single atom contact.

8.5 Conclusions

To conclude, we have investigated the role of dissipation during the formation of nanogaps due to electromigration. We find the following. First, some Joule heating is needed for gap formation to begin. The process does not start until a local temperature of typically 400 K is reached. This value is rather independent of the temperature of the surroundings. We relate this phenomenon to the activated behavior of the atomic mobility, which plays a crucial role in this diffusion process. Second, although Joule heating is important to start electromigration, it can also lead to unwanted effects. If no measures are taken, the temperature in the constriction can increase up to the melting point of gold, during slit formation. This leads to large gaps, possibly containing small gold islands. By minimizing the total series resistance of the system, we make sure the temperature keeps low during the electromigration process. In this way, we increased the number of samples with a gap < 2 nm to >90 percent, without the use of active feedback. With the improved samples, gap formation is much slower. Hence, it is also possible to observe the transition from the diffusive to the ballistic regime. In a number of cases, contacts have been achieved that consist of only a single or a few atoms.

We thank Gert ten Brink, Niko Tombros, Bernard Wolfs and Siemon Bakker for their assistance and advice. We thank Herre van der Zant and Hubert Heersche for useful discussions. This work was financed by the Nederlandse Organisatie voor Wetenschappelijk Onderzoek, NWO, via a Pionier grant.

References

[1] H. Park, J. Park, A. K. L. Lim, E. H. Anderson, A. P. Alivisatos, and P. L. McEuen, Nature (London), **407**, 57 (2000)

[2] W. Liang, M. P. Shores, M. Bockrath, J. R. Long, and H. Park, Nature (London), **417**, 725 (2002)

[3] J. Park, A. N. Pasupathy, J. I. Goldsmith, C. Chang, Y. Yaish, J. R. Petta, M. Rinkoski, J. P. Sethna, H. D. Abruna, P. L. McEuen, et al., Nature (London), **417**, 722 (2002)

[4] M. Mahadevan and R.M. Bradley, Phys. Rev. B. **59**, 11037 (1999)

[5] H. Park, A. K. L. Lim, J. Park, A. P. Alivisatos, and P. L. McEuen, Appl. Phys. Lett. **75**, 301 (1999)

[6] K. I. Bolotin, F. Kuemmeth, A. N. Pasupathy, and D. C. Ralph, Appl. Phys. Lett. **84**, 3154 (2004)

[7] D.R. Strachan, D.E. Smith, D.E. Johnston, T.-H. Park, M.J. Therien, D.A. Bonnel and A.T. Johnson, Appl. Phys Lett. **86**, 43109 (2005)

[8] H.B. Heersche, Z. de Groot, J.A. Folk, L.P. Kouwenhoven and H.S.J. van der Zant, A.A. Houck, J. Labaziewicz and I.L. Chuang, Phys. Rev. Lett. **96**, 017205, (2006)

[9] A.A. Houck, J. Labaziewicz, E.L. Chan, J.A. Folk and I.L. Chuang, Nano Letters **5**,1685, 9 (2005)

[10] G. Esen and M. S. Fuhrer , Appl. Phys Lett. **87**, 263101 (2005)

[11] H.S.J. van der Zant *et al.*, Faraday Discuss., **131**, 347 (2006)

[12] S.R. de Groot, Thermodynamics of irreversible processes, North-Holland Publishing company, Amsterdam, (1963)

[13] S.J. van der Molen, M.S. Welling and R. Griessen, Phys. Rev. Lett. **85**, 3882 (2000)

[14] King-Ning Tu, J.W. Mayer, L.C. Feldman, Electronic thin film science for electrical engineers and materials scientists, Macmillan, New York, (1992)

[15] J.I. Gonzalez, Tai-Hee Lee, M.D. Barnes, Y. Antoku and R.M. Dickson, Phys. Rev Lett. **93**, 147402(2004)

[16] R. Sordan, K. Balasubradamanian, M. Burghard and K. Kern, Appl. Phys Lett. **87**, 013106 (2005)

[17] For this manuscript we define the starting point of gap formation, when the increase in resistance reaches a speed of 100 $\mu\Omega$/s. We note that for other values, the starting temperature T_{start} will also change.

[18] Since we use a 1-dimensional model, the length of our constriction does not change with time.

[19] A comparison can also be made with a current source (Norton equivalent circuit) and a voltage source (Thevenin circuit). Gold wires with high series resistances are broken as if connected to an ideal current source. As the width of the wire decreases, the current density increases. Constrictions with negligible series resistances are broken as if connected to an ideal voltage source. As the width decreases, the current density stays approximately constant.

[20] J. Mendez, J. Gomez-Horrero, J.I. Pascual, J.J. Seanz, J.M. Soler and A.M. Baro, J. Vac Sci. Technol. B **14**, 1145 (1996)

[21] D. Huang, F. Yamaguchim, Y. Yamamoto, Jap. Journal Appl. Phys. **37**, 3824 (1998)

[22] M. F. Lambert, M. F. Goffman, J. P. Bourgoin, and P. Hesto, Nanotechnology **14**, 772 (2003).

[23] B. Stahlmecke and G. Dumpich, Defect and Diffusion Forum Vols. **237-240** 1163 (2005)

[24] C. Durkan, M.E. Welland, Ultramicroscopy **82**, 125, (2000)

[25] I.A. Blech, J. Appl. Phys. **47**, 1203 (1976)

[26] R.S. Sorbello, Solid State Phys. **51**, 159-231 (1998)

[27] A.H. Verbruggen, IBM J. Res. Develop. **32**, 93 (1988)

[28] N.T. Wilson, The structure and dynamics noble metal clusters. PhD thesis, University of Birmingham, (Sept. 2000)

[29] In our measurement range, the applied bias voltage is close to the Debye energy, leading to strong electron-phonon scattering. The inelastic scattering length does not exceed the contact size and the temperature in the contact can be described by the given relation. However, when temperatures around or below 1 Kelvin are considered, and the maximum voltage is in the mV range, electron-electron scattering is the dominant relaxation mechanism. The relation for the temperature becomes $T = \sqrt{T_0^2 + \beta j^2}$. For the measurement at Helium temperature, however, this will give only a minor change in the final maximum temperature (343 K instead of 330 K).

[30] B.J. van Wees *et al.*, Phys. Rev. Lett. **60**, 848 (1988)

[31] C.J. Muller, J.M. van Ruitenbeek and L.J. de Jongh, Phys. Rev. Lett. **69**, 140 (1992)

[32] J. Mizobata, A. Fujii, S. Kurokawa, A. Sakai, Phys. Rev. B **68**, 155428 (2003)

[33] Since it is not possible to vary the conductance back and forth, as with the mechanically controllable break junctions, we have not performed statistics. However, since the values are exactly equal to the conductance quantum, there is a strong indication that the conductance steps are due to single gold atoms.

Appendix: MCB-junction recipe

Below, the preparation of the lithographically defined break junctions is described in detail.

Metallization

- The processing starts by cutting Ph-Bronze substrates of 22.5 × 10.2 mm (thickness is 0.5 mm).
- At this stage, the surface of the substrate is too rough for the electron beam lithography process. Hence, the surfaces are first polished using a polishing machine. For this purpose, the samples are glued on top of a hot copper plate (8 samples maximum). Next, a heavy metal plate is put on top of the samples, while cooling the samples to room temperature.
- Polish for 1"40 minutes on Piano 1200 (type of polishing plate) with water, speed 300 rpm. Force 5 kg. If necessary, first polish with paper P320 (with water).
- Clean sample with water and continue with MD LARGO, speed 150 for 6"30 minutes. Use diamante suspension. Force 5 kg.
- Clean sample and continue with DAC, speed 150 for 6"30 minutes. Now, use both Diamante and Lubricant suspension. Force 4 kg.
- Clean sample and continue with MD NAP, speed 150 for 1"40 minutes. Use 1 μm. diamante spray. Force 2 kg. After NAP, rinse samples with ethanol, blow dry, and put samples on hot plate. Take the samples of the hot plate as soon as possible. Finally, clean the samples with aceton, ethanol and blow dry.

Polyimide

- To electrically insulate the wire from the substrate, an elastic polyimide layer is spined on top of the metal substrate: First, the substrates are put in aceton for a second time, and cleaned in a ultrasonic bath for 8 minutes. Subsequently, wash with ethanol and spin samples dry.

- Clean with an O_2 plasma for 4 minutes at 40 Watt, with parameters 9 sccm O_2 and 0.009 mbar.

- Spin Pyralin Polyimide (HD MicroSystems) at 500 rpm for 5 s. and 2000 rpm for 85 s. Prebake polyimide at 100^o C for 90 s. and 150^oC for 90 s.

- Cure polyimide at 330^oC for 30 minutes in a tube furnice in a N_2 environment on top of a glass plate. This results in an insulating, elastic polyimide layer of approximately 3 μm thickness.

Resist layers

- Spin PMMA 2010, 4 percent in Cl-benzene, at 2000 rpm for 60 s.

- Bake PMMA 2010 at 175^oC for 45 min.

- Spin PMMA 2041, 2.2 percent in O-xylene, at 3000 rpm for 60 s.

- Bake PMMA 2041 at 175^oC for 45 min.

E-beam Lithography

- For the electron beam lithography, we have used a Raith "e-line" system. First, the orientation and center of the sample is defined, by measuring each corner of the sample. Subsequently, the u,v coordinate system is defined along the edges of the substrate.

- For the sample design, both small structures (100 nm lines) and large structures (1 mm^2 bonding pads) are used. For this purpose, the small structures are written using a 10 μm aperture, while the large structures are written with a 120 μm aperture size. During the e-beam writing, the system automatically changes between these two aperture sizes. Doing so, the e-beam time is 90 minutes for each MCBJ sample. The settings are as follows: Voltage is 10 kV, area dose is 100. The small lines are written with a step size of 10 nm, dwell time of 2 μs, 0.1 mm write field, and a beam speed of 4-5 mm/s. For the large structures, we used a step size of 150 nm, 2 mm write field, and a beam speed of 40 mm/s.

Development of the resist layers

- Development of resist layers: IPA:MIBK 3:1 (usually 60cl:20cl), for 60 s. To stop the process, the samples are put in IPA for 60 s; Finally, clean the samples in IPA and spin dry.

Metals evaporation

- The metal evaporation is done in a home built cryo-pumped system, at a back pressure of 10^{-7} mbar. All metals are thermally evaporated.
- For better adhesion of the gold to the polyimide layer, we used a 1 nm thick Cr adhesion layer. The Cr is evaporated at a rate of about 0.009 nm/s.
- Subsequently, a 120 nm gold layer is evaporated. Before opening the shutter (and starting the actual evaporation), the gold pieces are first baked out during 1 minute. Next, the shutter is opened at an evaporation rate of about 0.05 nm/s. After the evaporation of the first 1 nm, the evaporation rate is increased to 1 nm/s. After evaporation, wait at least 15 minutes before venting the system with N_2.
- Lift-off in heated acetone. A syringe is used for easy lift-off (do not use the ultrasonic bath, since this will erase the whole gold layer). Finally, the samples are put in ethanol and spined dry.

Plasma Etching

- To create an undercut below the gold wire (and thus create a free hanging gold wire), part of the Polyimide is etched in a home built Reactive Ion Etching machine. First, the champer is cleaned for 5 minutes with an oxygen plasma. Settings: 20 sccm O_2, 0.02 mbar at 100 Watt. Next, the samples are inserted in the etching chamber. Before starting the etching, the chamber is flushed twice with O_2 for about 20 s.
- For an isotropic etch, a combination of CF_4 and O_2 is used. The gas flows are set to **15** sccm CF_4, and **60** sccm O_2.
- Set the pressure to 0.674 mbar, and plasma etch at 200 W. This leads to a vertical etching rate of approximately 100 nm/s. Stop etching after 65 s.

Summary

The research field of nanotechnology deals with structures below 100 nanometer (1 nanometer is 10^{-9} meter). It is expected that this technology will strongly develop in the next years. The ultimate question is whether one can control the process on the atomic scale, and use this for applications. Possibly, one could even make faster computer chips in the future consisting of molecules as the functional building blocks. At this moment, it is not yet clear if this will happen, more research is needed of the interactions on the atomic scale.

This thesis describes experimental research on electron transport through single atoms and molecules. This is possible by using a so called mechanically controllable break junction. Such a junction consists of a (golden) wire, which is fabricated on top of a flexible substrate (as shown on the cover page of this thesis). This wire can be stretched by bending the substrate and, with further stretching, the wire will break near the middle of the substrate. The interesting thing is that for metals like gold, the wire will become thinner and thinner upon stretching (like chewing gum). Just before rupture, the minimum diameter of the wire is only a single gold atom. After breaking, one has created 2 atomically sharp electrodes. By now bending back and forth the substrate, one can control the distance between the electrodes with a very high precision (with a precision in the order of picometers, or 10^{-12} meter). With this system, one can investigate the electronic and mechanical properties on atoms and molecules on the atomic scale.

First of all, it is crucial to know the precise distance between the electrodes. Therefore, one has to know the ratio between the bending of the substrate, and the change in electrode distance. This is not trivial. We show in chapter 3 that this depends on the exact geometry of the system. Luckily, there are experimental methods to measure the electrode distance, and to calibrate the break junctions. In this thesis, three independent methods are used. An example is to measure the tunnel current. At electrode distances smaller than 1 nm, electrons can quantum mechanically tunnel from one electrode to the other. This current can

be measured directly, and has an exponential dependence with distance. This way, one can accurately determine the electrode distance.

It is not possible to set the electrode distance at any given value. Instead, the two wires "jump" into contact at small electrode separations. This occurs at typical distances of 1.5 Ångstrom (1 Ångstrom = 10^{-10} m), and is investigated in chapter 4. This effect is a direct consequence of the binding energy of the opposing atoms of the two wires, which results in a attractive force between the wires. At small separations, this force is so strong that the wires are pulled towards each other, and even jumping into making contact. Subsequently, when pulling the wire, the wire will first be stretched before it breaks. Till thus far, it was not possible to model this process. The reason is plastic deformation. Every time the wire is broken, the atoms arrange themselves in a somewhat different configuration. We have found a method to eliminate this plastic deformation. This method is based on multiple times breaking and making of the wire. When this is done in a controllable way, then this "training" of the wire leads to an ordening of the gold atoms. For the new formed wires the breaking process can be modeled with high precision, with only the elasticity of the electrodes as fit parameter (between 5 and 32 N/m). This gives new insight in the electron transport on the atomic scale.

The process described above results in atomically sharp electrodes. With this system, one can "catch" a molecule for investigating its electrical properties. In this thesis, measurements are described on hydrogen molecules. Hydrogen, as a simple molecule, is an ideal system for studying the interactions on the atomic scale. An example of such interactions is the molecular vibrations of the hydrogen molecule. By measuring the electron transport through a hydrogen molecule, one can deduce the conductance of a single molecule. Subsequently, when the energy of the electrons is large enough (above a certain threshold voltage), the molecule can use the electron energy for the excitation of a molecular vibration. The molecule then vibrates in between the electrodes (comparable to a guitar string). However, the influence of these excitations on the conductance properties of the molecule is not yet completely understood. For example, these vibrations often result in a sudden changes of the current through the contact. This phenomenon is investigated and its results are reported in chapter 5. For this study, the molecules are vibrationally excited by a voltage pulse, after which the current response has been measured. This gave some unexpected results. Namely, the lifetime of a molecular vibration is expected to be small (smaller than 1 ns). Instead, we have observed response times as long as 200 ms. Apparently, a

large amount of energy has been put into the system, which needs a long time to flow away into the electrodes. Although it is difficult to draw a detailed conclusion, our observations are consistent with a phase change of the hydrogen. It is possible that the excitations of the molecules result in a strong heating of the molecules (including the molecules near the contact). This could result in a phase transition, for example from the solid phase to a liquid phase. Such heating effect by molecular vibrations has been theoretically predicted, but has never been shown experimentally. Another explanation could be the weak coupling between the molecules and the gold atoms. This could result in a long time scale, for the molecules to cool down.

The effect described above can even be used for an electronic switch (as described in chapter 6). With the help of small voltage pulses (as small as 2 mV), one can switch the system between two different conductance values. These voltage pulses are then added to a DC voltage, which is set equal to the vibration energy of the molecule. Also here, it is found difficult to give a precise description of the effect. However, it is clear that a heating effect plays a crucial role. It is possible to explain the results by a phase change depending on the exact molecular temperature. This could explain explain the energy difference between the different transitions (solid to liquid and vice versa). The results presented in chapters 5, 6 and 7 show that the vibration spectra of even simple molecules as hydrogen are not yet understood, and give interesting physics. Without any doubt this will result in new insights in the future.

All measurements described above are done with a break junction, where one breaks a gold wire with the help of a mechanical system. In the last chapter, we describe another method to create electrodes for molecular electronics. When a large current density is forced through a wire, the atoms in the wire will be pushed out their equilibrium position (at typical current densities of $10^8 \mathrm{A}/cm^2$). This process is called electromigration, and can result in breaking of the wire. After breaking, one ends up with two electrodes, separated by only a few ångstroms. The main advantage of this system is that it is relatively easy to fabricate a large number of electrodes, which can be used for molecular electronics. We have studied this method, as described in chapter 8. The main conclusion is that electromigration only occurs at a minimum local temperature (around 400 Kelvin). This threshold temperature increases the mobility of the atoms, and has one important consequence. For using electromigration induced contacts for molecular electronics, methods have to be used to minimize the local temperature

during breaking.

Samenvatting

Het vakgebied van de nanotechnologie houdt zich bezig met structuren onder de 100 nanometer (1 nanometer is 10^{-9} meter). De verwachting is dat deze technologie zich de komende jaren sterk verder zal ontwikkelen. De ultieme vraag daarbij is of men in de toekomst de processen die plaats vinden op atomaire schaal kan beheersen en gebruiken voor toepassingen. Wellicht kan men in de toekomst zelfs computerchips maken die bestaan uit moleculen als functionele bouwelementen. Het is op dit moment niet duidelijk of het zover gaat komen, er is nog veel onderzoek nodig naar de interacties op de atomaire schaal.

Dit proefschrift beschrijft experimenteel onderzoek aan elektronentransport door individuele atomen en moleculen. Zulk onderzoek is mogelijk door gebruik te maken van een zogenaamde breekjunctie. Zo'n breekjunctie bestaat uit een (gouden) draad, die van tevoren is gefabriceerd op een dun flexibel plaatje (zoals te zien op de kaft van het proefschrift). Wanneer we nu de plaat buigen, zal het draadje op de plaat mee buigen en uitgerekt worden. Bij verder buigen zal het draadje zelfs knappen, precies bij het midden van de plaat. Het interessante is nu dat voor metalen zoals goud, het uitrekken gepaard gaat met het langzaam dunner worden van het draadje (te vergelijken met kauwgom). Net voor het breken, heeft de gouddraad een diameter van slechts een enkel goud atoom. Na het breken, heeft men twee atomair scherpe gouddraadjes. En door nu de plaat weer terug te buigen, kan de afstand tussen de draadjes met een hoge precisie worden gecontroleerd (met een precisie van maar liefst enkele picometers, oftewel 10^{-12} meter). Met dit systeem kan men de elektronische en mechanische eigenschappen onderzoeken van atomen en moleculen op de atomaire schaal.

Om te beginnen is het cruciaal de precieze afstand te kennen tussen de elektrodes. Hiervoor moet men de verhouding weten tussen het buigen van het plaatje, en de verandering van de elektrode afstand. Dit is niet triviaal. Zo laten we zien aan de hand van een theoretisch model, dat dit sterk afhangt van de precieze geometrie van het systeem (als beschreven in hoofdstuk 3). Gelukkig zijn er experimentele methodes om de precieze elektrodeafstand te bepalen, en de

breekjuncties te kalibreren. In dit proefschrift worden 3 onafhankelijke methodes gebruikt. Een van de methodes is het meten van de zogenaamde tunnelstroom. Bij elektrodeafstanden kleiner dan 1 nanometer, kunnen elektronen kwantum mechanisch tunnelen van de ene elektrode naar de andere. Deze tunnelstroom is direct te meten, en hangt exponentieel af van de afstand. Hierdoor kan men direct op een nauwkeurige wijze de elektrodeafstand bepalen.

Overigens is het niet mogelijk om de elektrodes in te stellen op elke gewenste afstand. Zo "springen" de twee draadjes in contact bij kleine elektrodeafstanden. Dit gebeurt typisch op een afstand van 1.5 Ångstrom (1 Ångstrom = 10^{-10} m), en is onderzocht in hoofdstuk 4. Dit effect is een direct gevolg van de bindingsenergie tussen de tegenoverliggende atomen van de twee draadjes, dat zorgt voor een aantrekkende kracht tussen de elektrodes. Bij kleine elektrodeafstand is deze kracht zo sterk dat de draadjes naar elkaar toe worden getrokken en in contact springen. Wanneer de draad nu weer uit elkaar wordt getrokken, zal het draadje eerst verder uitrekken voordat het weer breekt. Tot nu toe was het alleen niet mogelijk om dit hele proces fysisch te modelleren. De reden hiervoor is dat er plastische vervorming optreedt. Elke keer dat het draadje wordt gebroken, rangschikken de atomen zich op een net iets andere manier. Wij hebben een methode gevonden om deze plastische vervorming te elimineren. Deze methode is gebaseerd op het meerder malen in en uit contact brengen van het draadje. Als men dit doet op een controleerbare manier, dan zorgt deze "training" van het draadje tot een ordening van de goud atomen. Voor de nieuw gevormde draadjes kan het breekproces met hoge precisie gemodelleerd worden, met enkel de elasticiteit van de elektrodes als fit parameter (tussen 5 en 32 N/m). Dit geeft een nieuw inzicht in het elektronen transport op de atomaire schaal.

Het hierboven beschreven proces resulteert dus in atomair scherpe elektrodes. Met dit systeem kan men nu een molecuul "vangen" voor het bestuderen van de elektronische eigenschappen. In dit proefschrift staan metingen beschreven aan waterstof moleculen. Waterstof, als een vrij simpel molecuul, is een ideaal systeem voor het bestuderen van de interacties op de atomaire schaal. Een voorbeeld is moleculaire vibraties van het waterstof molecuul. Door het meten van het elektronen transport door een waterstof molecuul, kan men de geleiding bepalen van een enkel molecuul. Wanneer nu de energie van de elektronen groot genoeg is (bij een bepaalde spanning), kan het molecuul deze energie gebruiken voor het aanslaan van een moleculaire vibratie. Het molecuul gaat dan vibreren tussen de elektrodes (te vergelijken met het aanslaan van een gitaarsnaar). Toch is de invloed van deze vibraties op de elektrische eigenschappen van het molecuul nog

niet compleet begrepen. Zo zorgen deze vibraties vaak voor een plotselinge verandering van de stroom door het moleculaire contact. Dit fenomeen is onderzocht en staat beschreven in hoofdstuk 5. Voor dit onderzoek werden de waterstof moleculen aangeslagen met een spanningspuls, waarna de stroom respons werd gemeten. Dit leidde tot onverwachtse resultaten. Zo is de verwachting dat de levensduur van een moleculaire vibratie zeer kort is (korten dan 1 ns). In plaats daarvan werden zeer lange responstijden gemeten, tot wel 200 ms. Kennelijk is er tijdens de spanningspuls een grote hoeveelheid energie gestopt in het systeem, wat een relatief lange tijd nodig heeft om weg te vloeien naar de elektroden. Alhoewel het moeilijk is om een gedetailleerde conclusie te trekken, zijn onze observaties consistent met een faseovergang van het waterstof. Het is mogelijk dat door het aanslaan van de vibraties van de waterstof moleculen, de moleculen sterk opwarmen (inclusief de moleculen in de directe omgeving van het contact). Dit kan leiden tot een faseovergang, van bijvoorbeeld de vaste fase naar de vloeibare fase. Zo'n opwarmeffect door moleculaire vibraties is inderdaad theoretisch voorspeld, maar nog nooit direct experimenteel aangetoond. Een andere mogelijkheid is dat de vibratie-energie van de moleculen moeilijk kan wegvloeien naar de electrodes. Inderdaad is de phonon phonon koppeling tussen de moleculen en de goud atomen verwaarloosbaar door het grote verschil in massa. Dit zou ertoe kunnen leiden dat het een relatief lange tijd duurt voordat de moleculen afgekoeld zijn.

Het effect kan zelfs gebruikt worden voor een elektronische schakelaar (als beschreven in hoofdstuk 6). Door gebruiken te maken van kleine spanningspulsen (tot slechts 2 mV), kan men de moleculen een hoge of lage vibratie-energie geven. Interessant is dat deze twee toestanden een verschillende geleiding hebben. Men kan het systeem dus aan of uit schakelen simpelweg door de moleculen te laten vibreren. Zo'n type schakelaar is nog nooit eerder vertoond. Wel geldt hier dat het nog onduidelijk is wat de precieze oorzaak is van het twee niveau systeem. Het is mogelijk dat ook hier een faseovergang plaatsvindt. Dit zou het verschil in energie kunnen verklaren tussen de ene overgang (vast naar vloeibaar) en terug (vloeibaar naar vast). Het onderzoek gepresenteerd in de hoofdstukken 5, 6 en 7 laat zien dat de vibratiespectra van zelfs simpele moleculen als waterstof nog niet volledig begrepen zijn, en dat dit resulteert in interessante fysica. Ook in de toekomst zal dit ongetwijfeld leiden tot nieuwe inzichten.

Alle bovengenoemde metingen zijn dus gedaan met een breekjunctie, waarbij een gouddraadje mechanisch uit elkaar wordt getrokken. In het laatste hoofdstuk beschrijven we een andere methode voor het creëren van elektroden voor molec-

ulaire elektronica. Door een sterke elektronenstroom te sturen door een draadje, zullen de atomen in het draadje weg geduwd worden uit hun evenwichtspositie (bij typische stroomdichtheden van $10^8 \mathrm{A}/cm^2$). Dit proces heet electro-migratie, en kan uiteindelijk leiden tot het breken van het draadje. Na het breken blijven dan twee elektrodes over, slechts enkele ångstroms verwijderd van elkaar. Het voordeel van deze methode is dat het relatief eenvoudig is om een groot aantal elektrodes te maken, die gebruikt kunnen worden voor moleculaire elektronica. Deze methode is onderzocht en de resultaten staan beschreven In hoofdstuk 8. De belangrijkste conclusie is dat electro-migratie alleen plaatsvindt bij een minimale locale temperatuur (typisch 400 Kelvin). Alleen zo hebben de atomen voldoende energie om zich te kunnen bewegen in het metaal. Deze bevinding heeft een belangrijke consequentie: Voor het gebruiken van electro-migratie contacten voor moleculaire elektronica, zal men methodes moeten toepassen om de locale temperatuur van het draadje te beperken tijdens het breekproces.

Epilogue

The work presented in this thesis was carried out in the Physics of Nanodevices group at the University of Groningen, in between 2004 and 2008. During these years, I found it surprising how diverse the job as a PhD researcher actually is. Giving presentations at (inter)national conferences, writing articles and conference proceedings, building experimental setups, setting up measurement plans, running measurements, supervising students, writing software, reading literature, having scientific discussions, designing graphics and teaching students. Furthermore, I had the luck to be surrounded with great people, which made my PhD research a very informative and fun time. Many thanks to all those people who created the great and inspiring atmosphere.

I would like to thank Sense Jan, who taught me so many research skills. Your physics knowledge, creative ideas and social talk in the bar made me have a fun time during my PhD and Master research. I will always remember the conferences in Venice, Salt Lake City, Ulm, Jülich and Paris, and the many (international) phone calls we had. It has been (and still is) an honor to work with you.

Bart van Wees, who gave me the possibility and freedom to find my scientific interests and to do research in the interesting field of nanotechnology. You always impressed me with the way you simplify problems which seem to complicated at first sight (and always turns out successful). Many thanks for letting me work in your great research group.

I would like to thank Ben Feringa, for being my second Ph. D. advisor and for giving me the opportunity to work with the photochromic switches. Even though we only had a small number of meetings, the discussions made a big impression on me. Furthermore, I thank the reading committee, Elke Scheer, Herre van der Zant en Dago de Leeuw for reading my thesis and for being there at the defence.

For the design and improvements of the experimental setup, Bernard Wolfs was always there for advise and help. Together with Siemon Bakker (thanks for all your help and unforgettable remarks during the coffee breaks), the technical staff forms a great team of crucial importance for the group.

I truly enjoyed being the supervisor of three M.Sc. students during their master research. Ponky, Simon and Frank, you were all absolutely fantastic! I would like to highlight the period with Frank. I found our cooperation fun and highly efficient, which formed the basis of a large part of my thesis. Together with Eek, we formed a superior molecular electronics team. Eek, our discussions and teamwork was incredible! And thanks for learning me to be more organized (it was needed).

Thanks to all the group members: Casper (not only for organizing the fun and efficient group meetings), Nikos, Erik, Alex, Mihai , Thorsten, Alina, Maksym, Bram, Csaba, Marius C., Ji, Steve Watts and Diana Dulic. The people who introduced me into the fantastic world of the scanning electron microscope, Gert ten Brink and Pim van den Dool. I would like to thank the secretary, for all your help (even in difficult times): Sonja Heimink-Groot and Renate Hekkema-Nieborg. Thank you Wigger Jonker, for helping me with the best electronic equipment for the job, and Ubel Linstra for the steady supply of helium. Furthermore, I enjoyed the inspiring discussions with the specialists in the research filed: many thanks to Jan van Ruitenbeek and his group members, who were always willing to discuss about each others results.

I could not have done all this work, without having a great free time with my friends. Jan willem van Noort, Peter Musschenga, and JC Solid, in particular Bram Bontrup, Paul Braat, Joost Ebeling Koning, Joost Hagedoorn, Harmen Nieuwenhuis, Joris Roggeveen, Splynter van Everdingen, Jeroen Visser, Maarten Vlemmings, Frans Went and Jan Maarten Zandbergen. And of course all the people who gave me a brilliant time in Groningen, I found the goodbye parties quite tough. Furthermore, I think it is amazing how relaxing a clubbing night (with far to much alcohol and not going to bed before 7 in the morning) can be.

Thanks to my family, my parents in particular, for always supporting me and having confidence. And finally, special thanks to my girlfriend Sietske Schudde. Thank you for all your support, love, and patience with my sometimes chaotic lifestyle. My most beautiful memories of the past years were with you, and because of you. The quality time we have together makes life *super toll*.

Marius Trouwborst
Zürich, November 2008

Curriculum vitae

Marius L. Trouwborst
Email address: M.L.Trouwborst@hotmail.com

29 March 1977	Born in Woerden, the Netherlands.
1983-1989	HAVO at the Sint Antonius college in Gouda.
1995-1997	Study Applied Physics at the Technische Hogeschool Rijswijk.
1997-2003	M.Sc. in Experimental Physics at Rijksuniversiteit Groningen. Graduate research in the Physics of Nanodevices group of prof. dr. ir. B.J. van Wees. Subject: Characterization of Gold Nanocontacts Fabricated by Electromigration.
2004-2008	Ph.D. research, Physics of Nanodevices, Zernike Institute of Advanced Materials, Rijksuniversiteit Groningen. Under supervision of Prof. dr. ir. B.J. van Wees. Dr. ir. S.J. van der Molen and Prof. dr. B.L. Feringa Topic: Molecular electronics.
2008-	Post-Doctoral researcher, Science and Technology Department, IBM Zürich Research Laboratory, Rüschlikon, Switzerland Project Topic: Molecular electronics.

List of publications

1. ***The role of Joule heating in the formation of nanogaps by electromigration.****
   M.L. Trouwborst, S.J. van der Molen, B.J. van Wees, *J. Appl. Phys.* **99**, 114316 (2006).

2. ***Single atom adhesion in optimized gold nano junctions.****
   M.L. Trouwborst, E.H. Huisman, F.L. Bakker, S.J. van der Molen and B.J. van Wees, Phys. Rev. Lett. **100**, 577052 (2008)

3. ***Molecular heating in hydrogen gold junctions.***
   M.L. Trouwborst, S.J. van der Molen, E.H. Huisman, and B.J. van Wees, *to be submitted to Phys. Rev. Lett.*.

4. ***Switching with hydrogen molecules.***
   M.L. Trouwborst, S.J. van der Molen, and B.J. van Wees, *in preparation.*.

5. ***Two level fluctuations in hydrogen affected gold tunnel junctions.***
   M.L. Trouwborst, S.J. van der Molen, F.L. Bakker and B.J. van Wees, *in preparation.*.

6. ***Mechanics of lithographically defined break junctions.****
   S.A.G. Vrouwe, E. van der Giessen, S.J. van der Molen, D. Dulic, *M.L. Trouwborst*, B.J. van Wees, *Phys. Rev. B* **71**, 035313 (2005).

7. ***Calibration of lithographically defined break junctions.***
   M.L. Trouwborst, F.L. Bakker, S.J. van der Molen and B.J. van Wees, *in preparation.*

8. ***Stabilizing single atom contacts by molecular bridge formation.***
   E.H. Huisman, *M.L. Trouwborst*, F.L. Bakker, B. de Boer, B.J. van Wees and S.J. van der Molen, *Nano letters **8**, 3381-3385 (2008).*

* These publications also appeared in the "Virtual Journal of Nanoscale Science & Technology".

Talks and poster presentations

Talks

- "Characterization of electromigration induced gold nanogaps", Nanoelectronics days 2005, February 10, 2005, Jülich, Germany.
- "Characterization of electromigration induced gold nanogaps", Transport through single molecules, March 11, 2005, Leiden, Netherlands.
- "Photochromically switchabele molecular devices", Transport in mesoscopic and single-molecule systems, August 22, 2005, Kopenhagen, Denmark.
- "Towards a low temperature switch based on a hydrogen molecule", IBM Zürich Research Laboratory, October 23, 2007, Rüschlikon, Switzerland.
- "Gold atoms and hydrogen molecules. Switching on the atomic scale", November 26, 2008, Alicante, Spain.

Poster presentations

- "Characterization of electromigration-induced nanogaps", Nano8 conference, June 28, 2004, Venice, Italy.
- "Electromigration in gold nanojunctions", Towards molecular devices, November 27, 2004, Ulm, Germany.
- "Electromigration in gold nanojunctions", Foundations of Nanoscience, April 25, 2005, Snowbird, Utah, USA.
- "Inelastic Tunneling spectroscopy on single molecules", ICNT2006, July 30, 2006, Basel Switzerland.

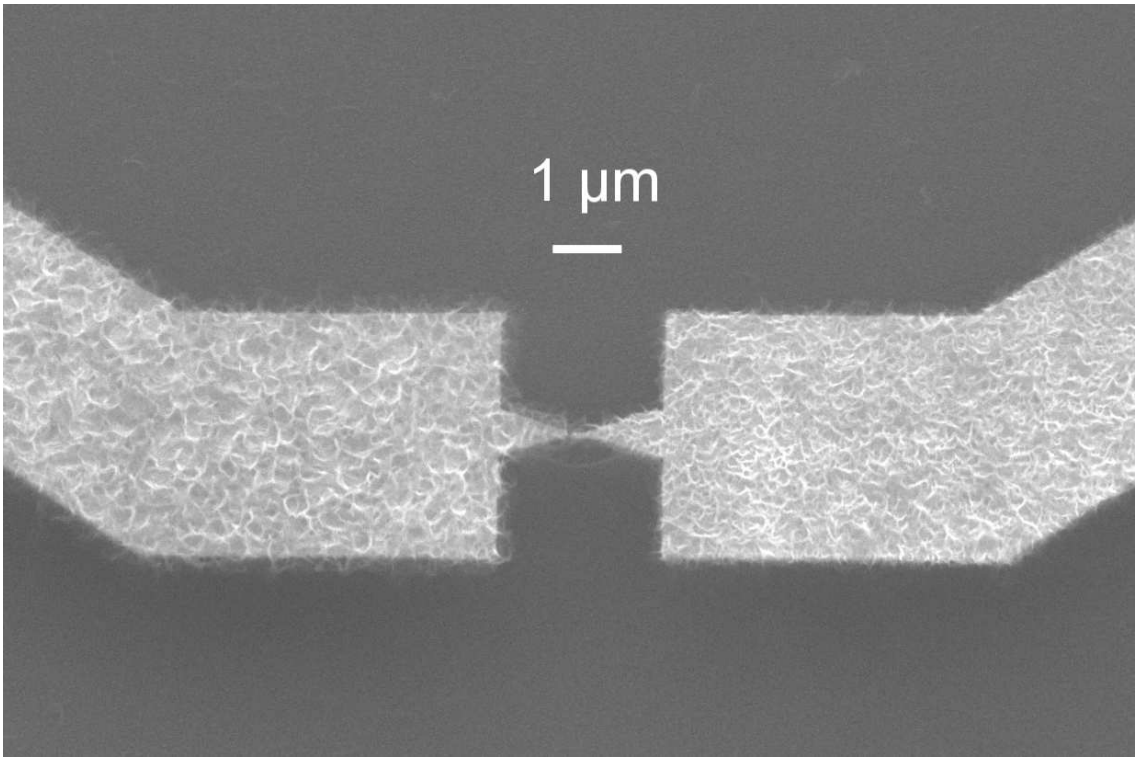

Figure 8.8: *Scanning electron micrograph of a "hairy" break junction, after the self assembly process with thiolated molecules (P3). Due to reaction with probably oxygen, polymerization occurs of the molecules. This process can especially show up in conjugated molecules.*